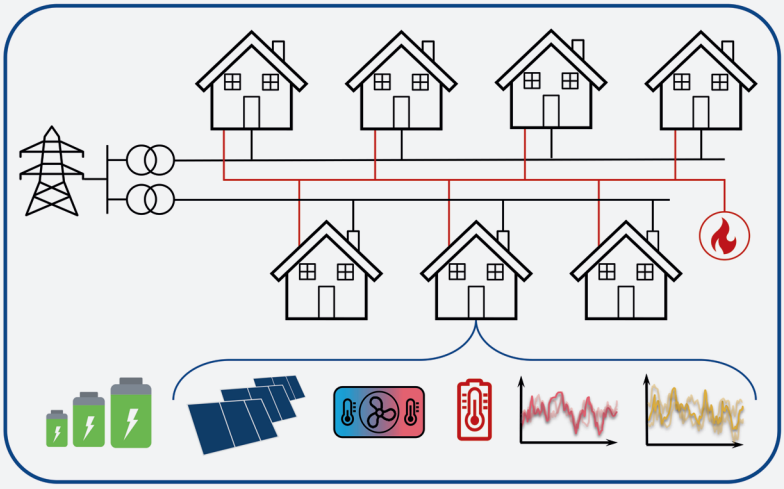

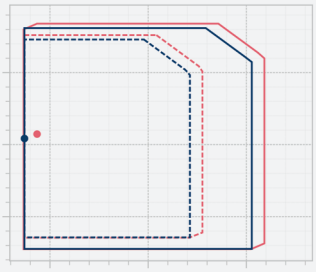

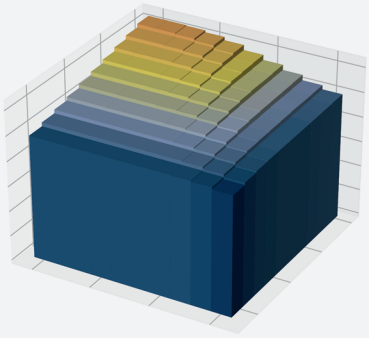

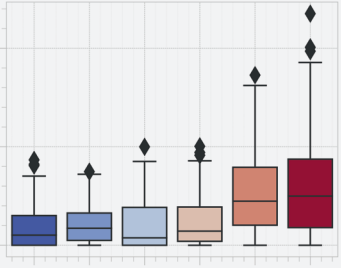

Design of Local Multi-Energy Systems: Impact of Coupled Energy Vector Integration and Grid Service Participation

Philipp Siegfried Glücker

Energie & Umwelt / Energy & Environment
Band / Volume 690
ISBN 978-3-95806-880-3

Mitglied der Helmholtz-Gemeinschaft

JÜLICH
Forschungszentrum

Schriften des Forschungszentrums Jülich
Reihe Energie & Umwelt / Energy & Environment Band / Volume 690

Forschungszentrum Jülich GmbH
Institute of Climate and Energy Systems (ICE)
Energiesystemtechnik (ICE-1)

Design of Local Multi-Energy Systems: Impact of Coupled Energy Vector Integration and Grid Service Participation

Philipp Siegfried Glücker

Schriften des Forschungszentrums Jülich
Reihe Energie & Umwelt / Energy & Environment Band / Volume 690

ISSN 1866-1793 ISBN 978-3-95806-880-3

Bibliografische Information der Deutschen Nationalbibliothek.
Die Deutsche Nationalbibliothek verzeichnet diese Publikation in der
Deutschen Nationalbibliografie; detaillierte Bibliografische Daten
sind im Internet über http://dnb.d-nb.de abrufbar.

Herausgeber und Vertrieb:	Forschungszentrum Jülich GmbH Zentralbibliothek, Verlag 52425 Jülich Tel.: +49 2461 61-5368 Fax: +49 2461 61-6103 zb-publikation@fz-juelich.de www.fz-juelich.de/zb
Umschlaggestaltung:	Grafische Medien, Forschungszentrum Jülich GmbH
Druck:	Grafische Medien, Forschungszentrum Jülich GmbH
Copyright:	Forschungszentrum Jülich 2026

Schriften des Forschungszentrums Jülich
Reihe Energie & Umwelt / Energy & Environment, Band / Volume 690

ISSN 1866-1793
ISBN 978-3-95806-880-3

Vollständig frei verfügbar über das Publikationsportal des Forschungszentrums Jülich (JuSER)
unter www.fz-juelich.de/zb/openaccess.

Abstract

As the energy transition transforms power systems towards decentralised systems dominated by renewable energy sources, the electrification of other energy vectors drives the development of integrated multi-energy systems (MESs), especially at the local level. Local MESs coupling electricity and heat can improve energy efficiency and autonomy, reduce carbon emissions, and minimise transmission losses by matching local generation and demand. However, during the design stage of local MESs, the technical and economic role of the coupled thermal vector, particularly for system sizing and leveraging its flexibility capability to provide ancillary services, remains unclear.

This thesis focuses on the optimal design of local MESs with coupled electricity and heat. A two-stage stochastic optimisation framework is developed which is adaptable and comprehensive, allowing to study several important aspects of local MES design: impact of component modelling choices on electrical storage systems; impact of individual and interdependent component sizing on technical system flexibility; integration of ancillary services and their role on optimal design; and uncertainty in future forecasting and market prices. Moreover, a novel method was developed that allows for constant flexibility calculation in relation to a time-varying reference schedule.

The framework is applied to real-world case studies to provide techno-economic insights in local MES design. The explicit modelling of the thermal vector avoids oversizing of the battery energy storage system (BESS) and reduces overall costs, highlighting the importance of incorporating coupled energy vectors in real-world electrical storage design. Moreover, the developed framework enables constant flexibility provision based on time-varying reference schedules, while accounting for internal grid constraints via a convex relaxation, which represents a suitable compromise between model accuracy and computational tractability. This allows energy system operators to assess the technical flexibility potential of their MESs across multiple market products. Furthermore, incorporating market participation for local MESs demonstrates their ability to provide multiple grid services, whose revenues shape the design of the BESS and solar PV. Despite the thermal vector participating in electricity markets, only modest oversizing of thermal storage is profitable. Additionally, risk-neutral investment positions favour large BESS capacities, while risk-averse positions prefer smaller BESSs to limit high-cost tail risks under uncertainty. Finally, the frameworks are adaptable to be used by system planners of MESs in techno-economic design studies, and can be extended to incorporate additional energy vectors.

Kurzfassung

Die Energiewende transformiert Energiesysteme hin zu dezentralen Systemen mit einem hohen Anteil an erneuerbaren Energien. Gleichzeitig treibt die Elektrifizierung anderer Energiesektoren die Entwicklung integrierter Multi-Energiesysteme (MES) voran, insbesondere auf lokaler Ebene. Lokale MES, die Strom und Wärmesektoren koppeln, steigern Energieeffizienz und Autonomie, senken Emissionen und minimieren Übertragungsverluste, indem sie lokale Erzeugung und Last optimal aufeinander abstimmen. In der Planungsphase lokaler MES bleibt die technische und wirtschaftliche Rolle des gekoppelten thermischen Vektors oft unklar, insbesondere in Bezug auf die Systemdimensionierung und die Nutzung von Flexibilität für Systemdienstleistungen.

Diese Arbeit untersucht die optimale Auslegung lokaler MES mit Strom und Wärme. Hierzu werden zweistufige stochastische Optimierungsmodelle entwickelt, die zentrale Fragestellungen der Dimensionierung lokaler MES adressieren: den Einfluss unterschiedlicher Komponentenmodelle auf Batterieenergiespeichersysteme (BESS); die Auswirkungen individueller und voneinander abhängigen Komponentengrößen auf das technische Flexibilitätspotenzial; die Integration von Systemdienstleistungen und den Einfluss dieser Einkommensströme auf das optimale Design; sowie die Berücksichtigung von Unsicherheiten in zukünftigen Prognosen und Marktbedingungen.

Praxisnahe Fallstudien liefern techno-ökonomische Erkenntnisse für die Auslegung lokaler MES. Die explizite Modellierung des thermischen Vektors verhindert eine Überdimensionierung von BESS und reduziert die Gesamtkosten. Eine neuartige Methodik zur konstanten Flexibilitätsbereitstellung auf Basis zeitlich variabler Fahrpläne ermöglicht die systematische Bewertung des technischen Flexibilitätspotenzial über mehrere Marktprodukte hinweg. Interne Netzbeschränkungen werden durch eine konvexe Relaxierung abgebildet, die einen Kompromiss zwischen Genauigkeit und Lösbarkeit darstellt. Darüber hinaus zeigt die Integration von Systemdienstleistungen, dass deren Erlöse die Auslegung von BESS und PV-Anlagen wesentlich beeinflussen. Trotz der Teilnahme des thermischen Systems an Strommärkten ist nur eine moderate Überdimensionierung des thermischen Speichers rentabel. Zudem hängen Investitionen stark von der Risikobereitschaft ab: risikoneutrale Positionen bevorzugen große BESS, während risiko-averse Positionen kleine BESS wählen, um hohe Tail-Risiken unter Unsicherheit zu begrenzen. Die entwickelte Methodik ist flexibel und kann von Systemplanern in techno-ökonomischen Designstudien genutzt und um zusätzliche Energieträger erweitert werden.

Declaration

This is to certify that

1. the thesis comprises only of my original work towards the degree of Doctor of Philosophy except where indicated in the preface,
2. due acknowledgement has been made in the text to all other material used, and
3. the thesis is less than 100,000 words in length, exclusive of tables, maps, bibliographies, and appendices.

Philipp Siegfried Glücker, August 2025

Preface

This thesis is partially based on research performed by the author during his time at the Institute for Energy Systems Engineering (ICE-1) of Forschungszentrum Jülich (FZJ) GmbH and The University of Melbourne (UoM). Parts of this thesis have been carried out in collaboration with Dr. Sleiman Mhanna (UoM), Dr. Thiemo Pesch (FZJ), Dr. Marco Langiu (FZJ), Dr. Manuel Dahmen (FZJ), and my supervisors Prof. Pierluigi Mancarella (UoM) and Prof. Andrea Benigni (FZJ, RWTH Aachen).

As per regulation of The University of Melbourne, I, Philipp Glücker, hereby declare that I have made a substantial contribution to the publications incorporated in this thesis. The list below identifies the chapters that include content from published works. The published works and the contributions from the authors are listed.

Chapter 2

1. **P. Glücker**, M. Langiu, T. Pesch, M. Dahmen, and A. Benigni, "Incorporating AC Power Flow into the Multi-Energy System Optimization Framework COMANDO." *2022 Open Source Modelling and Simulation of Energy Systems (OSMSES)*, Aachen, Germany, 2022, pp. 1-6, DOI: 10.1109/OSMSES54027.2022.9769138. © 2022 IEEE. Reprinted (adapted) with permission from IEEE.

P. Glücker wrote the first draft of the manuscript, validated the results and provided support for the implementation. M. Langiu led the coding implementation of the power grid formulations and provided substantial support in reviewing the manuscript. A. Benigni provided the original idea. T. Pesch, M. Dahmen and A. Benigni provided feedback, reviewed and revised the manuscript.

Chapter 3

2. **P. Glücker**, T. Pesch, and A. Benigni, "Optimal Sizing of Battery Energy Storage System for Local Multi-Energy Systems: The Impact of the Thermal Vector." *Applied Energy, Volume 372*, 2024, DOI: 10.1016/j.apenergy.2024.123732. © 2024 Elsevier. Reprinted (adapted) under a Creative Commons license (CC BY 4.0).

P. Glücker solely contributed to software, modelling, analysis of results, and writing the manuscript. A. Benigni assisted in the conceptualisation, supervised the project and provided feedback. T. Pesch and A. Benigni reviewed and revised the manuscript.

3. **P. Glücker**, S. Mhanna, T. Pesch, A. Benigni, and P. Mancarella, "Electrical Storage Design in Multi-Energy Systems: Impact of Component Model Choice." *2024 IEEE PES Innovative Smart Grid Technologies Europe (ISGT Europe)*, Dubrovnik, Croatia, 2024, pp. 1–5, DOI: 10.1109/ISGTEUROPE62998.2024.10863645. © 2024 IEEE. Reprinted (adapted) with permission from IEEE.

P. Glücker solely contributed to software, modelling, analysis of results, and writing the manuscript. S. Mhanna, T. Pesch and A. Benigni reviewed and revised the manuscript. P. Mancarella contributed proofreading.

Chapter 4

4. **P. Glücker**, S. Mhanna, T. Pesch, A. Benigni, and P. Mancarella, "Quantification of Electrical System Flexibility by Local Multi-Energy Systems: Impact of the System Design and Component Interdependencies." *Applied Energy, Volume 397*, 2025, DOI: 10.1016/j.apenergy.2025.126342. © 2025 Elsevier. Reprinted (adapted) under a Creative Commons license (CC BY 4.0).

P. Glücker solely contributed to implementation, modelling, case study, analysis of results, and writing the manuscript. S. Mhanna, A. Benigni and P. Mancarella assisted in the conceptualisation. S. Mhanna and A. Benigni reviewed and revised the manuscript. A. Benigni and P. Mancarella supervised the project. T. Pesch and P. Mancarella contributed proofreading.

Chapter 5

5. **P. Glücker**, S. Mhanna, T. Pesch, P. Mancarella, and A. Benigni, "Design Assessment of Local Multi-Energy System under Joint Energy and Reserve Market Participation." *in preparation*.

P. Glücker solely contributed to implementation, modelling, case study, analysis of results, and writing the manuscript. S. Mhanna and A.Benigni reviewed and revised the manuscript. A. Benigni and P. Mancarella assisted in the conceptualisation and contributed supervision. T. Pesch and P. Mancarella contributed proofreading.

6. **P. Glücker**, S. Mhanna, T. Pesch, P. Mancarella, and A. Benigni, "Optimal Design of Local Multi-Energy Systems: Impact of Reactive Power Provision." *2025 IEEE PES Innovative Smart Grid Technologies Conference Europe (ISGT Europe)*, Valletta, Malta, 2025, pp. 1–5, DOI: 10.1109/ISGTEurope64741.2025.11305385. © 2025 IEEE. Reprinted (adapted) with permission from IEEE.

P. Glücker solely contributed to conceptualisation, implementation, modelling, analysis of results, and writing the manuscript. S. Mhanna assisted in the modelling formulation. A. Benigni and S. Mhanna reviewed and revised the manuscript. T. Pesch proofread the manuscript.

Additional publications

7. **P. Glücker**, S. Germscheid, A. Ojeda, A. Benigni, M. Dahmen, and T. Pesch, "Unlocking Reactive Power Potential of Industrial Processes for Voltage Support through Scheduling Optimization." *in preparation*.

8. A. Pomarico, **P. Glücker**, D. Carta, T. Pesch, A. Berizzi and A. Benigni, "Python-based API for real-time control and monitoring of RSCAD models" *2024 Open Source Modelling and Simulation of Energy Systems (OSMSES)*, Vienna, Austria, 2024, pp. 1-6, DOI: 10.1109/OSMSES62085.2024.10668991.

9. D. Carta, M. Weber, **P. Glücker**, T. Pesch, V.Hagenmeyer, A. Benigni and U. Kühnapfel, "VILLASnode-based co-simulation of local energy communities." *2022 Open Source Modelling and Simulation of Energy Systems (OSMSES)*, Aachen, Germany, 2022, pp. 1-6, DOI: 10.1109/OSMSES54027.2022.9768933.

Acknowledgements

This thesis was developed during my time at the Institute of Energy Systems Engineering (ICE-1), Forschungszentrum Jülich, and at The University of Melbourne (UoM).

I would like to express my sincere gratitude to my supervisor, Prof. Andrea Benigni, for giving me the opportunity to start this journey and for his guidance and unwavering support. I am also sincerely grateful to my UoM supervisor, Prof. Pierluigi Mancarella, for the warm welcome and support during my time in Melbourne, and his inspiring passion for impactful research. I would further like to thank Dr. Sleiman Mhanna for his invaluable support in optimisation and scientific writing, and Dr. Thiemo Pesch for providing the framework to steer my research. I also thank the Jülich-University of Melbourne Postgraduate Academy (JUMPA) for the opportunity to work across both research environments.

I would like to extend my gratitude to my colleagues and friends at ICE-1. In particular, I would like to thank Marco for introducing me to optimisation and COMANDO, and his endless patience in answering my questions; Sonja, for the very enjoyable collaboration and her valuable advice; Jan, for many interdisciplinary discussions and shared car rides; Marcel, for all the shared coffee breaks, conversations over noodles, and his continuous encouragement and empathy; and Sina, for her willingness to listen and support. I would also like to thank Yifei, Diran, Daniele, Ariana, and several others for the work-related and non-scientific conversations, which I truly value.

Special thanks go to my colleagues and friends at the University of Melbourne: Cristian, Bastian, Pablo, Roger, Antonella, Lucas. Thank you for welcoming me into the team and the office, and for making my stay in the beautiful city of Melbourne truly special and memorable. Thanks Cristian, for bringing the fun with you, and for the table tennis sessions, bike rides and meaningful conversations we shared. Cheers mates!

My heartfelt gratitude goes out to my parents, Agathe and Helmut, and my siblings, Luise and Tobias, for their love, pride and support before and throughout this journey. I am also very grateful to my mother-in-law, Ronel, for her continuous interest and genuine curiosity in my work, and the many conversations we shared about science.

Finally, and most importantly, I would like to express my deepest gratitude and admiration to my wife, Niemke. You have sacrificed so much by moving across the world, leaving the people and the place you love, and rebuilding your life in an unfamiliar environment. Thank you for your endless support and encouragement, for always being there for me, and for the joy you bring into my life. On to new adventures!

Table of Contents

List of Figures

List of Tables

Acronyms

AC OPF AC optimal power flow.

aFRR automatic frequency restoration reserve.

AS ancillary services.

Bd building.

BESS battery energy storage system.

BTM behind-the-meter.

COP coefficient of performance.

CVaR Conditional Value-at-Risk.

DA day-ahead.

DEM demand.

DER distributed energy resources.

ED electric demand.

EV electric vehicle.

FCR frequency containment reserve.

FOM front-of-meter.

FR frequency reserve.

GWI global warming impact.

HD heat demand.

HP heat pump.

HWS hot water storage.

ID intraday.

ISOCP iterative second-order cone program.

LEC local energy community.

LinDistFlow linear distribution flow.

LTDH low-temperature district heating.

LWR least worst regret.

MES multi-energy system.

MILP mixed-integer linear problem.

NOE nodal operating envelope.

OPF optimal power flow.

PCC point of common coupling.

PL part-load.

PV photovoltaic.

RES renewable energy sources.

SoC state of charge.

SOCP second-order cone program.

TAC total annualised cost.

TES thermal energy storage.

TSO transmission system operator.

VPP virtual power plant.

WH waste heat.

Nomenclature

Indices and sets

$\epsilon, \mathcal{E}$	Individual data set, set of individual data sets
ω, Ω	Future scenario, set of future scenarios
$\tau, \mathcal{T}_\tau$	Time step index for flexibility duration, set of flexibility time steps
$c, \mathcal{C}$	Component, set of all components
$c, \mathcal{C}_{\text{st}}$	Storage component, set of all storage components
$c, \mathcal{C}_{\text{ds},ik}$	Component downstream of branch ik, set of all components downstream of branch ik
$f, \mathcal{F}$	Energy vector for flexibility calculation, set of energy vectors for flexibility calculation
$i, \mathcal{B}$	Electric bus, set of all electric buses
$ik, \mathcal{L}$	Branch connecting bus i and bus k, set of all branches
$ik, \mathcal{L}_{\text{tr}}$	Transformer (branch) connecting bus i and bus k, set of all transformers
$k, \mathcal{B}_i$	Electric bus connected to bus i, set of all buses connected to bus i
$k, \mathcal{K}_m$	Bidding period index of market m, set of bidding periods of market m
$m, \mathcal{M}$	Energy/reserve market, set of all participating energy/reserve markets
$n, \mathcal{N}$	Day index of original time series, set of days in original time series
$s, \mathcal{S}$	Representative scenario day index, set of representative scenario days
$t, \mathcal{T}$	Time step index, set of time steps
$t_k, \mathcal{T}_k$	Time step index in bidding period k, set of time steps in bidding period k
$v, \mathcal{V}$	Energy vector, set of all energy vectors

Parameters

$\cos\varphi$	Power factor (-)
$\Delta\mu$	Afternoon price shift for energy market price (€/kWh)
Δp	Pressure drop of pipe network (N/m^2)
Δt	Length of time step (h)
η^{pcc}	Electrical efficiency at PCC (%)
η_{pump}	Electric pump efficiency of the network (%)

$\eta_c^{\text{out/in}}$	(Dis)charging efficiency of component c (%)
γ^m	Price factor for frequency-balancing market m (-)
γ^p	Active power security margin of maximum market bid for storage systems (%)
γ_c^{soc}	Relative security margin for the state of charge of storage component c for market bids (%)
$\hat{\zeta}_{\epsilon,s(n)}$	Normalised daily profile of data set ϵ for day n assigned to representative day s (-)
κ_c	Self-discharge time constant of component c (1/h)
λ	Volatility factor for the energy market price (%)
$\text{SOC}_c^{\text{min/max}}$	Min./max. state of charge limits of storage component c (%)
π^{bkz}	Building cost subsidies for BESS instalment (€/kW)
π^{buy}	Variable cost for buying electricity (€/kWh)
π^{sell}	Variable price for selling electricity (€/kWh)
$\pi^{\text{buy},\omega}$	Variable cost for buying electricity for future price scenario ω (€/kWh)
π_c^{fix}	Annual fixed cost of component c (%)
ψ	Response time of flexibility (h)
$\rho_{\text{H}_2\text{O}}$	Density of water (kg/m^3)
τ_m	Response time of of market m (h)
ξ^{m}	Factor for reserve market revenues (%)
$\xi_{\text{fcr}}^{\text{act}}$	Bid activation probability in FCR market (%)
$\zeta_{\epsilon,n}$	Normalised daily profile of data set ϵ for day n (-)
A	Surface area of pipes (m^2)
A_{pv}	Installed area of solar PV (m)
a_{ik}	Voltage tap ratio of transformer connecting bus i and bus k (-)
b_{ik}	Susceptance of the branch connecting bus i and bus k (p.u.)
b_{ik}^{sh}	Shunt susceptance of the branch connecting bus i and bus k (p.u.)
$C_{\text{c}}^{\text{inv}}$	Total investment costs for component c (€)
d	Duration of flexibility (h)
d_m	Maximum activation duration of market m (h)
G	Global tilted irradiance (W/m^2)
g_{ik}	Conductance of the branch connecting bus i and bus k (p.u.)
h_{loss}	Heat transfer coefficient (W/m^{2}K)
I_{ik}^{max}	Maximum current across the branch connecting bus i and bus k (p.u.)
K_{bd}	Building capacity of building bd (kWh/°C)
k_c^{ann}	Annualisation factor of component c (-)
M_c^{ch}	Arbitrarily large number for big-M constraint (-)
$N_{\text{cyc}}^{\text{lim}}$	Cycle limit per day for BESS (-)
n_c	Lifetime of component c (a)
$P_c^{\text{min/max}}$	Minimum/maximum active power limit of component c (kW)
r	Interest rate (%)
r_{ik}	Resistance of the branch connecting bus i and bus k (p.u.)

$S_c^{\min/\max}$	Minimum/maximum apparent power limit of component c (kVA)
$V_i^{\min/\max}$	Minimum/maximum voltage magnitude at bus i
w_ϵ	Weight of data set ϵ in time series aggregation (-)
w_d	Weight of representative day d (-)
x_{ik}	Reactance of the branch connecting bus i and bus k (p.u.)

Design variables

$\dot{Q}_{\text{hp}}^{\text{des}}$	Maximum thermal output power of heat pump
$C_{\text{bess}}^{\text{des}}$	Battery energy storage system capacity
$C_{\text{hws}}^{\text{des}}$	Hot water storage capacity
$P_{\text{pv}}^{\text{nom}}$	Nominal active power output of solar PV array

Operational variables

$\dot{m}_{hp}^{\text{con}}$	Mass flow rate at the condenser of the heat pump
$\dot{m}_{hp}^{\text{evap}}$	Mass flow rate at the evaporator of the heat pump
$\dot{Q}_c^{\text{in/out}}$	Heating power input/output of component c
Λ_{ik}	Square of current I_{ik} across the branch connecting bus i and bus k
SOC_c	State of charge of storage component c
$\underline{V}_i$	Complex voltage at electric bus i
$b_{\text{hp}}^{\text{op}}$	Binary operating variable of heat pump
$b_{\text{pcc}}^{\text{cons}}$	Binary consumption variable at the PCC
b_c^{ch}	Binary charging variable of component c
b_c^{inst}	Binary installation variable of component c
E_i	Real part of complex voltage $\underline{V}_i$ at electric bus i
$f_{s,\tau}^{\text{c}}$	Value for vector f of component c at time (s,τ)
$f_{s,\tau}^{\text{pcc,ref}}$	Value for vector f at PCC for reference schedule at time (s,τ)
$f_{s,\tau}^{\text{pcc}}$	Value for vector f at PCC at time (s,τ)
F_i	Imaginary part of complex voltage $\underline{V}_i$ at electric bus i
$f_{s,\tau}^{\text{flex}}$	Flexibility for vector f at time (s, τ)
$f_{s,t}^{\text{down}\,\vert\,d}$	Downward flexibility for vector f at time (s,t) for duration d
$f_{s,t}^{\text{up}\,\vert\,d}$	Upward flexibility for vector f at time (s,t) for duration d
I_{ik}	Current across the branch connecting bus i and bus k
$o_{\text{s,t}}$	Operational variable value at scenario s and time t
$P_c^{\text{in/out}}$	Active power input/output of component c
$P_{c,m}^{\uparrow/\downarrow}$	Upward/downward market bid of component c in market m
P_c^{base}	"Normal" base operation bid of component c
$P_c^{\uparrow/\downarrow}$	Sum of upward/downward market bids of component c
P_{ik}	Active power flow across the branch connecting bus i and bus k
$P_{s,t}^{\text{down}\,\vert\,d}$	Downward active power flexibility at time (s,t) for duration d
$P_{s,t}^{\text{up}\,\vert\,d}$	Upward active power flexibility at time (s,t) for duration d
$Q_c^{\text{in/out}}$	Reactive power input/output of component c
Q_{ik}	Reactive power flow across the branch connecting bus i and bus k

$Q_{s,t}^{\text{down}\,\vert\,d}$	Downward reactive power flexibility at time (s,t) for duration d
$Q_{s,t}^{\text{up}\,\vert\,d}$	Upward reactive power flexibility at time (s,t) for duration d
S_{ik}	Apparent power flow across the branch connecting bus i and bus k
$T_{\text{hp}}^{\text{in/out}}$	Input/output temperature of heat pump
$T_{hp}^{\text{con,in/out}}$	Input/output temperature at the condenser of the heat pump
$T_{hp}^{\text{evap,in/out}}$	Input/output temperature at the evaporator of the heat pump
W_i	Square of voltage magnitude V_i at bus i

Subscripts and superscripts

act	activated
ann	annualised
bd	building
bkz	building cost subsidies (*German: Baukostenzuschuss*)
con	condenser
cons	consumption
ds	downstream
el	electrical
eva	evaporator
fix	fixed
fl	flow
flex	flexibility
gr	ground
in	input
inst	installed
inv	investment
nom	nominal
op	operating
out	output
ps	peak solar
ref	reference
th	thermal
var	variable

CHAPTER 1

Introduction

This chapter provides background, context and motivation of this thesis. An outline of the research scope is provided below, followed by the key research questions this thesis intends to address, as well as a description of the major contributions of this work. Finally, an overview of the remaining chapters of the thesis is presented.

1.1 Background and motivation

The energy transition towards carbon neutrality by 2050 leads to the decommissioning of conventional electricity generators and the increasing expansion of renewable energy sources (RES). This transition significantly changes traditional power systems, from a centralised fossil-fuel-based power system towards a decentralised power system fully relying on RES generation. The planned immense uptake of RES is depicted in Fig. 1.1 for Germany until 2045, where the projection of installed capacity of photovoltaic (PV) and wind power is evident. Especially for the solar PV, it can be seen that more decentralised rooftop PV will be deployed. Due to the time-varying nature of RES and their decentralised installation, the power system further shifts from a supply-driven system following varying demand towards an increasingly flexible demand-driven system, which ideally adapts its consumption based on the available power. In order to balance their time-varying power generation, battery energy storage systems (BESSs) are increasingly adopted to store surplus renewable energy and discharge in times of low availability.

As part of the energy transition, other energy vectors, such as transportation, gas, heat, or heavy industry, are also increasingly being electrified to reduce their carbon emissions. This includes replacing existing fossil fuel-based technologies with electric alternatives. For instance, the current increase in electric vehicles (EVs) electrifies the transportation sector from fossil fuels, while the heating sector moves from natural gas and oil towards electric

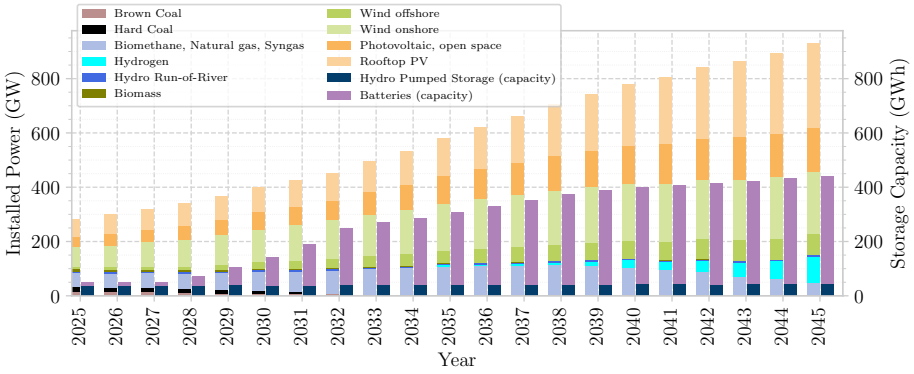

Fig. 1.1: Forecast of installed power generation and storage capacity for the scenario *technology open* in Germany, own representation adapted from [1].

heat pumps (HPs) and district heating networks [2]. In this context, multi-energy systems (MESs), integrating multiple energy vectors across different sectors as one overall system, are increasingly gaining attention, both on a local and a large-scale level. Local MESs are particularly beneficial, as generated and consumed energy is directly balanced on a local level, and synergies between energy vectors can be systematically coordinated for an optimised overall performance. Through storage systems or the coupling of energy carriers, local MESs can leverage their inherent flexibility potential to improve their local energy management or provide support to the upstream power grid [3]. This integrated approach of multiple energy vectors can improve the economic, technical and environmental performance compared to their independent counterparts [4].

Local MESs can be organised within local energy communities (LECs), which are geographically bound groups of individuals or organisations that collaboratively generate, distribute and consume energy, typically relying on a high share of RES [5, 6]. LECs are formally recognised in the European Union's Clean Energy Package as key features to involve individual households and value-driven citizen-led initiatives, rather than profit-driven companies [7]. The interest in LECs or local MESs is driven by several factors, e.g., increasing the share of renewable energy in the grid, creating a more decentralised energy system, attracting sustainable community-driven benefits, and promoting energy efficiency by reducing transmission losses over long distances [6, 8, 9].

At the level of large-scale power systems, the decommissioning of conventional synchronous generators reduces the overall system inertia, which makes the grid frequency more susceptible to disturbances and thus might increase frequency instability. Moreover, conventional power plants typically provide reactive power for voltage stability, which could face more instability with the phase-out of conventional power plants. Due to these challenges in frequency and voltage stability, future power systems will require new providers and might further increase the need for ancillary services (AS) [10, 11]. AS are deployed by grid operators to ensure a secure and reliable operation of the power sys-

tem [12]. Two types of AS exist: frequency-related services and non-frequency-related ones. While frequency-related AS ensure frequency stability via meeting active power demand with generation, non-frequency-related AS focus on non-frequency stability, such as voltage stability via reactive power provision, black start capabilities or virtual inertia response, among others [13]. When equipped with appropriate control and communication capabilities, local MESs can provide some of these services to the upstream power grid, e.g., frequency reserve or reactive power support [14–17].

The aforementioned aspects of local MESs, specifically the integration of coupled energy vectors, their inherent flexibility potential, and their potential to provide AS to the upstream power grid, are gaining more attention recently, especially during the system operation. However, these capabilities might not only impact the optimal operation of local MESs, but can significantly impact the optimal sizing, placement and selection of individual components within the local system. Therefore, it is crucial that grid service provision and the explicit modelling of coupled energy vectors within MESs are explicitly considered and integrated within the design stage. Building on these aspects, this thesis investigates the optimal design of local MESs with electricity and heat, with a particular focus on the impact of the explicit integration of the coupled thermal vector, multiple modelling choices for individual components and grid service participation. Through the presented thesis, this research aims to provide comprehensive modelling guidelines and valuable design insights to unlock the technical and economic potential of local MESs within future decentralised and decarbonised power systems.

1.2 Scope of this work

This work focuses on the techno-economic design of local multi-energy systems comprising the commodities of electricity and heat. A core part of this work is the integration and modelling of the thermal energy carrier, its impact and the quantification of operational flexibility during the design stage, and AS that can be provided to the upstream power grid and their effect on system design.

Note that while LECs and local MESs are related, they differ conceptually. On the one hand, LECs are social and legal organisations that focus on community ownership, democratic participation and fair allocation from local energy generation and consumption [6, 7]. On the other hand, local MESs primarily focus on the technical integration of multiple energy carriers at a local level [3, 4]. While both concepts have similar advantages, such as improved efficiency, enhanced energy independence and reduced carbon emissions, their focus differs. This thesis focuses on local MESs, and further provides technical insights into the optimal design of electricity-heat systems, which might include LECs, but not exclusively. In the following, the specific scope of this work is presented.

1.2.1 Design framework for local multi-energy systems

This thesis develops an optimisation-based modelling framework for the optimal design of local MESs. It explicitly models electricity and the thermal energy carrier, including their underlying network constraints and individual components. Furthermore, the inherent flexibility of local MESs is provided to energy and AS markets. The modelling framework is based on a two-stage stochastic problem formulation. In the first stage, design decisions such as placement or component sizing are determined. The second stage optimises all operational decisions and incorporates future scenarios to account for uncertainty. A centralised control structure is considered, which coordinates all considered components within the whole MES. The analysis focuses on residential and commercial systems on a local level, where electricity and heat are the most common energy carriers. While the electrification of the transport sector is well underway, the focus of this thesis lies on stationary energy systems; thus EVs and their associated challenges (e.g., optimal charging station placement and stochastic human factors [18, 19]) are excluded from the scope of this thesis. Additionally, as the local MES is assumed as a closed entity, aspects related to fairness or internal allocation of benefits are not addressed within this work.

1.2.2 Impact of component modelling choice

The coupling of multiple energy vectors, particularly electricity and heat on a local level, shifts the focus of separate optimisation of each energy vector towards an integrated analysis for improved technical and economic performance. The computational burden of modelling integrated MESs typically leads to neglecting or simplifying the connected thermal vector, especially for design studies. Yet, it is not fully known how the coupled thermal vector influences design studies in the electrical domain. This work provides a comprehensive analysis of the impact of modelling choices within local MESs on the optimal sizing of a BESS. The component models of interest of the thermal vector include electric HPs, the thermal building representation, and the heating network. Additionally, the internal power grid formulation with its inherent constraints plays a significant role in electrical storage design, thus different formulations are investigated in terms of BESS sizing and computational tractability.

Besides the detailed component models, the scope of this work extends to other factors affecting the design of BESSs. While constant electricity tariffs were typically deployed for small-scale consumers, time-varying tariffs are gaining importance to discourage electricity consumption at times of high demand, and encourage consumption in hours of excess RES generation. Comparing a constant tariff with a time-varying one, and analysing their impact on optimal sizing of BESSs, can reveal how effectively pricing signals can incentivise electrical storage design.

Through a comprehensive comparative analysis, a deeper techno-economic understanding of different modelling choices within local electricity-heat systems is gained. The scope

of this work further includes how the modelling choice implicates the computational workload. Overall, this work aims to provide practical modelling guidelines for the design of local MESs with electricity and heat.

1.2.3 Quantification of flexibility under time-varying operation

Electrical operational flexibility of multi-energy systems can be defined as the technical ability to adjust the operating point dynamically by effectively utilising interconnected energy carriers, subject to a specific duration and response time. However, this definition does not account for an operational adjustment over subsequent time steps in relation to a reference schedule, which may change due to time-varying demand or RES generation. This is especially important for large consumers such as industrial facilities or virtual power plants that must submit their operational schedule one day prior to delivery. For the participation in frequency-balancing markets, the offered bids of negative or positive active power must remain constant in relation to their time-varying planned schedule, thus requiring a flexibility calculation that incorporates the constant deviation from a time-varying reference schedule. The scope of this work lies in developing a technical framework that calculates the maximum constant upward or downward flexibility in relation to a predetermined time-varying reference schedule over successive time steps. This flexibility calculation is essential for accommodating constant flexibility offers for a specified duration, which can be adjusted to any market regulation.

1.2.4 Component sizing for operational flexibility

While the focus of flexibility provision typically lies on the operation, this work extends the operational aspect by investigating how flexibility provision is affected by individual component sizing within MESs, for both upward and downward flexibility. The scope of this work lies in the technical flexibility potential of MESs and the interdependencies between components, while the economic analysis for utilising flexibility to provide services to the upstream power grid is conducted at a later stage within this thesis, as described in Section 1.2.5. The technical analysis includes a comprehensive sensitivity analysis of individual component sizes to study their impact on the overall system flexibility potential. To allow for comparison between different designs and components, the system flexibility is quantified over the operation by aggregating all flexibility values and determining their mean value. This enables a detailed analysis of individual component size and the identification of key components that enhance or hinder overall system flexibility. In particular, the impact of the HP as the key energy vector-coupling component in combination with its thermal storage is investigated, and the interdependence and an optimal ratio between HP and hot water storage (HWS) are identified. This allows for a deeper technical understanding of the electrical flexibility and interactions between MES components.

1.2.5 Participation in multiple electricity markets under uncertainty

With an increasing electricity price volatility due to the rising penetration of RES, large-scale BESSs are increasingly adopted to benefit from these price spreads. Additional revenue streams can be generated through AS, which are measures to ensure a secure and reliable operation of the power system deployed by grid operators [12]. Active power measures are required to maintain frequency stability, while there are further non-frequency related AS such as reactive power provision, among others [13]. Besides BESSs, other components within local MESs have the technical capabilities to provide AS to the upstream power grid.

Rather than solely focusing on the optimal operational schedule, this work explicitly considers AS markets as a key factor during the design stage. The design of electrical and thermal components within local MESs is jointly optimised under energy and AS market participation. While this approach is applicable to other regions and market structures, this work is applied to the current German regulations, incorporating two frequency-balancing reserve markets within the framework. Additionally, it is analysed how potential future markets, e.g., a reactive power market, can affect the optimal design of local MESs.

The uncertainty faced by decision-makers concerning the price evolution of these markets must further be incorporated within design studies. The framework enables scenario-based integration of uncertainty via varying parameters of interest. This allows for evaluating the optimal design under a wide range of uncertain parameter values. In this case, the input parameters accounting for uncertainty factor in imperfect foresight, a possible decline in frequency reserve prices, an increasing volatility in electricity prices, as well as different values for a location-dependent fee for the BESS grid connection. The goal is to highlight the importance of incorporating the most relevant market participation options and associated revenue streams during the design phase, and taking uncertainty in key market parameters into account for optimal investment decision-making under uncertainty.

1.3 Research questions

The design of local multi-energy systems and their investment decisions pose several research questions, which this thesis aims to answer:

1. **How does the level of modelling detail in local MESs with electricity and heat impact the optimal size of electrical storage?**

   With the increasing interconnection of various energy carriers within MESs, a detailed modelling of all considered components within design studies significantly increases the problem complexity. Therefore, a systematic comparison of modelling choices within local MESs comprising electricity and heat for the optimal design of

electrical storage systems is required, which will support decision-making in their planning studies. Some specific questions related to design studies of BESSs within local MESs are stated below:

(a) How does the exact modelling of electricity and heating components influence the design of electrical domain components, e.g., electrical storage system?

(b) What is the impact of explicitly integrating the coupled thermal vector on the design of BESSs compared to an electricity-only system?

(c) What are the implications of different modelling choices on the computational tractability of the design optimisation?

(d) How does a time-varying electricity tariff affect the BESS design in comparison to a constant electricity tariff?

2. **How can operational flexibility be calculated to ensure constant flexibility provision across multiple time steps?**

Frequency-balancing markets such as frequency containment reserve (FCR) or automatic frequency restoration reserve (aFRR), which allow for remuneration of active power flexibility, require bids to offer constant upward or downward deviation from their reference schedule for a given duration. Existing approaches define flexibility as a single time-step deviation from the current operating point. However, this definition neglects time-varying demands or renewable generation within the operating schedule over multiple time steps. To address this, this research question requires a framework development which calculates the maximum constant upward or downward flexibility in relation to a time-varying reference schedule over successive time steps. This framework is designed to the following specific questions:

(a) How can a predetermined time-varying schedule be incorporated into the calculation of operational flexibility?

(b) How should operational flexibility be defined and quantified relative to a time-varying reference schedule over multiple time steps?

(c) How can the maximum constant upward and downward flexibility be calculated for a specified duration and response time, while taking inherent component and network constraints into account?

(d) To what extent can the developed methodology be generalised and applied across energy vectors?

3. **How does the sizing of individual and interdependent components of local MESs affect operational system flexibility?**

Multi-energy systems can provide electrical flexibility by effectively utilising their interconnected energy carriers. To fully leverage this flexibility, a deeper technical understanding of how operational flexibility is affected during the investment process is

required. For instance, how much flexibility can be provided by which components, how can interdependencies between individual components be identified, and how does the flexibility potential depend on the component sizing? More specifically, the detailed scope of this work is clarified through the following questions:

(a) To what extent does the explicit integration of the thermal vector affect the overall system flexibility potential?

(b) How can operational flexibility be embedded within and quantified at the design stage?

(c) Which key components in multi-energy systems enable or hinder electrical flexibility provision?

(d) Are there interdependencies or ideal ratios between component sizes over which no further flexibility can be provided?

4. **How does the integration of current and future grid service provision shape investment decisions in local MESs under uncertainty?**

Local MESs could become a key local provider of AS within decentralised RES-based energy systems. For instance, their controllable assets can adjust their active power to provide frequency-balancing reserve or adjust reactive power for voltage stability. When integrating the revenue streams from these markets during the design stage, uncertainty sources such as market price evolution and forecasting inaccuracy must be taken into account for informed decision-making. Given the broad research question, below are specific questions related to the grid service integration in the design stage of local MESs:

(a) To what extent is local MES investment shaped by the participation in ancillary service markets?

(b) How does an increasing volatility in electricity prices affect the design of local MESs?

(c) Is it economically feasible to invest in oversizing thermal components for additional ancillary service revenue?

(d) How do key uncertainty sources impact investment in local MESs?

(e) How can a future reactive power market impact controllable assets within local MESs investment?

1.4 Research aims and objectives

The general objective of this work is to investigate the design of local multi-energy systems, specifically how the explicit consideration of the thermal vector coupling can lead

to better planning decisions, while grid services can be provided. The specific objectives are summarised below:

(i) Examine the current state-of-the-art of the design of local MESs comprising electricity and heat

(ii) Investigate the impact of different component modelling choices on the design of electrical storage systems within MESs

(iii) Identification of practical modelling guidelines for the design of electrical storage systems in local MESs

(iv) Develop a framework that calculates operational flexibility over multiple time steps in relation to a predetermined reference schedule

(v) Determine interdependencies between individual components that enable or hinder the potential to provide operational flexibility

(vi) Assess and quantify the impact of individual component design on the provision of operational flexibility within MESs

(vii) Develop a techno-economic design analysis model under energy and reserve market participation for local MESs considering future uncertainty

(viii) Investigate the impact of frequency-reserve and future reactive power markets on optimal investment decisions of local MES components

1.5 Novelty and contributions

The outcomes presented in this work contribute to the improved understanding of key factors that shape and impact the design of local MESs, focusing on the explicit integration of the coupled thermal vector into the electrical system and its technical and economic implications. Several contributions introduced below have been published in different articles and proceedings, as outlined in the preface. The key novelties and contributions of this work can be summarised in the following.

1.5.1 Comprehensive analysis of modelling impact in multi-energy systems

This work presents an extensive analysis of the impact of component model choice within a local MES with electricity and heat for the design of electrical storage. Within BESS design studies, previous literature typically employs simplified models or completely neglects the coupled thermal vector, thus overlooking the impact of the thermal vector on electrical component sizing. Therefore, this work investigates the impact of modelling

choices of individual components on the BESS design, focusing on, but not exclusively, the thermal vector. This includes the thermal building representation, the heat pump model, the district heating network, and the internal power grid representation. Moreover, the computational workload of these component models is analysed. This novel contribution is developed and demonstrated in Chapter 3, providing valuable insights into practical modelling guidelines for designing electrical storage systems in local MESs and understanding their computational implications.

1.5.2 Flexibility assessment in relation to time-varying reference schedule

Another contribution of this work is the operational flexibility assessment relative to a time-varying reference schedule. Existing literature typically calculates operational flexibility relative to the current operating point given certain ramping and duration limits. However, this approach does not account for a time-varying operating schedule due to fluctuating demand or variable renewable energy generation. This work, therefore, presents a framework that evaluates operational flexibility in relation to a *time-varying reference schedule*. This predetermined reference schedule is especially important for large consumers that need to submit their operational schedule one day in advance in a day-ahead market. The novel flexibility calculation approach is presented in Chapter 4, enabling the provision of constant marketable flexibility across multiple time steps.

1.5.3 Framework of operational flexibility assessment within design phase

This work presents a framework that embeds operational flexibility within the design phase of an MES. A framework is presented that systematically quantifies the influence of individual component sizing on the operational flexibility potential of local MESs. The framework identifies key design components that hinder or enhance the technical flexibility potential, embedding the capability of local MESs to provide flexibility during operation into the design phase. Through a sensitivity analysis, the precise impact of each component design on the overall system flexibility can be quantified, and interdependencies between individual components can be identified. This contribution is developed and demonstrated in Chapter 4, providing a comprehensive technical understanding of system behaviour and identifying key components that enable system flexibility. This flexibility can then be reliably offered to the upstream power grid or utilised to improve internal system efficiency.

1.5.4 Uncertainty-aware design analysis for market participation

Another contribution of the presented work is a detailed uncertainty-aware design analysis framework which incorporates the participation of several grid service markets. This

techno-economic framework allows for the detailed assessment of potential market revenues during the design phase of local MESs for electricity and heat components, including revenues from both energy and reserve markets, as well as future markets such as a reactive power market. Uncertainty can be incorporated into future scenarios by varying input parameters, with this work focusing on different energy price volatility levels, achievable revenue limited by imperfect foresight, and varying reserve price levels. This uncertainty-aware assessment is presented in Chapter 5, allowing for optimal decision-making by quantifying the impact of market participation and future uncertainty on investment decisions.

1.6 Thesis overview

This thesis investigates various aspects of the optimal design of local MESs with electricity and heat. Fig. 1.2 presents an overview of the thesis, its research questions, and the connections between individual chapters. Chapter 2 presents the methodological and modelling foundations required to answer the research questions outlined in Section 1.3. Chapters 3 to 5 then address these questions by demonstrating the novel contributions listed in Section 1.5. The remainder of this thesis is structured as follows:

Chapter 2 presents the modelling framework of this thesis by first outlining the model formulations of the considered components, which include the commodities electricity and heat. Second, the formulation of the optimisation problem as a two-stage stochastic problem is presented, which optimises both the design and operation of the system. Moreover, the aggregation of the time series into representative days is demonstrated, which is crucial for the computational workload of the optimisation problem. The presented formulations and time series aggregation are used within the remainder of the thesis.

Chapter 3 presents a comparative analysis of different component modelling choices in local MESs and their impact on the design and placement of BESSs. The analysis is applied to an individual building and a community BESS within a local energy community. The study focuses on the modelling detail of the thermal vector, and extends it to the internal power grid. Moreover, different solar irradiance years and electricity tariffs are investigated. Through this analysis, practical modelling guidelines are provided for electrical storage design in local MESs comprising heat and electricity, along with their computational implications.

Chapter 4 presents a technical framework that is capable of quantifying the impact of component sizing on the electrical flexibility potential in local MESs during their design phase. The framework further allows for a quantified flexibility analysis over multiple time steps, which depends on a predetermined time-varying reference schedule. The adopted case studies, an individual building and a small energy community, highlight the capabilities of the presented framework and its applicability to energy systems with internal network constraints. Through a sensitivity analysis, the study provides valuable technical insights, including a comprehensive technical understanding of limiting factors and interdependencies between components across energy vectors.

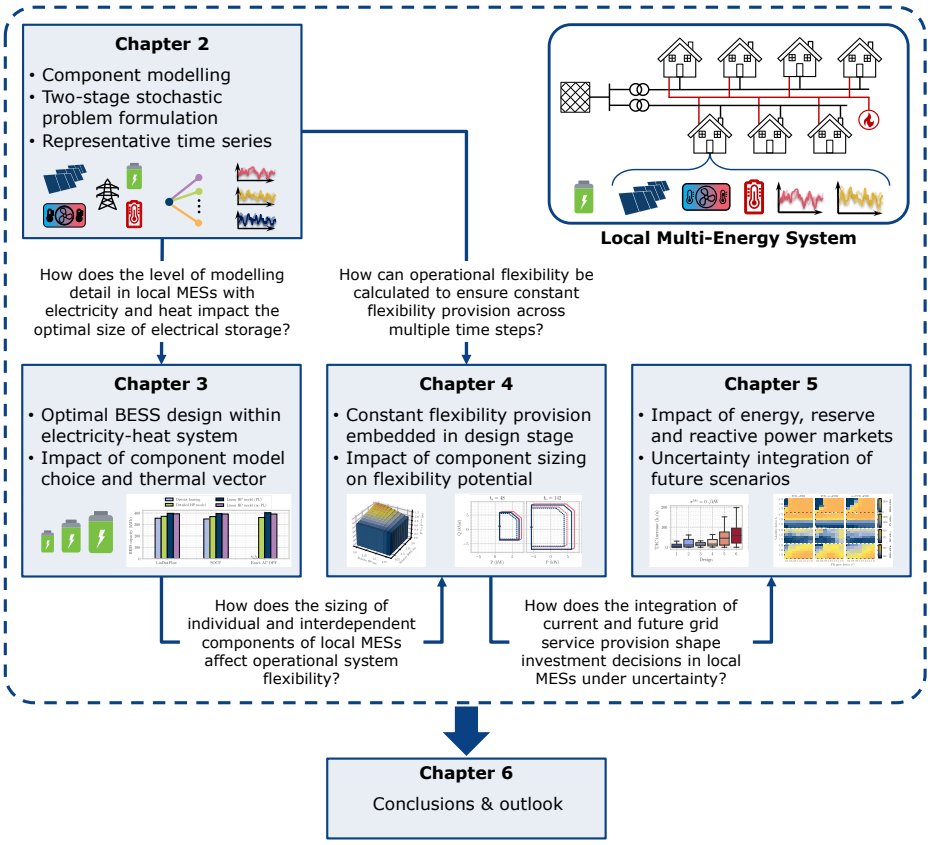

Fig. 1.2: Guiding research questions and structure of the thesis. Chapter 2 outlines the methodological and modelling foundations of this thesis, while Chapter 3 presents the first contribution listed in Section 1.5.1, Chapter 4 addresses the second and third contribution outlined in Sections 1.5.2 and 1.5.3, and Chapter 5 demonstrates the fourth contribution described in Section 1.5.4.

Chapter 5 investigates how the explicit integration of ancillary service participation impacts the optimal design of local MESs. The analysis integrates reserve markets, energy markets and a potential future reactive power market while accounting for varying future market conditions to support uncertainty-aware investment decisions. The adopted case study in the German market setup highlights the importance of considering relevant potential market revenues and uncertainty during the design phase, as these revenues can cause a shift in investment decisions.

Chapter 6 concludes the thesis and gives an outlook for future work.

CHAPTER 2

Modelling framework

This chapter presents the underlying modelling framework, which is deployed in the remainder of this work. Additional methodological aspects which are specific to individual investigations are presented in the respective chapter. This work adopts a component-oriented modelling approach, which enables scalable and modular energy system design and operation. This modularity is particularly important within local MESs, which typically comprise multiple similar components. It further allows for the investigation of different model formulations for the same type of component, enabling how various levels of modelling details impact investment decisions during the planning stage. Section 2.1 introduces the models of the individual components, which are employed in the remaining part of this thesis. Section 2.2 outlines the overall problem formulation, focusing on the two-stage stochastic problem formulation and the time series aggregation, which is used to balance computational efficiency and model accuracy.

2.1 Component model formulations

In this section, the energy components included in the MES under consideration are introduced, and their functionalities are briefly presented. This includes the BESS, the solar PV array, the internal power grid representation, the heating network, the HP, the thermal building model and the upstream power grid. Chapter 3 presents a thorough analysis of the impact of the different models on the design of a BESS within local MESs, with a particular focus on the thermal vector. The identified suitable models are then used for the remaining studies in Chapter 4 and Chapter 5.

2.1.1 Notation

Before introducing the component models, the notation and associated indices used within the following models are introduced. The operation of the energy system is modelled through a set of representative scenario days $s \in \mathcal{S}$. Within each representative scenario, discrete time steps $t \in \mathcal{T}$ are considered. Both of these indices are used consistently in the following component model formulations. The method used to derive representative scenarios and time series reduction is described in Section 2.2.2.

2.1.2 Battery energy storage system

The BESS is modelled as a lithium-ion battery system interfaced via a bidirectional power inverter, which allows for both active and reactive power exchange. The model accounts for energy losses through distinct charging and discharging efficiencies, incorporates a self-discharge rate, and further enforces thermal limits via apparent power constraints. The BESS model is governed by the following equations:

$$\begin{aligned}
\mathrm{SoC}_{\mathrm{bess},s,t+1} = (1-\kappa_{\mathrm{bess}}\Delta t)\,\mathrm{SoC}_{\mathrm{bess},s,t} + \\
\left(\eta^{\mathrm{in}}_{\mathrm{bess}} P^{\mathrm{in}}_{\mathrm{bess},s,t} - P^{\mathrm{out}}_{\mathrm{bess},s,t}/\eta^{\mathrm{out}}_{\mathrm{bess}}\right)\Delta t, \qquad & s\in\mathcal{S},\ t\in\mathcal{T}, && \text{(2.1a)}\\
b^{\mathrm{inst}}_{\mathrm{bess}}\,\mathrm{SoC}^{\mathrm{min}}_{\mathrm{bess}} \le \mathrm{SoC}_{\mathrm{bess},s,t} \le b^{\mathrm{inst}}_{\mathrm{bess}}\,\mathrm{SoC}^{\mathrm{max}}_{\mathrm{bess}}, \qquad & s\in\mathcal{S},\ t\in\mathcal{T}, && \text{(2.1b)}\\
P^{\mathrm{min}}_{\mathrm{bess}} \le P^{\mathrm{in}}_{\mathrm{bess},s,t} \le P^{\mathrm{max}}_{\mathrm{bess}}, \qquad & s\in\mathcal{S},\ t\in\mathcal{T}, && \text{(2.1c)}\\
P^{\mathrm{min}}_{\mathrm{bess}} \le P^{\mathrm{out}}_{\mathrm{bess},s,t} \le P^{\mathrm{max}}_{\mathrm{bess}}, \qquad & s\in\mathcal{S},\ t\in\mathcal{T}, && \text{(2.1d)}\\
b^{\mathrm{ch}}_{\mathrm{bess},s,t}\,P^{\mathrm{min}}_{\mathrm{bess}} \le P^{\mathrm{in}}_{\mathrm{bess},s,t} \le b^{\mathrm{ch}}_{\mathrm{bess},s,t}\,M^{\mathrm{ch}}_{\mathrm{bess}}, \qquad & s\in\mathcal{S},\ t\in\mathcal{T}, && \text{(2.1e)}\\
\left(1-b^{\mathrm{ch}}_{\mathrm{bess},s,t}\right)P^{\mathrm{min}}_{\mathrm{bess}} \le P^{\mathrm{out}}_{\mathrm{bess},s,t} \le \left(1-b^{\mathrm{ch}}_{\mathrm{bess},s,t}\right)M^{\mathrm{ch}}_{\mathrm{bess}}, \qquad & s\in\mathcal{S},\ t\in\mathcal{T}, && \text{(2.1f)}\\
-Q^{\mathrm{max}}_{\mathrm{bess}} \le Q_{\mathrm{bess},s,t} \le Q^{\mathrm{max}}_{\mathrm{bess}}, \qquad & s\in\mathcal{S},\ t\in\mathcal{T}, && \text{(2.1g)}\\
\left(P^{\mathrm{in}}_{\mathrm{bess},s,t} - P^{\mathrm{out}}_{\mathrm{bess},s,t}\right)^2 + Q^2_{\mathrm{bess},s,t} \le S^{\mathrm{max}}_{\mathrm{bess}}, \qquad & s\in\mathcal{S},\ t\in\mathcal{T}, && \text{(2.1h)}\\
b^{\mathrm{inst}}_{\mathrm{bess}}\,C^{\mathrm{min}}_{\mathrm{bess}} \le C^{\mathrm{des}}_{\mathrm{bess}} \le b^{\mathrm{inst}}_{\mathrm{bess}}\,C^{\mathrm{max}}_{\mathrm{bess}}. && && \text{(2.1i)}
\end{aligned}$$

Here, the state of charge (SoC) change is described in (2.1a), where $\mathrm{SoC}_{\mathrm{bess},s,t}$ denotes the SoC at operational scenario s and time step t, $\eta^{\mathrm{in}}_{\mathrm{bess}}$ and $\eta^{\mathrm{out}}_{\mathrm{bess}}$ are the respective constant efficiencies, $P^{\mathrm{in}}_{\mathrm{bess},s,t}$ and $P^{\mathrm{out}}_{\mathrm{bess},s,t}$ represent the charging and discharging power, and κ_{bess} denotes the discharging rate per hour. The SoC is bounded by the minimum and maximum limits $\mathrm{SoC}^{\mathrm{min/max}}_{\mathrm{bess}}$ in (2.1b), while upper and lower power limits constrain the (dis)charging power in (2.1c) and (2.1d), respectively. (2.1e) and (2.1f) prevent simultaneous charging and discharging via the binary variable $b^{\mathrm{ch}}_{\mathrm{bess},s,t}$ and a big-M formulation $M^{\mathrm{ch}}_{\mathrm{bess}}$ to avoid bilinear terms. The reactive power $Q_{\mathrm{bess},s,t}$ is limited by $Q^{\mathrm{max}}_{\mathrm{bess}}$ in (2.1g), and the apparent power limit $S^{\mathrm{max}}_{\mathrm{bess}}$ in (2.1h). Finally, the design capacity $C^{\mathrm{des}}_{\mathrm{bess}}$ is constrained with upper and lower bounds in (2.1i), with the binary variable $b^{\mathrm{inst}}_{\mathrm{bess}}$ indicating whether the BESS is installed.

2.1.3 Photovoltaic array

The PV array is modelled as an active power source interfaced with the AC grid via a DC-AC power inverter, which controls the exchange of active and reactive power. The governing equations are the following:

$$0 \leq P_{\mathrm{pv},s,t} \leq \eta_{\mathrm{pv}} \cdot A_{\mathrm{pv}} \cdot G_{s,t} \,, \qquad s \in \mathcal{S},\, t \in \mathcal{T}, \tag{2.2a}$$

$$P_{\mathrm{pv},s,t} \leq P_{\mathrm{pv}}^{\mathrm{nom}}, \qquad s \in \mathcal{S},\, t \in \mathcal{T}, \tag{2.2b}$$

$$Q_{\mathrm{pv},s,t} \leq \tan(\varphi) P_{\mathrm{pv},t} \,, \qquad s \in \mathcal{S},\, t \in \mathcal{T}, \tag{2.2c}$$

$$P_{\mathrm{pv},s,t}^2 + Q_{\mathrm{pv},s,t}^2 \leq S_{\mathrm{pv}}^{\mathrm{max}}, \qquad s \in \mathcal{S},\, t \in \mathcal{T}. \tag{2.2d}$$

Here, $P_{\mathrm{pv},s,t}$ denotes the active power generation of the solar PV array at operational scenario s and time step t, which is constrained by its inherent efficiency η_{pv}, the installed area A_{pv}, and the global tilted irradiance $G_{s,t}$. $P_{\mathrm{pv}}^{\mathrm{nom}}$ denotes the installed nominal capacity, representing the upper bound for the solar PV array power output. $Q_{\mathrm{pv},s,t}$ represents the reactive power of the power inverter, which is limited by a predefined power factor range for $\cos\varphi$. The maximum apparent power limit of the power inverter further limits the combined active and reactive power generation.

2.1.4 Heat pump

The implemented HP model represents a water-to-water system, extracting thermal energy from a district heating network at the evaporator side and supplying it to the building energy system at higher temperatures via the condenser. In the following, two models are presented: the non-convex model in Section 2.1.4.1, explicitly modelling the reduced efficiency of the compressor under low utilisation, and the linear model in Section 2.1.4.2, which includes the part-load behaviour by minimum part-load limit.

2.1.4.1 Non-convex detailed model

The HP is modelled as a component with two ports, one at the condenser and one at the evaporator. Each port is characterised by a supply temperature, a return temperature, and an associated mass flow rate. The coefficient of performance (COP) of the HP varies non-linearly, particularly under part-load conditions, due to enhanced heat transfer and cycling losses. This non-linearity is captured through a detailed model based on previous work by our research group [20]. The part-load characteristics are represented using a Glover reformulation as proposed in [21, 22], resulting in a quadratic formulation of the

HP efficiency. The governing equations are as follows:

$$P_{\mathrm{hp},s,t} = \dot{Q}^{\mathrm{con}}_{\mathrm{hp},s,t} - \dot{Q}^{\mathrm{eva}}_{\mathrm{hp},s,t}\,, \qquad s \in \mathcal{S},\ t \in \mathcal{T}, \tag{2.3a}$$

$$\dot{Q}^{\mathrm{eva}}_{\mathrm{hp},s,t} = \dot{m}^{\mathrm{eva}}_{\mathrm{hp},s,t} \cdot c_{\mathrm{p}} \cdot \left(T^{\mathrm{eva,in}}_{\mathrm{hp},s,t} - T^{\mathrm{eva,out}}_{\mathrm{hp},s,t}\right), \qquad s \in \mathcal{S},\ t \in \mathcal{T}, \tag{2.3b}$$

$$\dot{Q}^{\mathrm{con}}_{\mathrm{hp},s,t} = \dot{m}^{\mathrm{con}}_{\mathrm{hp},s,t} \cdot c_{\mathrm{p}} \cdot \left(T^{\mathrm{con,out}}_{\mathrm{hp},s,t} - T^{\mathrm{con,in}}_{\mathrm{hp},s,t}\right), \qquad s \in \mathcal{S},\ t \in \mathcal{T}, \tag{2.3c}$$

$$P_{\mathrm{hp},s,t} \cdot \eta_{\mathrm{hp}} \cdot \eta^{\mathrm{pl}}_{\mathrm{hp},s,t} = \left(\frac{T^{\mathrm{con,out}}_{\mathrm{hp},s,t} - T^{\mathrm{eva,out}}_{\mathrm{hp},s,t}}{T^{\mathrm{con,out}}_{\mathrm{hp},s,t}}\right) \cdot \dot{Q}^{\mathrm{con}}_{\mathrm{hp},s,t}\,, \qquad s \in \mathcal{S},\ t \in \mathcal{T}, \tag{2.3d}$$

$$P_{\mathrm{hp},s,t} \cdot T^{\mathrm{con,out}}_{\mathrm{hp},s,t} \cdot \eta_{\mathrm{hp}} = \left(T^{\mathrm{con,out}}_{\mathrm{hp},s,t} - T^{\mathrm{eva,out}}_{\mathrm{hp},s,t}\right) \cdot \left(0.029 \cdot \dot{Q}^{\mathrm{max}}_{\mathrm{hp}} \cdot b^{\mathrm{op}}_{\mathrm{hp},s,t} + 0.993 \cdot \dot{Q}^{\mathrm{con}}_{\mathrm{hp}}\right), \qquad s \in \mathcal{S},\ t \in \mathcal{T}, \tag{2.3e}$$

$$\dot{Q}^{\mathrm{out}}_{\mathrm{hp},s,t} \leq \dot{Q}^{\mathrm{des}}_{\mathrm{hp}}, \qquad s \in \mathcal{S},\ t \in \mathcal{T}, \tag{2.3f}$$

$$Q_{\mathrm{hp},s,t} = \tan(\varphi_{\mathrm{hp}}) \cdot P_{\mathrm{hp},s,t}\,, \qquad s \in \mathcal{S},\ t \in \mathcal{T}. \tag{2.3g}$$

Here, $P_{\mathrm{hp},s,t}$ denotes the electric power consumption of the HP. The thermal power at the condenser and evaporator are represented by $\dot{Q}^{\mathrm{con}}_{\mathrm{hp},s,t}$ and $\dot{Q}^{\mathrm{eva}}_{\mathrm{hp},s,t}$, respectively, with their corresponding input and output temperatures $T^{\mathrm{eva,in/out}}_{\mathrm{hp},s,t}$ and $T^{\mathrm{con,in/out}}_{\mathrm{hp},s,t}$, and mass flow rates $\dot{m}^{\mathrm{eva/con}}_{\mathrm{hp},s,t}$. The overall efficiency is modelled as the product of the constant device efficiency $\eta_{\mathrm{hp}} = 0.6$ and a part-load efficiency $\eta^{\mathrm{pl}}_{\mathrm{hp},s,t}$. The part-load efficiency is integrated into (2.3e) based on the maximum thermal output $\dot{Q}^{\mathrm{max}}_{\mathrm{hp}}$ and a binary variable $b^{\mathrm{op}}_{\mathrm{hp},s,t}$ indicating the operation of the HP. To reduce model complexity, a fixed temperature difference of $\Delta T = 10\,\mathrm{K}$ is assumed at the evaporator. Discontinuous operation of the HP is allowed, without time-coupling minimum operational or shutdown time constraints, following [23]. The coefficients in (2.3e) were calibrated to experimental data representing the part-load efficiency of water-to-water HPs from [22].

2.1.4.2 Linear model

The linear model of the HP assumes a constant efficiency independent of its utilisation. The lower part-load efficiency is included by a minimum part-load limit $P^{\mathrm{min}}_{\mathrm{hp}}$, leading to the following governing equations:

$$\dot{Q}^{\mathrm{out}}_{\mathrm{hp},s,t} = \eta_{\mathrm{hp},s,t}\, P_{\mathrm{hp},s,t}\,, \qquad s \in \mathcal{S},\ t \in \mathcal{T}, \tag{2.4a}$$

$$\eta_{\mathrm{hp},s,t} = \eta^{\mathrm{carnot}}_{\mathrm{hp},s,t}\, \eta^{\mathrm{sys}}_{\mathrm{hp}}, \qquad s \in \mathcal{S},\ t \in \mathcal{T}, \tag{2.4b}$$

$$\eta^{\mathrm{carnot}}_{\mathrm{hp},s,t} = \frac{T^{\mathrm{out}}_{\mathrm{hp},s,t}}{T^{\mathrm{out}}_{\mathrm{hp},s,t} - T^{\mathrm{in}}_{\mathrm{hp},s,t}}\,, \qquad s \in \mathcal{S},\ t \in \mathcal{T}, \tag{2.4c}$$

$$b^{\mathrm{op}}_{\mathrm{hp},s,t}\, P^{\mathrm{min}}_{\mathrm{hp}} \leq P_{\mathrm{hp},s,t} \leq b^{\mathrm{op}}_{\mathrm{hp},s,t}\, P^{\mathrm{max}}_{\mathrm{hp}}, \qquad s \in \mathcal{S},\ t \in \mathcal{T}, \tag{2.4d}$$

$$\dot{Q}^{\mathrm{out}}_{\mathrm{hp},s,t} \leq \dot{Q}^{\mathrm{max}}_{\mathrm{hp}}, \qquad s \in \mathcal{S},\ t \in \mathcal{T}, \tag{2.4e}$$

$$Q_{\mathrm{hp},s,t} = \tan(\varphi_{\mathrm{hp}}) \cdot P_{\mathrm{hp},s,t}\,, \qquad s \in \mathcal{S},\ t \in \mathcal{T}. \tag{2.4f}$$

Here, one temperature at the evaporator $T^{\mathrm{eva}}_{\mathrm{hp},s,t}$ and at the condenser $T^{\mathrm{con}}_{\mathrm{hp},s,t}$ is assumed, respectively, which determine the COP of the HP via the Carnot efficiency $\eta^{\mathrm{carnot}}_{\mathrm{hp},s,t}$.

The COP, which is equivalent to the efficiency of the device $\eta_{\mathrm{hp},s,t}$, is depicted in Fig. 2.1 for both models. The quadratic model shows a decreasing COP with a lower relative load, whereas the linear model has a constant COP. To represent the decreasing COP with lower utilisation for the linear model, a minimum relative load of 0.25 can be assumed.

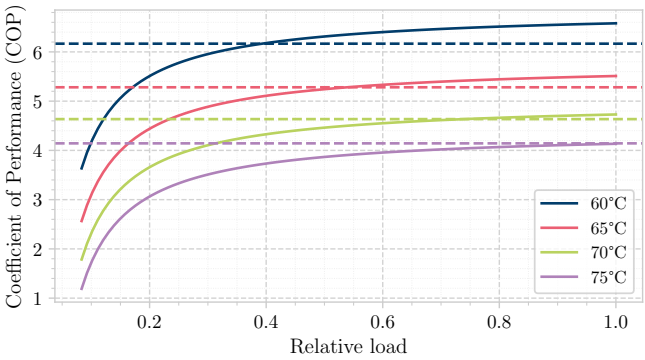

Fig. 2.1: Coefficient of performance (COP) of the HP depending on the load utilisation for the detailed non-convex model (solid lines) and the linear model (dashed lines) for different condenser temperatures for an evaporator temperature of 33 °C.

2.1.5 Thermal storage systems

In this work, two types of thermal storage systems within a building are considered: the HWS as a storage buffer, and the thermal capacity of the building dwellings.

The HWS serves as a supply-side buffer by storing heated water for space heating, while the building dwellings act as a passive thermal storage by internally absorbing, storing and releasing heat over time, which mitigates indoor temperature fluctuations caused by external conditions [24]. These two elements can be combined into a single lumped parameter, referred to as the thermal energy storage (TES) within this work. In the following, the models for both thermal storage systems are presented.

2.1.5.1 Building thermal energy storage

The building TES is characterised by its building capacity K_{bd}, with the following governing equations:

$$\frac{\mathrm{d}T_{\mathrm{bd},s,t}}{\mathrm{d}t} = \frac{\dot{Q}^{\mathrm{in}}_{\mathrm{tes},s,t} - \dot{Q}^{\mathrm{out}}_{\mathrm{tes},s,t}}{K_{\mathrm{bd}}}, \qquad s \in \mathcal{S},\ t \in \mathcal{T}, \tag{2.5a}$$

$$T^{\mathrm{min}}_{\mathrm{bd}} \leq T_{\mathrm{bd},s,t} \leq T^{\mathrm{max}}_{\mathrm{bd}}, \qquad s \in \mathcal{S},\ t \in \mathcal{T}. \tag{2.5b}$$

The temperature $T_{\mathrm{bd},s,t}$ represents the indoor temperature of the building, which is constrained within the comfort limits $T^{\mathrm{min}}_{\mathrm{bd}}$ and $T^{\mathrm{max}}_{\mathrm{bd}}$, assumed to be between 19 °C and

22 °C. The building TES is heated by the thermal input power $\dot{Q}^{\text{in}}_{\text{tes},s,t}$ and supplies its thermal output power $\dot{Q}^{\text{out}}_{\text{tes},s,t}$ to a deterministic heat demand (HD).

2.1.5.2 Hot water storage

The HWS works together with the HP to act as a storage buffer for space heating. It is assumed without mixing effects with an allowed temperature difference of 30 °C. The governing equations are as follows:

$$\begin{aligned}
\text{SoC}_{\text{hws},s,t+1} = (1-\kappa_{\text{hws}}\Delta t)\,\text{SoC}_{\text{hws},s,t} + \\
\left(\eta^{\text{in}}_{\text{hws}}\dot{Q}^{\text{in}}_{\text{hws},s,t} - 1/\eta^{\text{out}}_{\text{hws}}\dot{Q}^{\text{out}}_{\text{hws},s,t}\right)\Delta t, \qquad & s\in\mathcal{S},\ t\in\mathcal{T}, && \text{(2.6a)}\\
\text{SoC}^{\text{min}}_{\text{hws}} \le \text{SoC}_{\text{hws},s,t} \le \text{SoC}^{\text{max}}_{\text{hws}}, \qquad & s\in\mathcal{S},\ t\in\mathcal{T}, && \text{(2.6b)}\\
\dot{Q}^{\text{min}}_{\text{hws}} \le \dot{Q}^{\text{in}}_{\text{hws},s,t} \le \dot{Q}^{\text{max}}_{\text{hws}}, \qquad & s\in\mathcal{S},\ t\in\mathcal{T}, && \text{(2.6c)}\\
b^{\text{ch}}_{\text{hws},s,t}\,\dot{Q}^{\text{min}}_{\text{hws}} \le \dot{Q}^{\text{in}}_{\text{hws},s,t} \le b^{\text{ch}}_{\text{hws},s,t}\,M^{\text{ch}}_{\text{hws}}, \qquad & s\in\mathcal{S},\ t\in\mathcal{T}, && \text{(2.6d)}\\
\dot{Q}^{\text{min}}_{\text{hws}} \le \dot{Q}^{\text{out}}_{\text{hws},s,t} \le \dot{Q}^{\text{max}}_{\text{hws}}, \qquad & s\in\mathcal{S},\ t\in\mathcal{T}, && \text{(2.6e)}\\
\left(1-b^{\text{ch}}_{\text{hws},s,t}\right)\dot{Q}^{\text{min}}_{\text{hws}} \le \dot{Q}^{\text{out}}_{\text{hws},s,t} \le \left(1-b^{\text{ch}}_{\text{hws},s,t}\right)M^{\text{ch}}_{\text{hws}}, \qquad & s\in\mathcal{S},\ t\in\mathcal{T}, && \text{(2.6f)}\\
\text{with } 0 \le \left[\text{SoC}^{\text{min}}_{\text{hws}}, \text{SoC}^{\text{max}}_{\text{hws}}\right] \le C^{\text{des}}_{\text{hws}}. && && \text{(2.6g)}
\end{aligned}$$

Here, (2.6a) describes the SoC between two time steps, which depends the previous time step, as well as the self-discharge rate κ_{hws} and the respective input and output heating power $\dot{Q}^{\text{in/out}}_{\text{hws},s,t}$ with their corresponding (dis)charging efficiencies $\eta^{\text{in/out}}_{\text{hws},s,t}$. Simultaneous charging and discharging is avoided by the binary variable $b^{\text{ch}}_{\text{hws},s,t}$ and the big-M formulation $M^{\text{ch}}_{\text{hws}}$. Even though the (dis)charging efficiency of the HWS depends on the temperature [25], temperature-specific efficiency rates are not incorporated for computational efficiency.

2.1.6 Energy vector balancing

To create an MES, its components must be interconnected. For this purpose, the respective energy vectors of the components within the MES are connected and balanced.

For each energy vector $v \in \mathcal{V}$, a balancing-node constraint ensures that at every time step t and for every representative scenario s, the total generation and consumption of the respective energy vector across all components $c \in \mathcal{C}$ is balanced. The energy balancing constraint is formulated as follows:

$$\sum_{c\in\mathcal{C}} v_{c,s,t} = 0, \qquad v\in\mathcal{V},\ s\in\mathcal{S},\ t\in\mathcal{T}, \tag{2.7}$$

where the set of energy vectors is defined as $\mathcal{V} = \{P, Q, \dot{Q}\}$, with P denoting active power, Q reactive power, and $\dot{Q}$ thermal heating power. Both imports and exports of active and reactive power are incorporated in the component-specific contribution $v_{c,s,t}$.

As an alternative to balancing nodes, dedicated components can be created to represent energy networks and their underlying equations. This is explicitly implemented for the energy vectors active power P and reactive power Q to represent the power grid, with different formulations as described in Section 2.1.7, as well as for the heating power $\dot{Q}$ via the heating network presented in Section 2.1.8.

2.1.7 Power grid

Three different power grid formulations are presented: the exact nonlinear AC optimal power flow (AC OPF) formulation in Section 2.1.7.1, the convex second-order cone program (SOCP) formulation in Section 2.1.7.2, and the linear distribution flow (LinDistFlow) equations in Section 2.1.7.3. Note that the single-phase representation of the balanced three-phase AC electrical network is considered in this work, with the branch $ik \in \mathcal{L}$ connecting electric bus $i \in \mathcal{B}$ with electric bus k, with $\mathcal{B}_i$ denoting the set of all buses connected to bus i. $\mathrm{j} = \sqrt{-1}$ is the imaginary unit in the complex domain.

2.1.7.1 Exact AC optimal power flow formulation

The original nonlinear trigonometric terms of the polar voltage representation of the AC optimal power flow (OPF) formulation are implemented in rectangular coordinates, i.e., the complex voltage $\underline{V}_i$ at the electric bus i consists of a real part E_i and an imaginary part F_i. This implementation allows for a bilinear, non-convex quadratic formulation, which can be solved with Gurobi [26]. The governing equations are implemented as follows [27]:

$$\underline{V}_{i,s,t} = E_{i,s,t} + \mathrm{j}F_{i,s,t}\,, \qquad i \in \mathcal{B},\ s \in \mathcal{S},\ t \in \mathcal{T}, \tag{2.8a}$$

$$P_{i,s,t} = \sum_{k \in \mathcal{B}_i} P_{ik,s,t}, \qquad i \in \mathcal{B},\ s \in \mathcal{S},\ t \in \mathcal{T}, \tag{2.8b}$$

$$Q_{i,s,t} = \sum_{k \in \mathcal{B}_i} Q_{ik,s,t}\,, \qquad i \in \mathcal{B},\ s \in \mathcal{S},\ t \in \mathcal{T}, \tag{2.8c}$$

$$\begin{aligned} P_{ik,s,t} = {} & g_{ik} a_{ik}^2 (E_{i,s,t}^2 + F_{i,s,t}^2) \\ & - g_{ik} a_{ik} (E_{i,s,t} E_{k,s,t} + F_{i,s,t} F_{k,s,t}) \\ & - b_{ik} a_{ik} (F_{i,s,t} E_{k,s,t} - E_{i,s,t} F_{k,s,t}), \end{aligned} \qquad ik \in \mathcal{L},\ s \in \mathcal{S},\ t \in \mathcal{T}, \tag{2.8d}$$

$$\begin{aligned} Q_{ik,s,t} = {} & -a_{ik}^2 (E_{i,s,t}^2 + F_{i,s,t}^2) \left(b_{ik} + \tfrac{b_{ik}^{\mathrm{sh}}}{2} \right) \\ & + b_{ik} a_{ik} (E_{i,s,t} E_{k,s,t} + F_{i,s,t} F_{k,s,t}) \\ & - g_{ik} a_{ik} (F_{i,s,t} E_{k,s,t} - E_{i,s,t} F_{k,s,t}), \end{aligned} \qquad ik \in \mathcal{L},\ s \in \mathcal{S},\ t \in \mathcal{T}, \tag{2.8e}$$

$$P_{ik,s,t}^2 + Q_{ik,s,t}^2 \leq (S_{ik}^{\max})^2, \qquad ik \in \mathcal{L},\ s \in \mathcal{S},\ t \in \mathcal{T}, \tag{2.8f}$$

$$(V_i^{\min})^2 \leq E_{i,s,t}^2 + F_{i,s,t}^2 \leq (V_i^{\max})^2, \qquad i \in \mathcal{B},\ s \in \mathcal{S},\ t \in \mathcal{T}. \tag{2.8g}$$

Here, (2.8a) presents the voltage in rectangular coordinates. $P_{i,s,t}$ and $Q_{i,s,t}$ in (2.8b) and Eq. (2.8c) denote the active and reactive power injected at bus i during operational scenario

s and time step t, while $P_{ik,s,t}$ and $Q_{ik,s,t}$ denote the active and reactive power transfers across a branch ik from bus i to bus k, respectively, as defined in (2.8d) and Eq. (2.8e). b_{ik} is the branch susceptance, g_{ik} is the branch conductance, b_{ik}^{sh} is the shunt susceptance, and a_{ik} represents the transformer voltage tap ratio with a default value of 1. $V_i^{\min}$ and $V_i^{\max}$ in (2.8g) are the lower and upper voltage magnitude limits, which are implemented as functional inequality constraints [27]. The apparent power of each branch is limited by $S_{ik}^{\max}$ in (2.8f).

2.1.7.2 Second-order cone program approximation

For the convex SOCP relaxation, the two new operational variables $W_i = |V_i|^2$ and $\Lambda_{ik} = |I_{ik}|^2$ are introduced. This representation does not explicitly enforce Kirchhoff's voltage law, i.e., the voltage angles around a loop are not enforced to sum to zero. However, for radial networks, this angle requirement is not needed, thus no information is lost [28]. The power flow constraints (2.8) are replaced by the following convex set of equations [29]:

$$P_{i,s,t} = \sum_{k \in \mathcal{B}_i} P_{ik,s,t} \ , \qquad i \in \mathcal{B},\ s \in \mathcal{S},\ t \in \mathcal{T}, \quad (2.9a)$$

$$Q_{i,s,t} = \sum_{k \in \mathcal{B}_i} Q_{ik,s,t} \ , \qquad i \in \mathcal{B},\ s \in \mathcal{S},\ t \in \mathcal{T}, \quad (2.9b)$$

$$P_{ik,s,t} + P_{ki,s,t} = r_{ik}\Lambda_{ik,s,t} \ , \qquad ik \in \mathcal{L},\ s \in \mathcal{S},\ t \in \mathcal{T}, \quad (2.9c)$$

$$Q_{ik,s,t} + Q_{ki,s,t} = x_{ik}\Lambda_{ik,s,t} \ , \qquad ik \in \mathcal{L},\ s \in \mathcal{S},\ t \in \mathcal{T}, \quad (2.9d)$$

$$W_{k,s,t} = W_{i,s,t} - 2(r_{\text{ik}}P_{ik,s,t} + x_{\text{ik}}Q_{ik,s,t}) + (r_{ik}^2 + x_{ik}^2)\Lambda_{ik,s,t} \ , \qquad ik \in \mathcal{L},\ s \in \mathcal{S},\ t \in \mathcal{T}, \quad (2.9e)$$

$$(V_i^{\min})^2 \leq W_{i,s,t} \leq (V_i^{\max})^2, \qquad ik \in \mathcal{L},\ s \in \mathcal{S},\ t \in \mathcal{T}, \quad (2.9f)$$

$$\Lambda_{ik,s,t} \leq (I_{ik}^{\max})^2, \qquad ik \in \mathcal{L},\ s \in \mathcal{S},\ t \in \mathcal{T}, \quad (2.9g)$$

$$\left\| [2P_{ik,s,t},\ 2Q_{ik,s,t},\ \Lambda_{ik,s,t} - W_{i,s,t}]^\top \right\|_2 \leq \Lambda_{ik,s,t} + W_{i,s,t} \ , \qquad ik \in \mathcal{L},\ s \in \mathcal{S},\ t \in \mathcal{T}. \quad (2.9h)$$

Here, (2.9a) and (2.9b) denote the active and reactive power balance at each electric bus i, while (2.9c) and (2.9d) represent the active and reactive power losses across branch ik, with r_{ik} being the branch resistance and x_{ik} being the branch reactance. (2.9e) represents the voltage drop across each branch, while (2.9g) limits the current via its maximum current $I_{ik}^{\max}$. (2.9h) denotes the relaxed convex Euclidean norm.

2.1.7.3 Linear distribution flow formulation

The linear distribution flow (LinDistFlow) equations are a linear representation of the AC power flow equations applying to radial medium and low-voltage networks, which do not consider losses, but include the voltage drop across lines. The governing equations

based on [30] for a directed graph are the following:

$$\sum_{k:i\to k} P_{ik,s,t} = P_{ji,s,t} + P_{i,s,t}\ , \qquad i \in \mathcal{B},\ s \in \mathcal{S},\ t \in \mathcal{T}, \tag{2.10a}$$

$$\sum_{k:i\to k} Q_{ik,s,t} = Q_{ji,s,t} + Q_{i,s,t}\ , \qquad i \in \mathcal{B},\ s \in \mathcal{S},\ t \in \mathcal{T}, \tag{2.10b}$$

$$W_{k,s,t} = W_{i,s,t} - 2(r_{ik}P_{ik,s,t} + x_{ik}Q_{ik,s,t}), \qquad ik \in \mathcal{L}_k,\ s \in \mathcal{S},\ t \in \mathcal{T}, \tag{2.10c}$$

$$(V_i^{\max})^2 \leq W_{i,s,t} \leq (V_i^{\max})^2, \qquad i \in \mathcal{B},\ s \in \mathcal{S},\ t \in \mathcal{T}, \tag{2.10d}$$

$$|P_{ik,s,t}| + |Q_{ik,s,t}| \leq \sqrt{2}\, S_{ik}^{\max}, \qquad ik \in \mathcal{L}_k,\ s \in \mathcal{S},\ t \in \mathcal{T}, \tag{2.10e}$$

$$\left[|P_{ik,s,t}|, |Q_{ik,s,t}|\right] \leq \left[S_{ik}^{\max}, S_{ik}^{\max}\right], \qquad ik \in \mathcal{L}_k,\ s \in \mathcal{S},\ t \in \mathcal{T}. \tag{2.10f}$$

Here, i, j and k represent electric buses, where j is the unique upstream parent of bus i, and $k \in \mathcal{L}_k$ is a downstream bus of bus i. Similarly to the SOCP formulation, W_k is an auxiliary operational variable defined as the square of the voltage magnitude V_k, while r_{ik} represents the branch resistance, and x_{ik} is the branch reactance. The voltage drop across lines is integrated with (2.10c), the voltage magnitude at each bus is kept within its limits by (2.10d), while (2.10e) and (2.10f) constrain the active and reactive power flow across lines. Note that these equations do not consider losses but include line voltage drops.

2.1.8 Heating network

The considered heating network is a low-temperature district heating (LTDH) system, supplied by low-temperature waste heat (WH) from sources such as industrial processes or high-performance computers. The LTDH network transports this heat to connected buildings, where HP elevates the temperature level to meet the required indoor temperature level. All buildings receive the same inlet temperature at the evaporator side of their HP. The governing equations of the LTDH network are as follows [20]:

$$\dot{m}_{\mathrm{ltdh},s,t} = \sum_{bd\in\mathcal{B}} \dot{m}_{bd,s,t}^{\mathrm{evap}}\ , \qquad s \in \mathcal{S},\ t \in \mathcal{T}, \tag{2.11a}$$

$$\dot{Q}_{\mathrm{loss},s,t} = \left(T_{\mathrm{lthd},s,t}^{\mathrm{fl}} - T_{\mathrm{gr}}\right) \cdot h_{\mathrm{loss}} \cdot A + \left(T_{\mathrm{lthd},s,t}^{\mathrm{ret}} - T_{\mathrm{gr}}\right) \cdot h_{\mathrm{loss}} \cdot A, \qquad s \in \mathcal{S},\ t \in \mathcal{T}, \tag{2.11b}$$

$$P_{\mathrm{pump},s,t} = \frac{\Delta p \cdot \dot{m}_{\mathrm{ltdh},s,t}}{\eta_{\mathrm{pump}} \cdot \rho_{\mathrm{H_2O}}}, \qquad s \in \mathcal{S},\ t \in \mathcal{T}. \tag{2.11c}$$

Here, $\dot{m}_{\mathrm{ltdh},s,t}$ denotes the mass flow rate of the LTDH network, while $\dot{m}_{bd,s,t}^{\mathrm{evap}}$ represents the mass flow rate of the HP at the evaporator side of the respective building bd. $T_{\mathrm{ltdh},s,t}^{\mathrm{fl}}$ and $T_{\mathrm{ltdh},s,t}^{\mathrm{ret}}$ denote the flow and return temperature of the network, respectively, while T_{gr} represents the ground temperature surrounding the network pipes. The heat transfer coefficient is denoted by h_{loss}, the surface area of the pipes is represented by A, and the pressure drop of the pipe network is denoted as Δp, which are used to calculate the network losses by a heat loss correlation in (2.11b). The active power consumption of the heating network pump is denoted as $P_{\mathrm{pump},s,t}$, η_{pump} is its efficiency and $\rho_{\mathrm{H_2O}}$ is the water density.

2.1.9 Upstream power grid

The upstream power grid is connected to the local MES under investigation at the point of common coupling (PCC). It is characterised by separate feed-in and consumption limits and prices, respectively, with the following governing equations:

$$0 \leq (1 - b^{\text{cons}}_{\text{pcc},s,t}) P^{\text{feedin}}_{\text{pcc},s,t} \leq P^{\text{feedin,max}}_{\text{pcc}}, \qquad s \in \mathcal{S},\ t \in \mathcal{T}, \tag{2.12}$$

$$0 \leq b^{\text{cons}}_{\text{pcc},s,t} P^{\text{cons}}_{\text{pcc},s,t} \leq P^{\text{cons,max}}_{\text{pcc}}, \qquad s \in \mathcal{S},\ t \in \mathcal{T}. \tag{2.13}$$

Here, the binary variable $b^{\text{cons}}_{\text{pcc},s,t}$ avoids simultaneous consumption $P^{\text{cons}}_{\text{pcc},s,t}$ and feed-in $P^{\text{feedin}}_{\text{pcc},s,t}$, while the maximum values $P^{\text{cons,max}}_{\text{pcc}}$ and $P^{\text{feedin,max}}_{\text{pcc}}$ can limit the maximum respective active power flows. The price for consumption $\pi^{\text{buy}}_{\text{el},s,t}$ and the remuneration $\pi^{\text{sell}}_{\text{el},s,t}$ for feeding into the grid typically differ due to network charges or constant feed-in tariffs [31, 32]. More details on the price assumptions are presented in the data input section of each chapter.

2.2 Optimisation problem formulation

There are several optimisation methods to tackle the design and operation of energy systems under uncertainty. Robust optimisation (RO) aims to minimise the worst-case scenario of integrated predefined uncertainty sets without constraint violations, and thus its solutions are conservative and feasible [33, 34]. Chance-constrained (CC) optimisation aims to limit the probability of violating a certain constraint below a certain threshold value, i.e., its solutions allow for a specific amount of constraint violations and are therefore less conservative [35–37]. Stochastic programming (SP) is particularly suited for optimisation problems with uncertain parameters, as it allows for the consideration of multiple scenarios simultaneously to account for the uncertainty of future stages during earlier stages [38, 39]. SP can be applied to the design and operation of an energy system through a two-stage problem formulation, with the design as the first stage and the operation as the second stage [40]. The operation and its uncertain operational parameters can be integrated as multiple scenarios during the second stage, and thus SP is a suitable approach to optimise the design and operation of an energy system within one holistic problem formulation. In the following, the structure of the two-stage stochastic problem is presented.

2.2.1 Two-stage stochastic problem formulation

A two-stage stochastic problem formulation is adopted, where design decisions such as component sizing or placement are determined in the first stage, while all decisions related to the operational conditions are optimised in the second stage. In order to account for uncertainty during the operation of the energy system, different scenarios can be generated

which can integrate the uncertain nature of various parameters, e.g., demands, prices or solar irradiance. The design decisions during the first stage are subject to the operational decisions in the second stage, and likewise, the operational decisions are subject to the design decisions in the first stage [36, 40]. This problem formulation allows for investment decision-making under uncertainty, as future scenarios can be integrated and weighted within the second stage. The mathematical formulation of the two-stage stochastic problem is as follows [40]:

$$\min_{\boldsymbol{y}\in\mathcal{Y}} \boldsymbol{q}(\boldsymbol{y}) + \sum_{s\in\mathcal{S}} w_s f(\boldsymbol{y}, s) \tag{2.14a}$$

$$\text{s.t.}\, \boldsymbol{g}(\boldsymbol{y}) \leq \boldsymbol{0}, \tag{2.14b}$$

$$\boldsymbol{h}(\boldsymbol{y}) = \boldsymbol{0}, \tag{2.14c}$$

$$\text{with}\, f(\boldsymbol{y}, s) = \min_{\boldsymbol{x}_s} f(\boldsymbol{y}, \boldsymbol{x}_s) \tag{2.14d}$$

$$\text{s.t.}\, \boldsymbol{g}_s(\boldsymbol{y}, \boldsymbol{x}_s) \leq \boldsymbol{0}, \tag{2.14e}$$

$$\boldsymbol{h}_s(\boldsymbol{y}, \boldsymbol{x}_s) = \boldsymbol{0}. \tag{2.14f}$$

Here, $\boldsymbol{y} \in \mathcal{Y}$ denotes the design decision vector in the first stage, while $\boldsymbol{x}_s$ represents the operational decision vector during the second stage for each scenario s, which are associated with an occurring probability w_s, with $\sum_{s\in\mathcal{S}} w_s = 1$. The set of constraints $\boldsymbol{g}$, $\boldsymbol{h}$, $\boldsymbol{g}_s$ and $\boldsymbol{h}_s$ determine the set of feasible design and operational variables. Furthermore, the objective function of the first stage consists of the total costs of the design decisions $\boldsymbol{q}$, typically the investment costs of the system, and the expected costs of optimally operating the system $\boldsymbol{f}$, typically the total operating costs minus the total revenue [41]. While the objective function typically reflects the economic performance of the energy system, it could also incorporate other metrics, such as environmental impact, energy autonomy or loss minimisation. The two-stage stochastic approach allows for a flexible problem formulation which can be adjusted to various planning and policy goals. The detailed structure and assumptions of the objective functions are described in the corresponding sections of each chapter.

2.2.2 Time series aggregation

To reduce the computational complexity of the optimisation problem, time series aggregation is a common approach that allows for a compact and representative formulation of time-dependent input data [42–44]. One effective method to first identify and then aggregate operational data with typical representative time series is k-medoids, which has been proven to be an effective algorithm for aggregating time series data in energy systems [43]. Therefore, this work adopts the k-medoids clustering approach to identify a set of typical representative days from a full year of operational data, following the methodology adapted from [45]. These representative sets of data can be integrated within the two-stage stochastic problem formulation as scenarios during the operational stage.

In this method, the original time series is first segmented into daily profiles. The orig-

inal time series comprises different types of data, such as power demand, heat demand, solar irradiance, and several electricity market prices. Each of these time series is individually normalised to a range between zero and one. Subsequently, a weighting factor is assigned to each input variable to reflect its relative importance in the clustering process, with the total of all weights equalling one. The clustering problem is formulated as a mixed-integer linear problem (MILP), minimising the weighted sum of Euclidean distances between each original day and its assigned representative day across all data sets. This problem formulation explicitly quantifies the time series aggregation error introduced by representing the original time series with a limited number or representative days. The clustering objective value is expressed as follows:

$$\min \sum_{\epsilon=1}^{\mathcal{E}} \sum_{n=1}^{\mathcal{N}} w_\epsilon \left\| \zeta_{\epsilon,n} - \hat{\zeta}_{\epsilon,s(n)} \right\|_2, \tag{2.15}$$

where $\zeta_{\epsilon,n}$ denotes the normalised daily profile of data set ϵ on day n, $\hat{\zeta}_{\epsilon,s(n)}$ is the representative day s assigned to day n, and w_ϵ the weighting factor of data set ϵ, which are all chosen to be equal. $\mathcal{N}$ and $\mathcal{E}$ represent the total number of days in the original time series and the number of data sets, respectively. After solving the optimal time series aggregation, each day of the original data set is assigned to one representative day, resulting in a weight for each representative day. Note that a single number of representative days is used for all datasets to maintain temporal alignment and preserve interdependencies between time series. The cluster weights are then used in the energy system optimisation model to weigh each representative scenario day accordingly, with the sum of all weights equal to one.

Finding an appropriate number of representative days is typically a trade-off between modelling accuracy and computational burden. A high number of representative days yields high accuracy in representing the original time series, while a low number of representative days results in fewer variables and constraints, and thus a model that is computationally easier to solve. A useful visualisation of the accuracy of the representative days is duration curves, which arrange the values of the data set in descending order. The difference in the duration curves for each original data set can be calculated depending on the number of representative days, as depicted in Fig. 2.2 for the four sets of input data of the district-scale MES presented in Chapter 3.

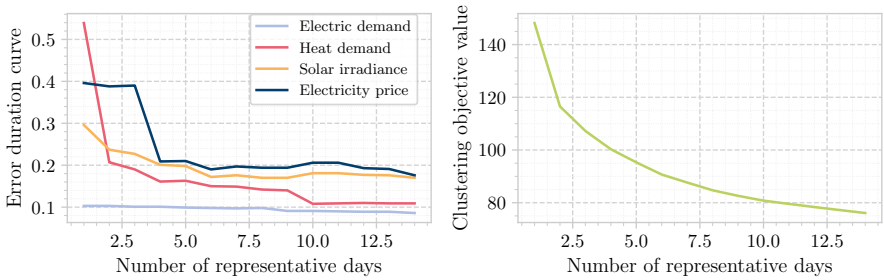

Fig. 2.2: Error duration curves (left) and objective value of k-medoids clustering optimisation (right) depending on the number of representative days for the local district case study in Chapter 3.

A significant drop in the error duration curve of the electricity price can be seen for four representative days, followed by a shallow further decline of all data sets. Due to the increased computational burden with an increasing number of representative days, four representative days are chosen. Additionally, the objective value of the clustering optimisation is presented on the right of Fig. 2.2, representing the minimal sum of all Euclidean distances of all data sets, which is decreasing with an increasing number of representative days.

Fig. 2.3 depicts the duration curves for the four input data sets: electric demand, heat demand, solar irradiance and electricity price. The non-dashed line represents the duration curve of the original data set, while the dashed line represents the duration curve of the clustered data set for four representative days. As the time series aggregation depends on the input data and the complexity of the considered problem, the input data is collected for each optimisation problem, and its time series is aggregated. This enables adaptive handling of different input data, which depends on the considered complexity of the problem. The (error) duration curves and the clustering objective value for the respective studies are depicted in Appendix C and Appendix D, respectively.

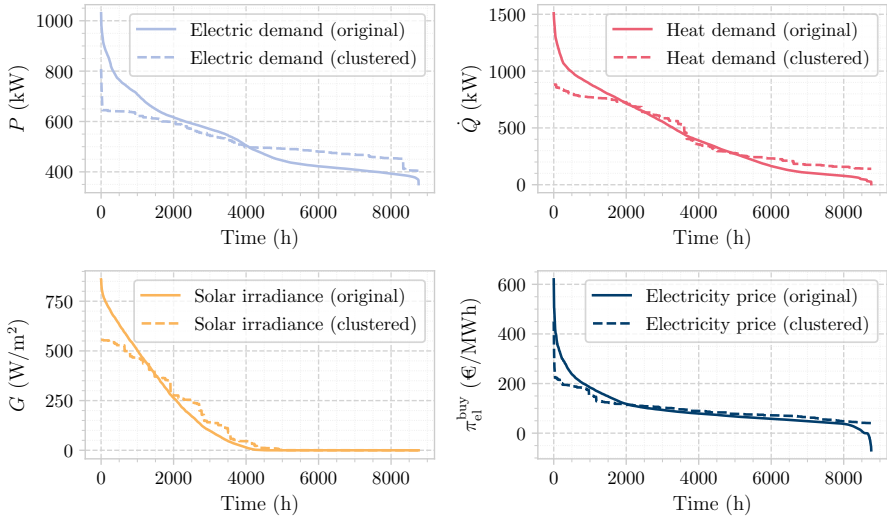

Fig. 2.3: Duration curves for the local district case study in Chapter 3 for four representative clustering days, with the non-dashed line representing the original data set, while the dashed lines depict the duration curves of the clustered data set.

2.2.3 Assumptions and justifications

This work assumes a centralised controller that controls the overall local MES and its components. Unlike local control systems that focus on individual components, a cen-

tralised coordinated control system optimises the operation of the entire MES, accounting for all integrated energy carriers and their interactions. Such a systematic approach enables the coordinated integration of distributed RES, electrical energy storage systems, and the interaction among different energy vectors.

All optimisation problems are solved on a 1.8 GHz Intel Core i7-1265U CPU with 32 GB of RAM, using Gurobi 11.0.2 [26].

CHAPTER 3

Impact of the thermal vector and component model choice on the design of battery energy storage systems

This chapter presents the optimal design and placement of a BESS within a local MES. In particular, the focus lies on the modelling choice of several MES components, specifically the internal power grid formulation, the heating network representation, as well as the HP model and the thermal building representation. Moreover, constant and time-varying electricity tariffs are investigated in terms of their impact on the optimal BESS capacity. Additionally, the computational workload of the incorporated models is investigated and applied to two case studies, a residential building and a real-world district-scale MES, for which the location and size of a community BESS are retrofitted. The presented work aims to provide valuable insights into practical modelling guidelines for MESs and their computational implications.

3.1 Introduction

Local MESs, which couple several energy sectors at a district level, are becoming more prominent as other energy carriers, such as heating or transportation, are increasingly electrified. By an integrated approach of coupled energy vectors, operating costs [46] can be reduced through exploiting synergies between energy carriers [47], e.g., surplus RES generation can heat buildings [48], or waste heat from industrial processes can supply district heating [49]. Nevertheless, design studies of one energy carrier often simplify models of the other coupled energy carriers, despite their interconnection and possible impact on each other. Therefore, this part of the work aims to answer the question of how the thermal vector and component model choices impact the optimal sizing of a BESS within a local MES.

The remainder of this section is structured as follows: Section 3.1.1 presents design

studies of local MESs and community BESSs within, followed by an outline of different methodological approaches in Section 3.1.2. A summary of the existing literature and the identified gap is presented in Section 3.1.3.

3.1.1 Design of local multi-energy systems

Significant research has been conducted regarding the optimal design and operation of local MESs. In this context, an important objective is minimising economic costs and the impact of global warming on greenhouse gas emissions. Both economic and ecological objectives have been investigated in several studies through a multi-objective optimisation aiming to minimise both objectives, e.g., for sustainable district energy systems [50], an urban multi-energy hub [51], or an MES considering residential buildings, electric mobility and industrial applications [52]. Another objective to consider for planning local MESs is reliability or resilience. In [53], an integrated energy system was planned considering resilience indicators to account for energy interruption scenarios such as the uncertainty of natural disaster occurrence or component failure. Furthermore, this study highlights the capacity of RES to limit load loss and storage systems to reduce durations of energy disruptions.

There are a significant number of studies regarding the optimal placement, sizing, and economic benefits of BESSs in local energy systems. On a local level, the adoption of a BESS is a common way to increase the self-sufficiency of LECs or a building equipped with local RES such as solar PV arrays [54, 55]. Within both single buildings and energy communities, BESSs can reduce the peak power of the electricity import and export, increase the self-consumption rate of the energy system combined with RES, and reduce annual costs [56–58]. Additionally, BESSs can mitigate over-voltages arising from extensive rooftop PV feed-in or under-voltages induced by increasing loads of electric vehicles in distribution networks [59]. Within energy communities consisting of several residential or commercial buildings with rooftop PV arrays, one central community BESS has been identified as the most promising solution to exploit the full potential of energy systems [60]. Compared to individual household BESSs, shared energy storage is beneficial in terms of electricity cost savings, energy storage utilisation and self-consumption rate compared to individual BESSs [57, 61, 62]. The optimal size of one community BESS is only two-thirds of the aggregated optimal sizes of individual household BESSs due to the common sharing of the BESS. Moreover, each kWh of the community BESS is significantly more effective at reducing exports, thus increasing the self-sufficiency of the energy community compared to individual household BESSs [63].

Identifying the optimal location of the community BESS has been the topic of several studies. The optimal placement within the power grid was studied in [64]. Its findings reveal that placing the BESS at the head of the feeder reduces grid congestion of distribution grids and is economically the optimal location. Another study found that within small distribution systems, the BESS should be placed at the same electric bus as the local

distributed energy resources (DER) generation for an overall cost minimisation [65]. From a reliability enhancement perspective, the optimal BESS location within radial distribution networks is at the end of the feeder [66].

There are several options for the operation of a shared community BESS: capacity sharing allocates a fixed capacity per user who can operate their share of the BESS independently. Another alternative involves an independent operator who invests in the shared storage and provides storage services to the users based on their requests [60]. Alternatively, an aggregator controls the entire system and coordinates the capacity allocation and the stored energy distribution according to an overarching objective, e.g., cost minimisation of the whole community. In the present work, the latter is assumed, i.e., a centralised coordinated control system that optimises the operation of the overall community, including the interaction of different energy vectors with each other. This systematic approach enables the coordinated integration of BESSs, RES and the interaction between different energy vectors.

3.1.2 Methodological approaches

Model-based optimisation is a suitable tool for the operation and planning of energy systems [67]. However, the design and operation of MES can be technically challenging due to the integration of multiple technologies and interdependent commodities. Since the design of components determines the optimal operation of a multi-energy system, energy flows between sources, conversion units, and storage options must be jointly coordinated during their design stage [4, 68]. This leads to complex optimisation problems that require detailed multi-energy models, which can be computationally expensive. To address these challenges, existing work often adopts iterative solution approaches or employs MILP models to balance model accuracy and computational tractability.

MILP models are widely used for the optimisation of both design and operation of distributed MESs within a single holistic problem formulation [69, 70]. In these models, nonlinear behaviour of energy components, such as the power grid or heating network, is linearised. This linearisation approach is applied across various studies, including seasonal storage systems [71, 72], large-scale transmission and investment planning [73, 74], and the representation of an MES as an energy hub that models the conversion of different energy carriers as multiple input multiple output components [75]. For instance, this concept is used in the optimal capacity design and operation of islanded energy hubs integrating electricity, heat, gas and hydrogen [76]. The study employs chance-constrained optimisation and robust counterpart formulations to incorporate stochastic RES generation and load uncertainty while balancing robustness and cost efficiency. Both gas and electrical networks are explicitly modelled, with the electrical network represented via the linear DC power flow approximation. While this approximation is accurate for high-voltage networks, it is not valid for medium- and low-voltage networks. Similarly, [77] presents a MILP formulation combined with energy hubs for the integrated design and operation of

DER and optimal heating network layouts. While these approaches offer valuable insights into the optimal design and operation of energy hubs, they often overlook BESS sizing and rely on linearisations of physical component and network behaviours. However, neglecting nonlinear effects or power grid losses may lead to suboptimal design choices. In another study, [78] investigates the optimal design and operation of PV-battery systems that are coupled with HPs. Their MILP model highlights the impact of increased HP penetration on the returns of PV-battery systems, but does not consider the electrical or heating network explicitly.

Another option to mitigate the computational burden of modelling local MESs that include energy networks is an iterative optimisation approach [79, 80]. These approaches typically employ an iterative two-stage process: in the first stage, a linear operational optimisation of the components without energy networks is performed. Based on the output of the first stage, the second stage then simulates the nonlinear operation of the energy networks and identifies power losses and possible network constraint violations. Subsequently, these deviations are linearised and incorporated into the next iteration of the linear optimisation model. This process is repeated until the violation error has fallen below a predefined convergence threshold. Several studies have employed iterative methods for the operational optimisation of MESs integrating electricity, heat and gas networks [79, 81]. However, these approaches either assume linear behaviour of networks and components, or focus exclusively on the system operation, while neglecting component sizing.

3.1.3 Summary

The presented literature shows the benefits of a shared community BESS within local energy systems. However, due to the computational complexity associated with detailed models, simplified models are frequently employed due to their computational benefits and faster computation times. Depending on the main focus of the study, the models of other energy sectors are often simplified or neglected. In MESs comprising electricity and heat, the thermal vector is often completely disregarded, or only included within so-called *all-electric* demands, which implicitly considers the electricity consumption of the heating sector [82, 83]. Nevertheless, with the increasing adoption of electric HPs, the thermal vector plays a more prominent role in the power system, and thus is crucial for investment decisions in the electrical system. Therefore, Chapter 3 investigates the impact of the modelling choice of several MES components on the electrical storage design. More specifically, this chapter analyses how different levels of modelling details impact the decision-making at the planning stage and the computational workload of solving the problem, with a specific focus on the coupled thermal vector and the power grid formulation. The optimal placement and sizing of a community BESS are retrofitted for a real-world district-scale MES, considering the commodities of electricity and heat. This chapter aims to provide valuable insights into practical modelling guidelines for MESs and their computational implications.

The remainder of this chapter is structured as follows: Section 3.2 presents the methodology, followed by outlining the two case studies in Section 3.3, namely an individual building and a local MES. Section 3.4 presents the impact of explicitly considering the thermal demand on the optimal BESS capacity, and further investigates how different modelling choices of the HP, the power grid and the heating network influence the location and placement of a community BESS. Finally, a summary in Section 3.5 concludes this chapter.

3.2 Objective function

In this section, the objective function for this analysis is presented, as well as the calculation of the global warming impact (GWI), which is analysed within this chapter as well. Note that the presented component models, as described in Section 2.1, are investigated regarding the optimal BESS design and their implications on the computational workload.

3.2.1 Design and operational objective

This study aims to determine the cost-optimal capacity of a BESS for an existing MES. The optimisation is conducted by minimising the total annualised cost (TAC) of the MES, which is incorporated as follows:

$$\mathrm{TAC} = C^{\mathrm{inv}} + C^{\mathrm{fix}} + C^{\mathrm{var}}, \tag{3.1}$$

where C^{inv} represents the investment costs, C^{fix} denotes the fixed costs including maintenance, and C^{var} represents the variable operating costs. Note that for both case studies, all the components, i.e., PV arrays, heat pumps, thermal energy storage, power grid and heating network, are already installed, except the BESS. Therefore, only the investment cost for the BESS is included in the optimisation objective at the design stage, yielding the following objective function:

$$\min \left\{ \left(C^{\mathrm{inv}}_{\mathrm{bess}} \cdot k^{\mathrm{ann}}_{\mathrm{bess}} + \pi^{\mathrm{fix}}_{\mathrm{bess}} \cdot C^{\mathrm{inv}}_{\mathrm{bess}} \right) + \sum_{s \in \mathcal{S}} w_s \sum_{t \in \mathcal{T}} \pi^{\mathrm{var}}_{s,t} \cdot o_{s,t} \cdot \Delta\tau \right\}, \tag{3.2a}$$

$$\text{with} \quad k^{\mathrm{ann}} = \frac{(1+r)^n \cdot r}{(1+r)^n - 1}. \tag{3.2b}$$

Here, the overall investment cost $C^{\mathrm{inv}}_{\mathrm{bess}}$, the annual fixed cost $\pi^{\mathrm{fix}}_{\mathrm{bess}}$ as a relative percentage of the investment cost, and the variable operating cost $\pi^{\mathrm{var}}_{s,t}$ are considered. $o_{s,t}$ represents the value of an operational quantity with associated cost, e.g., electricity or heat, for a scenario day s and time step t. w_s represents the weight accounting for the number of days assigned to each representative scenario day, Δt represents the chosen time step duration in hours, and f_{ann} is the annuity factor of approximately 0.103 per year, consider-

ing a lifetime n of 12 years and an interest rate i of 6 %. Note that the investment cost for small-scale BESS is higher than for large-scale ones. More details on the price assumptions are listed in Section 3.3.3.

3.2.2 Global warming impact

The GWI quantifies the contribution to climate change by aggregating the greenhouse gas emissions, typically expressed in CO_2-equivalents [84]. It includes the emitted greenhouse gases from the BESS capacity production and the consumed electricity from the upstream grid. Note that the GWI is not directly included within the objective, but it is further calculated to assess the impact of the expected annual GWI. The expected annual GWI is included within this study as follows:

$$\mathrm{GWI} = \sum_{s \in \mathcal{S}} w_s \sum_{t \in \mathcal{T}} \mathrm{GWI}^{\mathrm{el}}_{s,t} \Delta t + \mathrm{GWI}_{\mathrm{bess}} \frac{C^{\mathrm{des}}_{\mathrm{bess}}}{n_{\mathrm{bess}}}. \tag{3.3}$$

Here, $\mathrm{GWI}^{\mathrm{el}}_{s,t}$ is the hourly average GWI of the external power grid and $\mathrm{GWI}_{\mathrm{bess}}$ represents the GWI per capacity of the installed BESS size $C^{\mathrm{des}}_{\mathrm{bess}}$ over its lifetime n_{bess}.

3.3 Case studies

In this section, two case studies are introduced: a single building and a district-scale MES. Each case study is modelled both as a multi-energy system and as an *all-electric* system, with the latter serving as a benchmark approach for comparison. Finally, the input data used for both two case studies is presented. Both case studies consider an existing energy system for which a BESS is to be retrofitted. Therefore, only the investment cost of the BESS is considered. A perfect energy management system is assumed, which can centrally control the optimal operation of the MES.

3.3.1 Single building

The single building case study represents an office building and considers two modelling approaches: the multi-energy building model and the *all-electric* building model, as depicted in Fig. 3.1. The multi-energy model incorporates the HD and the TES, and allows for flexible operation of the thermal vector. The TES in the multi-energy model represents a lumped parameter that combines both the HWS and the thermal inertia of the building dwellings. The HP can be modelled using a detailed non-convex formulation, a linear representation with part-load constraint, or a linear model without part-load considerations, as described in Section 2.1.4. The HP output supplies the TES, which in turn supplies the

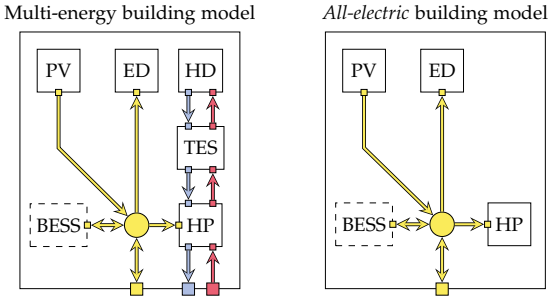

Fig. 3.1: Internal structure of the multi-energy and *all-electric* building models: The system includes solar photovoltaic (PV) array, electric demand (ED), heat demand (HD), thermal energy storage (TES), heat pump (HP), and a battery energy storage system (BESS) which is to be sized and installed. Electricity flows are depicted in yellow, hot water in red and cold water in blue. Arrows indicate the direction of energy carrier flows.

HD of the building. The building has an external connection to both the power grid and the district heating network.

In contrast, the *all-electric* model represents the thermal vector solely from an electrical perspective, i.e., the heating demand is directly converted into a fixed electric load profile for the HP, and any operational flexibility of heating components is neglected. The key distinction between the two models lies in the active power consumption of the HP: it is an operational variable in the multi-energy model, and a fixed parameter for the *all-electric* model directly determined by the HD.

Both models comprise an electricity balancing node that ensures electricity demand from the electric demand (ED) and the HP is met by the solar PV array, the BESS and the power grid. While active and reactive power are balanced independently within the building, the yellow energy carrier flows in Fig. 3.1 represent electricity without distinguishing between active and reactive power. The solar PV array can generate active power, and consume or inject reactive power. Note that this modelling framework can be adapted to any building type or component configuration.

3.3.2 District-scale multi-energy system

The second case study represents a real-world district-scale MES which is located at Forschungszentrum Jülich in Germany. The system comprises the commodities electricity and heat. Fig. 3.2 provides a schematic representation of the case study, including the single-phase diagram of the internal power grid and its integration with the district heating network. The district-scale MES is connected to the external power grid at the 110 kV level. The voltage is transformed to 35 kV and subsequently to 10 kV, from where it is distributed to two bus bars. Each bus bar supplies one feeder with several buildings. A single shared community BESS is to be sized and installed at the electric bus of one of the seven buildings, which include office and laboratory buildings. These buildings are

connected to the internal grid at 400 V via transformers, with buildings two (Bd2) and three (Bd3) sharing a common bus at 10 kV. Additionally, a large-scale solar PV array is connected directly to the upper bus bar.

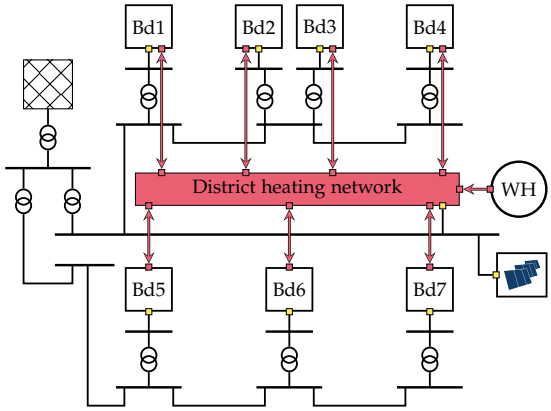

Fig. 3.2: District-scale energy system comprising seven buildings (Bd), which are interconnected via an internal power grid and a low-temperature district heating network supplied by waste heat (WH). Each building is equipped with a rooftop solar PV array.

Similarly to the single building case, the district case study is represented as a multi-energy district model, and as an *all-electric* district model. For the multi-energy model, each building is represented by the multi-energy building model introduced earlier in Fig. 3.1. All buildings are connected to a LTDH network that is supplied by WH from a high-performance computing facility. The evaporator mass flow of the HP in each building is connected to the district heating network, enabling the exchange of warm and cold water with the network.

The active and reactive power at each electrical bus is determined by the aggregated active and reactive power consumption and generation of the connected building. In particular, active power is determined by the sum of the active power consumption of the ED and the HP, and the power generation or consumption of the BESS and the solar PV array. The ED is implemented as a fixed time series, while the active power of the HP, the solar PV array and the BESS are operational variables determined within the optimisation. The same approach is applied to reactive power. The reactive power consumption of the ED is based on a constant power factor. In contrast, the reactive power contributions of the HP, the BESS and the solar PV array are optimisation variables that determine the overall reactive power at each bus.

In the *all-electric* district model, only the electricity domain is considered, while the thermal vector is integrated from an electrical perspective. All buildings are represented using the *all-electric* building model depicted in Fig. 3.1, while the LTDH network and the WH are omitted. The HD is implicitly integrated through the electrical consumption of the HPs, which is included as a fixed deterministic time series from the HD profile.

3.3.3 Input data

The representative scenario days for ED, HD, solar PV irradiance, ambient temperature and electricity price are derived from historical data. PV irradiance time series were generated for the location of Jülich, Germany, based on [85]. Electrical and heat demand profiles are based on measurement data collected at Forschungszentrum Jülich. Following the methodology time-series aggregation and k-medoids clustering as described in Section 2.2.2, representative scenario days are identified, alongside their respective weight representing the number or days assigned to the cluster. For the single-building case study, six representative days are used, whereas four representative days are selected for the district-scale case study, both with a time step length of one hour. The weights of the representative scenario days are given in Tab. 3.1.

To ensure that no energy can be transferred between representative scenario days, the state of charge (SoC) of the BESS and the indoor building temperature are constrained to be equal at the first and last time step of each representative day, while the specific values can be varied for each day. Both case studies evaluate a time-varying and a constant electricity price tariff. The time-varying tariff incentivises load shifting towards off-peak periods with lower electricity prices, which can lead to peak shaving and economic benefits for buildings with batteries [86]. The constant tariff is set to the mean of the time-varying price. The input parameters for the BESS, the solar PV data and the electricity tariff values are listed in Tab. 3.2.

The seven buildings in the district-scale MES vary in size and construction year (1960 - 2011), with thermal storage capacity ranging from 100 kWh/°C to 600 kWh/°C, depending on building mass and material. The buildings are divided into two groups with design supply temperatures of 85 °C and 70 °C, which are corresponding to the temperature requirements for an ambient temperature of −12 °C. These temperatures are implemented as the condenser output temperature of the respective HP.

BESS maintenance is incorporated as a fixed annual cost of $c_{\text{bess,fix}} = 2.5\,\%$ of the annualised investment cost [87], with the investment cost for the BESS being based on [88]. The data for the GWI emissions of the external power grid is based on licensed data from the ecoinvent database 3.9.1 as implemented in [89]. The data for the GWI emissions of the BESS production is based on the lifecycle assessment of a rechargeable, prismatic LiMn2O4 lithium-ion battery [90].

Tab. 3.1: Weights of the representative days for the building-scale multi-energy system (MES) and the district-scale MES.

Building-scale MES	Day	4	48	174	223	231	319
	Weight	37	69	60	93	64	42
District-scale MES	Day	48	180	231	317	-	-
	Weight	84	152	62	67	-	-

Tab. 3.2: Key input parameters for the considered components.

Component	Description	Parameter	Value
PV	High irradiance year	capacity factor	15.2 %
PV	Medium irradiance year	capacity factor	14.0 %
PV	Low irradiance year	capacity factor	12.6 %
BESS	charging efficiency	$\eta_{\text{bess}}^{\text{in}}$	95 %
BESS	discharging efficiency	$\eta_{\text{bess}}^{\text{out}}$	95 %
BESS	self-discharge rate	τ_{bess}	0.5 %/h
BESS	maintenance coefficient	c_{fix}	2.5 %
BESS (large-scale)	Investment cost	$C_{\text{bess}}^{\text{inv}}$	457 €/kWh
BESS (small-scale)	Investment cost	$C_{\text{bess}}^{\text{inv}}$	700 €/kWh
Grid	Average time-varying tariff	$\overline{\pi}_{s,t}^{\text{buy}}$	29.78 ct/kWh
Grid	Feed-in tariff	$\pi_{s,t}^{\text{sell}}$	5 ct/kWh

3.4 Results

In this section, the results for both case studies are presented. Section 3.4.1 presents the findings for a single building, focusing on the operational results of the multi-energy building compared to the *all-electric* model, which implicitly considers a non-flexible electricity consumption of the thermal vector. Moreover, the impact of the modelling detail of the thermal vector is investigated, and a constant electricity tariff is compared to a time-varying tariff. Subsequently, Section 3.4.2 presents the results for the local MES, focusing similarly on the comparison between constant and time-varying tariffs, as well as the representation of electrical and thermal networks, the impact of the solar irradiance and the computational implications of different modelling choices. Finally, Section 3.5 summarises the chapter.

3.4.1 Case study I: Single building

3.4.1.1 Design results for electricity tariffs and building models

The BESS sizing results for the single-building case study are presented in Tab. 3.3, comparing the multi-energy and the *all-electric* models. For the time-varying electricity tariff, the optimal BESS capacity is significantly larger for the *all-electric* building (52.4 kWh) than for the multi-energy model (33.7 kWh). For the constant electricity tariff, the optimal BESS capacities for both models are substantially reduced due to a lack of economic incentives for load shifting from price differences. However, the *all-electric* building model results in a larger BESS capacity compared to the multi-energy model.

The reduction in BESS capacity for the multi-energy model, particularly for the time-varying tariff, can be attributed to the integration of the TES, which is coupled to the electrical system via the HP. The thermal inertia of the building, represented by the TES, provides additional flexibility that can replace part of the electrical flexibility otherwise

Tab. 3.3: Optimal BESS capacity, total annualised cost (TAC) and global warming impact (GWI) emissions for both the *all-electric* and the multi-energy building models, for both time-varying and constant electricity price tariffs, respectively.

Electricity tariff	Building model	BESS capacity	TAC	GWI
Time-varying	Multi-energy	33.7 kWh	16.4 k€/a	30.0 t_{CO_2}/a
	All-electric	52.4 kWh	18.6 k€/a	31.0 t_{CO_2}/a
Constant	Multi-energy	2.5 kWh	17.2 k€/a	35.2 t_{CO_2}/a
	All-electric	5.5 kWh	19.6 k€/a	38.9 t_{CO_2}/a

offered by the BESS. Consequently, the integrated MES relies less on electrical flexibility, resulting in a smaller BESS capacity.

The TAC of the multi-energy model is 13.4 % to 14.0 % lower than that of the *all-electric* building model. This highlights the economic benefits of explicitly modelling the operational flexibility of the thermal vector. Moreover, the TAC for the constant electricity tariff increases by 4.9 % to 5.4 % compared to the corresponding case of the time-varying tariff. These overall cost increases highlight the inability to capitalise on time-varying tariffs and benefit from shifting demand to low-price periods.

3.4.1.2 Operational results for building models

The operational schedule for the *all-electric* building is depicted in Fig. 3.3a and for the multi-energy building in Fig. 3.3b. Positive values represent consumption, while negative values denote generation. Active power is depicted with the SoC of the BESS, and for the multi-energy building model, heat is depicted with the indoor temperature of the building.

It is evident from the top part of Fig. 3.3a that the heat output of the HP directly follows the heat demand, which creates a deterministic active power profile of the HP for the *all-electric* model in the bottom part of the figure. Charging the BESS corresponds to active power consumption and thus positive values, while BESS discharging represents an internal power generation and thus negative active power values. The BESS is fully charged and discharged at least once during each day, taking advantage of the price fluctuations during each representative day and the electricity generation of the solar PV array. The BESS is typically charged during periods of low electricity prices or high solar irradiance hours and discharged during periods of high electricity prices to maximise energy arbitrage.

For the multi-energy building shown in Fig. 3.3b, a notable difference can be observed in the operation of the HPs. Rather than directly following the heat demand, the HP primarily operate during periods of low electricity prices and high solar irradiation. By charging the TESs during these hours, the HP leverages the thermal inertia of the buildings by heating before high-price periods as indicated by the increasing building temperature, and thus reducing the need for heating during high-priced periods. This pattern of heating during high-solar irradiance and exploiting the thermal storage during evening hours is particularly evident on the representative days 174, 223 and 231, which represent warmer months with low heat demand and high solar availability. Moreover, the HP mainly operates at full load as its efficiency increases with a greater load utilisation. While the BESS

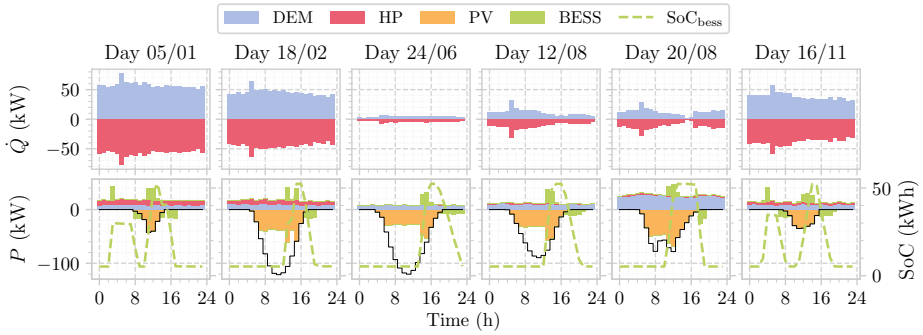

(a) *All-electric* building model

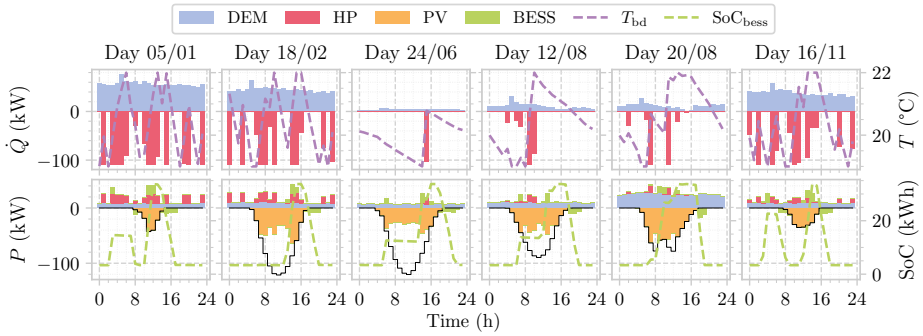

(b) Multi-energy building model

Fig. 3.3: Operational results of heat (top) and active power (bottom) for a time-varying electricity tariff. Positive values represent demand, while negative values represent generation. For conciseness, electric demand (ED) and heat demand (HD) are referred to as demand (DEM).

for the multi-energy building model is significantly smaller than for the *all-electric* model, its operating pattern remains similar. This suggests that the key driver behind the larger BESS capacity in the *all-electric* building model is the lack of thermal flexibility. By explicitly modelling the heating system and integrating the flexibility offered by the TES in the multi-energy building, investing in additional electrical flexibility by a large BESS capacity is not required. Instead, the thermal domain provides substantial flexibility, which can be effectively exploited by considering the coupling between electricity and heat.

3.4.1.3 Impact of thermal modelling detail and electricity tariff

The impact of using different HP models as well as the impact of considering the thermal vector on the optimal BESS capacity are depicted in Fig. 3.4. Note that the 'detailed HP model' refers to the previous multi-energy model incorporating the detailed non-convex quadratic model, while the 'all-electric demand' refers to the *all-electric* building model.

The difference in BESS size between the detailed HP model and the linear model is marginal for the time-varying tariff, with a change in BESS size from 33.7 kWh to 30.9 kWh as depicted in Fig. 3.4a. Simplifying the HP model further by omitting the minimum part-

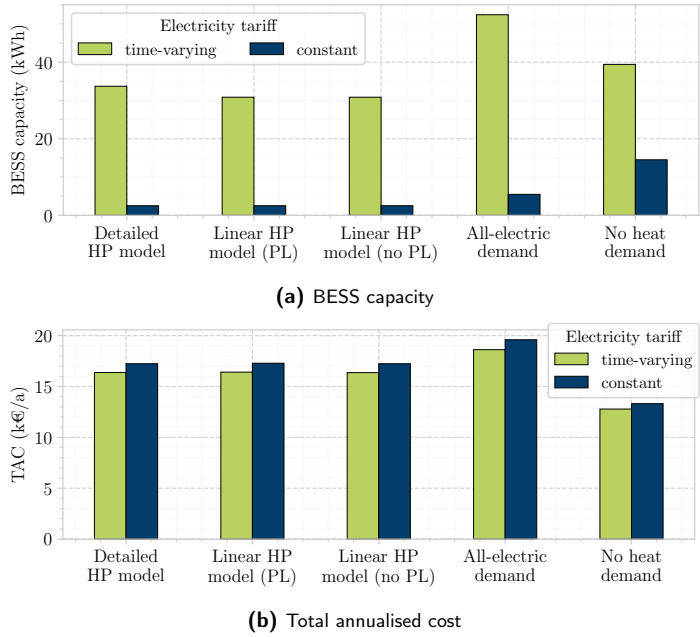

(a) BESS capacity

(b) Total annualised cost

Fig. 3.4: BESS capacities (top) and TAC (bottom) for the detailed HP model, the linear HP model with minimum part-load (PL) limit, the linear HP model without PL limit, for the *all-electric* demand model, and without considering heat demand, for both time-varying and constant electricity tariff, respectively.

load limit results in identical BESS capacities for both tariffs. For the presented local MES, the level of detail in the HP model does not significantly impact the BESS size. However, in case studies featuring an overloaded or unbalanced power grid, precise HP modelling could affect BESS sizing, which could specifically be utilised to mitigate peak loads and thus not overload electrical lines or transformers. Nevertheless, as described above in Section 3.4.1.2, neglecting the thermal building flexibility by modelling an *all-electric* demand results in a significantly BESS oversizing to compensate for the lack of thermal flexibility.

Moreover, Fig. 3.4b depicts the TAC for the different HP and thermal building models for both electricity tariffs. The constant tariff leads to a TAC increase by 3.9 % – 6.1 %. For the three HP models, the TAC remain within a range of 0.3 %, indicating that the varying efficiency of the detailed HP through its COP is negligible in terms of overall costs for the presented local MES. Moreover, the inflexible *all-electric* demand significantly increases the expected TAC by around 13 % for both electricity tariffs, respectively. Finally, it is evident that completely ignoring the heating sector by not modelling any heat demand or electricity consumption of the HP results in unrealistically low TAC.

The presented findings indicate that the heating sector and its accompanying thermal inertia must be considered for electrical storage design within an individual building. While the different HP models only slightly impact the BESS sizing and annualised cost estimation, the explicit modelling of the thermal inertia has the biggest impact on BESS size and overall costs, and thus should be included in design studies within local MESs.

3.4.2 Case study II: District-scale multi-energy system

In this section, the results for the design of the community BESS within the district-scale MES are analysed. First, Section 3.4.2.1 presents the design and operational results depending on the chosen electricity tariff and building model. Second, Section 3.4.2.3 investigates the impact of the power grid formulation and heating network inclusion on the optimal community BESS design. Third, the impact of different solar irradiation years is analysed in Section 3.4.2.2. Finally, Section 3.4.2.4 analyses the impact of the different component models on the computational performance of the optimisation problems.

3.4.2.1 Design and operation

For the local district-scale energy system, both the multi-energy model and the *all-electric* model for the thermal building representation were implemented, similarly to the individual building. Here, the multi-energy model further includes the explicit modelling of the heating network, and the SOCP formulation for the internal power grid. The shared community BESS is to be sized and located at the electric bus of one of the seven buildings. The optimal size and location of the BESS, as well as the corresponding TAC and GWI, are listed for both electricity tariffs in Tab. 3.4.

Similarly to the building case study, the *all-electric* community BESS is oversized by 81.8 % compared to the multi-energy model for the time-varying electricity tariff. For the constant electricity tariff, the BESS capacity for the *all-electric* model is oversized by 68.9 % compared to the *all-electric* district model. These results show that the explicit consideration of the heating sector coupled with the electricity sector significantly impacts the BESS design capacity. The modelled TESs enable a more flexible HP operation, which directly impacts the electricity sector and the BESS sizing. The optimal location of the community BESS for the all-electric models is located at building 6 for the time-varying and building 2 for the constant electricity price, respectively. Without thermal storage, the community BESS is primarily located to shave local demand peaks, which are most dominant in building 6, as it can be seen in Tab. A.2. By placing the BESS at the bus bar of the building with the highest fluctuation and peaks in electric demand, the peaks are smoothed with minimal losses, particularly during high price periods. In the absence of price-demand shifting incentives, the location is rather chosen by physical network factors such as minimising load losses or maintaining voltage magnitudes, resulting in the bus bar at building 2 for

Tab. 3.4: Optimal building (Bd) bus bar location and size of the community BESS, total annualised cost (TAC) and global warming impact (GWI) for both the multi-energy and *all-electric* district models, as well as for the time-varying and constant electricity price tariffs, respectively.

Tariff	District model	Location	BESS size	TAC	GWI
Time-varying	Multi-energy	Bd 5	346 kWh	308.6 k€/a	443.5 t_{CO_2}/a
	All-electric	Bd 6	629 kWh	341.4 k€/a	472.1 t_{CO_2}/a
Constant	Multi-energy	Bd 5	302 kWh	311.0 k€/a	445.0 t_{CO_2}/a
	All-electric	Bd 2	510 kWh	345.6 k€/a	479.2 t_{CO_2}/a

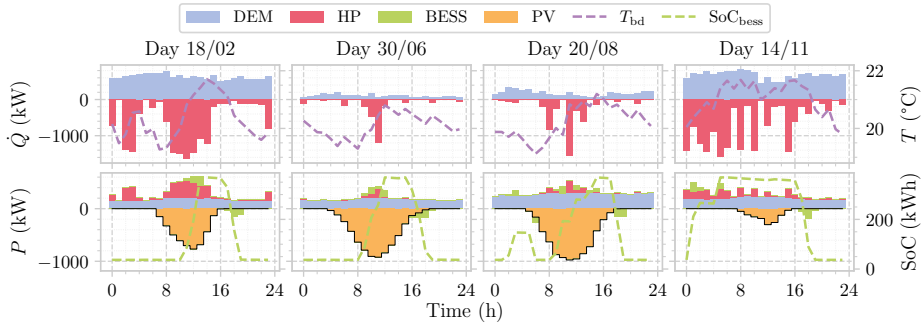

(a) Time-varying electricity tariff

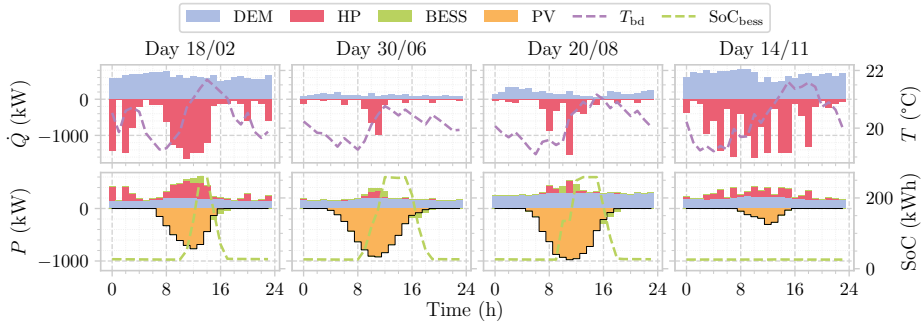

(b) Constant electricity tariff

Fig. 3.5: Operational results of heat (top) and active power (bottom) for the multi-energy district model. The values for demand (ED and HD), solar PV generation and indoor temperatures are aggregated from all buildings within the district-scale MES.

the constant electricity tariff. For the multi-energy model, the strategic location at the head of the feeder at the bus bar of building 5 enables the community BESS to control the voltage magnitudes of the whole downstream feeder and minimise losses more effectively. Moreover, the TAC for the *all-electric* district model is between 10.6 % and 11.1 % higher than for the multi-energy model, despite excluding the operational cost of the LTDH network in the *all-electric* case. Additionally, the annual GWI of the district-scale MES increases by 7.6 % – 10.1 % when the heating sector coupled to the electrical system is not explicitly modelled.

The operational results of the multi-energy district system are presented in Fig. 3.5a for the time-varying electricity tariff, and in Fig. 3.5b for the constant tariff. Apart from the community BESS, the depicted values are aggregated across all buildings. In both modelling approaches, the HPs operate in a way that leverages the thermal inertia of the buildings, following a similar pattern. A notable difference between the electricity tariffs is evident for day 14/11, which represents a typical winter day with high heat demand and low solar PV generation. For the time-varying electricity tariff, the BESS charges in the morning when electricity prices are low, and discharges during the early evening hours when prices peak. In contrast, for the constant electricity tariff, the BESS remains at its

lower SoC limit as there is no financial incentive for load shifting, and the solar PV generation directly supplies parts of the ED.

3.4.2.2 Impact of solar irradiance

The influence of different solar irradiance years on BESS sizing is presented in Fig. 3.6. For all cases, the same input data is used, except for the variation in solar irradiance profiles. Regardless of the selected modelling approach or electricity tariff, lower solar irradiance results in smaller optimal BESS capacities, whereas higher irradiance levels lead to larger BESS capacities. In years with high solar irradiance, the increased electricity generation from solar PV arrays incentivises investment in larger BESS, enabling energy storage during surplus generation periods and discharge during times of low solar irradiance or high electricity prices. Across all three solar irradiance scenarios, the multi-energy models consistently result in smaller BESS capacities compared to their *all-electric* counterpart for the same tariff. This again highlights the additional flexibility provided by the integrated modelling of the thermal system. Furthermore, the bottom row of Fig. 3.6 indicates that the contribution of the BESS to the annual GWI is negligible compared to that of the external power grid import. The overall GWI decreases with higher solar irradiance levels, as the additional power generated by solar PV with low CO_2 emissions replaces the higher CO_2 emissions of the external power grid.

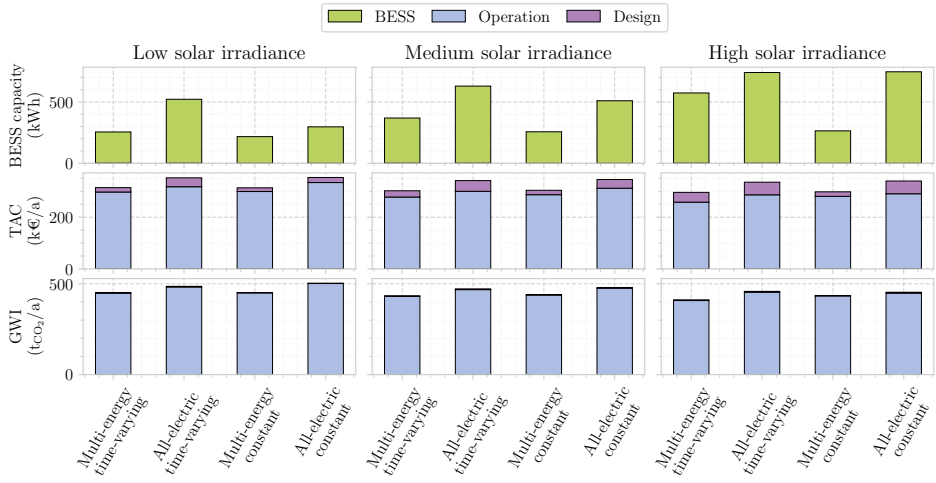

Fig. 3.6: BESS capacity (top), total annualised cost (TAC) (middle) and annual global warming impact (GWI) emissions (bottom) for the multi-energy *all-electric* models, as well as for time-varying and constant electricity tariffs for the district-scale MES.

The results show that higher solar irradiance levels lead to larger BESS capacities, reduced TAC, and lower annual GWI. This is especially the case for the *all-electric* model, which lacks thermal storage and thus relies entirely on the BESS to store excess PV energy. For the high solar irradiance year, this results in large BESS capacities for both electricity tariffs. For the low solar irradiance year, surplus PV generation is limited, which reduces

the opportunity and the economic value of electrical storage. The role of the BESS shifts towards energy arbitrage, charging during hours of low electricity prices and discharging during high-price hours. Therefore, the difference in BESS sizing between time-varying and constant tariffs is more pronounced for low solar irradiance years, which aligns with existing literature [91]. Conversely, in high solar irradiance years, both electricity tariffs result in similar BESS capacities for the *all-electric* model. While the time-varying tariff still deploys energy arbitrage, it plays a secondary role, as the main driver for BESS sizing becomes storing excess PV energy.

For the multi-energy building, the need for electrical storage is significantly lower than for the *all-electric* demand due to the availability of thermal storage. As solar irradiance increases, the difference in BESS capacity between electricity tariffs becomes more significant. While the time-varying tariff enables additional revenue through energy arbitrage, which outweighs the higher investment cost of the BESS, the constant tariff solely offers PV self-consumption, which is economically not sufficient to justify a larger BESS investment. These findings highlight that besides electricity tariffs and thermal building model, the economic value and the sizing of the BESS are significantly impacted by solar availability, and thus various solar irradiance years should be considered during the design stage of electrical storage systems.

3.4.2.3 Impact of internal network representation

In this section, the representation of both the internal power grid and the heating network is analysed in terms of optimal BESS sizing. Fig. 3.7 depicts the optimal BESS capacities for the three implemented internal power grid representations. While the light-blue bars represent the model with the explicit modelling of the district heating network (with the detailed HP model), the remaining models assume an energy balance vector for the heating network while adjusting the HP model.

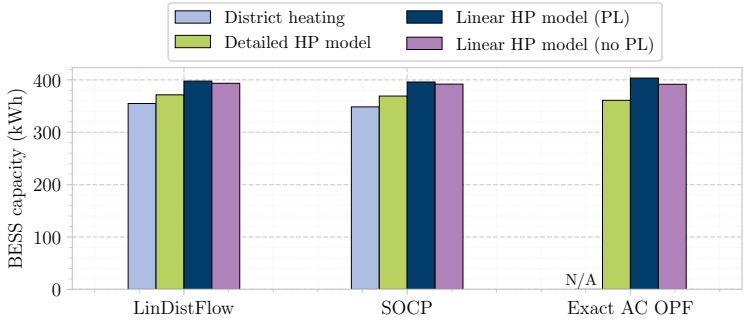

Fig. 3.7: Optimal BESS capacities for three power grid representations: linear distribution flow (LinDistFlow), convex second-order cone program (SOCP) approximation, and exact AC optimal power flow (OPF) formulation.

It can be seen that the BESS capacities are very similar for both LinDistFlow and for SOCP. When explicitly modelling the district heating network, the optimal BESS size is

slightly smaller than deploying only the detailed HP model. This can be explained by the thermal and operational constraints of the heating network, which may limit the flexible operation of the connected HPs in response to time-varying prices. Additionally, the electricity consumption of the electric pump in the district heating network is relatively constant. The inflexible additional electricity consumption combined with the reduced thermal volatility introduced by internal heating network constraints, reduces the requirement and economic benefit of a larger BESS. Therefore, both LinDistFlow and SOCP result in slightly smaller community BESS when explicitly modelling the district heating network.

The modelling choice of the HP model also impacts the optimal BESS size. When simplifying the detailed model with a linear HP model including a minimum part-load constraint, the BESS capacity increases by around 7 %. This can be attributed to the assumed fixed COP, which differs from the variable COP of the detailed HP model. Depending on the load, the fixed COP under- or overestimates the efficiency and thus the electricity consumption of the HPs. Removing the minimum part-load limit results in a slight reduction in BESS capacity. While it can be seen that the detailed HP model affects the optimal BESS capacity, its impact is not significant when compared to general uncertainty within design studies, e.g., thermal and electric demand profiles, or specific user behaviour.

Moreover, for both linear HP models and the detailed model, the exact AC OPF equations result in almost identical BESS sizes. However, the difficulty in finding a solution for a large non-convex problem formulation is evident in the explicit modelling of the district heating network in combination with the exact AC OPF formulation. No feasible solution is found within five days of computation, highlighting the challenges of non-convex problems. More information on the computational time and tractability of the different formulations is presented in the following in Section 3.4.2.4.

3.4.2.4 Computational assessment

In this section, the computational workload of the deployed models is assessed for both heating and electrical networks, and the heat pump representation.

Power grid and heating network

Fig. 3.8 depicts the computational time and the corresponding optimality gap for the three different power grid formulations. Note that the computational time is on a logarithmic axis, with the scales between Fig. 3.8a and Fig. 3.8b being different. Fig. 3.8a represents the energy balance model for the heating network. It can be seen that the global optimality for the AC OPF formulation can not be proven due to its non-convexity, evident by its optimality gap of 41 % after three days. The linear LinDistFlow formulation reaches the optimality gap of 0.01 % the quickest, while the SOCP formulation finds the optimal solution within three minutes. These findings show that both LinDistFlow and SOCP present suitable alternatives for closely representing the physical grid while maintaining computational tractability. As the LinDistFlow neglects power losses, the SOCP is more suited if the computational workload allows.

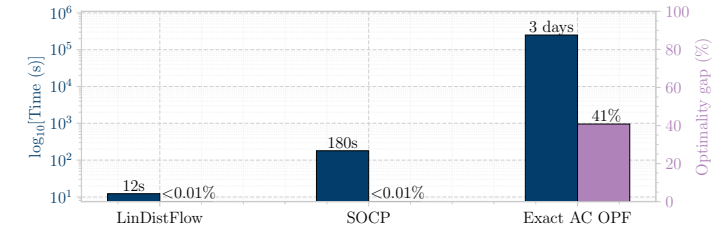

(a) No explicit modelling of district heating network (energy balance).

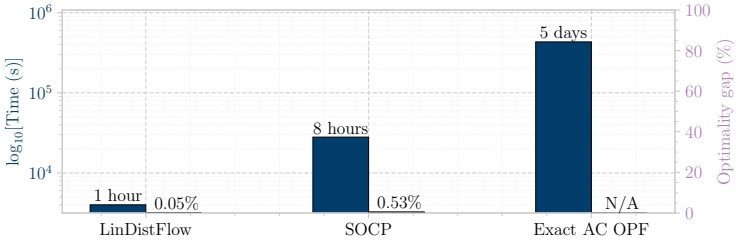

(b) Explicit modelling of district heating network.

Fig. 3.8: Computational time and optimality gap for three power grid representations: linear distribution flow (LinDistFlow), convex second-order cone program (SOCP) relaxation, and exact AC optimal power flow (OPF) formulation. The detailed HP model, the multi-energy building demand model and the time-varying tariff are deployed.

Conversely, Fig. 3.8b shows the explicit modelling of the district heating model. The non-convex formulation of the heating network adds computational complexity to all models, with the LinDistFlow and SOCP not reaching the optimality gap within several hours. Note that the optimisation problems for both LinDistFlow and SOCP were performed for five days, but no significant decrease in the optimality gap was achieved after one hour and eight hours, respectively. Moreover, the combination of a non-convex heating network with an exact, non-convex AC OPF poses significant computational challenges, as no solution was found within five days.

Heat pump representation

The computational impact of employing different HP models is investigated in the following. The SOCP is used for the internal power grid, the heating network is represented via an energy balance approach, and the multi-energy building model is deployed. It is evident from Fig. 3.9 that the detailed HP model with its non-convex equations takes significantly more computational time to solve to global optimality than for the linear HP models. Nevertheless, for design studies like the presented work, all three HP are computationally easy to solve, despite the detailed HP model also comprising non-convex constraints.

The difference between the complexity of the non-convex constraints of the HP model and networks lies in the coupling of the network constraints across the whole energy system. Since the thermal and electrical networks interconnect all buildings, their non-convex

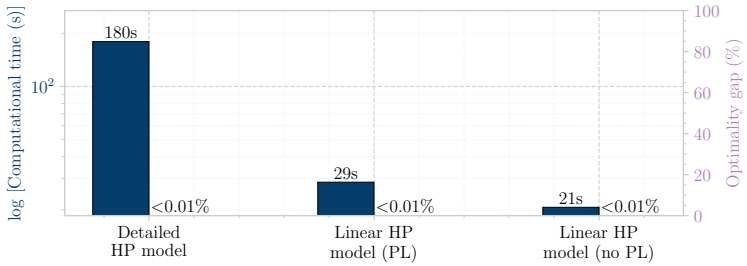

Fig. 3.9: Computational time and optimality gap for three different HP models (with the SOCP grid approximation, and the multi-energy building model): detailed non-convex model, linear HP model with minimum part-load (PL), and linear HP model without minimum PL limit.

constraints couple all nodes, which significantly increases complexity and leads to convergence or computational tractability issues. Nevertheless, it is essential to represent the physical behaviour of underlying networks accurately. Therefore, it is crucial to find a balance between accurately representing the physical behaviour and computational workload and tractability.

3.4.3 Key findings & discussion

The two adopted case studies, an office building and a district-scale MES, explored the impact of different modelling choices within local MESs on the optimal sizing of BESS. One of the key findings is that explicitly modelling the thermal vector, including its thermal storage, avoids BESS oversizing. By exploiting the thermal building inertia via the coupling between electricity and heat, investment in additional electrical flexibility via a larger BESS capacity is not required. Additionally, the TAC and the GWI are reduced when explicitly modelling the thermal vector, which highlights the economic and environmental benefits of integrated modelling of MESs.

A time-varying electricity tariff leads to larger BESS capacity and lower costs, as it enables demand shifting into low-price hours besides the benefits of complementing solar PV generation, which outweighs the higher investment costs. Different HP models only show a slight impact on the BESS sizing and annualised costs, thus the findings suggest that linear models for the HP are suitable. The value and sizing of BESSs are significantly impacted by solar availability, thus various solar irradiance years should be considered. Incorporating the heating network within the design study reduces the BESS capacity slightly, but it increases the computational workload due to its non-convex model formulation. The internal power grid formulation significantly impacts the computational tractability and time, especially the exact non-convex AC OPF formulation, where the solution might get stuck in a local minimum, or does not find a feasible solution at all. Therefore, the SOCP formulation proves to be a suitable alternative for closely representing the physical grid while maintaining computational tractability.

However, there are various factors not considered that influence the BESS sizing and thus the generalisation of the presented findings. The adopted heating network model only considers operational constraints and heating losses, but it does not account for storing thermal energy within its pipes. The specific impact of heating network storage on the design of BESSs should be investigated in future work. While the impact of different levels of PV irradiation on the optimal BESS capacity is demonstrated, the influence of climate types, as well as energy consumption patterns, could further affect the BESS sizing. The heating demand in colder climates is significantly higher compared to warmer climate regions, which could in turn increase the influence of the coupled thermal vector on the sizing of the BESS capacity. Furthermore, the particular building characteristics, e.g., the construction materials or the insulation levels, affect the overall thermal inertia of the building, which might further influence the BESS sizing. Moreover, uncertainty in the input data for the heat demand, the power demand, the time series for electricity prices or solar PV irradiance, is another potential limitation of the investigated planning problem. The presented findings are thus limited to the assumed input data and the specific location. Finally, while the GWI emissions of the BESS production and instalment are taken into account within this study, it is important to acknowledge that other factors such as recycling processes or disposal, also contribute to their overall environmental impact. For a greenfield design study, the GWI associated with other component installations, such as a solar PV array or HP, must be considered as well.

3.5 Chapter Summary

This chapter investigated the impact of component modelling choices on the optimal sizing of a BESS within local MESs comprising electricity and heat. Besides focusing on different models of the coupled thermal vector, the internal power grid and heating network, time-varying and constant electricity tariffs were compared, and the influence of different solar irradiance years on the optimal design of a BESS was analysed. Additionally, the computational workload and tractability of the different models were further assessed. Through two real-world case studies, this chapter highlighted the importance of integrated multi-energy modelling and further provided practical modelling guidelines for electrical storage sizing in local MES with electricity and heat. These guidelines can be summarised as follows: explicitly model the thermal vector and the thermal building capacity to avoid BESS oversizing; use the SOCP relaxation of the internal power grid for a suitable compromise between model accuracy and computational tractability; deploy a linear HP model which is sufficient for optimal BESS sizing; and do not explicitly model the heating network, as its substantially increased computational workload outweighs the slight reduction in optimal BESS capacity.

CHAPTER 4

Component design assessment for electrical system flexibility quantification

This chapter investigates the impact of individual component design within local MES on its overall operational flexibility capabilities to the upstream power grid. By embedding operational flexibility provision in the design phase of local MES, the proposed framework presents a quantitative assessment of how the sizing of individual and interdependent components affects technical flexibility. By identifying key components that either enhance or reduce the flexibility of MESs through a sensitivity analysis, this chapter aims to provide a deeper understanding of limiting factors and interdependencies between components across energy vectors. The framework is applied to a residential building and a district-scale MES, highlighting the capabilities of the framework and its applicability to energy systems with internal network constraints.

4.1 Introduction

Due to the increasing share of time-varying RES in electricity generation, the need for flexibility in power systems is growing to ensure a reliable and secure power supply [92–94]. This flexibility can be provided either by electrical assets or by assets from interconnected energy vectors within MESs [4]. As demonstrated in Chapter 3, explicitly considering the thermal vector has a significant impact on the optimal design of a community BESS. It was shown that the thermal vector plays a crucial role in optimally sizing a community BESS, and that explicitly modelling the coupled thermal vector significantly affects the optimal community BESS capacity.

Based on these findings, this chapter aims to answer the question of how the thermal vector quantitatively influences electrical operational flexibility. It further investigates the technical constraints and inherent interdependencies within MESs comprising electricity and heat. By identifying components that might hinder or enable flexibility potential, the

framework merges the design aspect of MESs with their technical capabilities to provide operational flexibility.

The remainder of this section is structured as follows: Section 4.1.1 presents the concept of operational flexibility. Section 4.1.2 presents studies regarding operational flexibility provided by MESs in Section 4.1.2, followed by related work of integrating flexibility during the design phase Section 4.1.3. Finally, Section 4.1.4 presents a summary of the existing literature and the identified gap.

4.1.1 Concept of operational flexibility

The general concept of operational flexibility in power systems has been defined as the "technical ability of a component to regulate its power exchange with the grid" [95]. Further metrics such as response time and cost have been included [96]. In a comprehensive work about the characterisation of flexibility from DER in [97], an optimisation-based nodal operating envelope (NOE) modelling framework for power systems was presented. Here, the operational flexibility of DER was modelled and characterised through key flexibility metrics (notice time, response time, duration length, maximum cost) and the application to market services was demonstrated. Furthermore, different types of dynamic flexibility were defined, the most important being capability (virtually aggregated flexibility), feasibility (including power network constraints), dynamic flexibility (including ramping and duration constraints), economic flexibility (including costs for deviating from the operating point), and market-specific flexibility (including market-specific techno-economic constraints).

Besides flexibility assets in the electrical domain, such as reservoir-based hydropower and pumped storage plants [98], conventional power plants or BESSs [93], a comprehensive analysis of interconnected energy vectors within MESs can provide further electrical flexibility [4, 99]. In particular, DER that are connected via various energy networks can provide flexibility to the power system by shifting generation and demand across energy vectors [3]. Following the definitions of [3], key examples of electrical flexibility that are enabled by interconnected energy vectors are: i) replacing an input energy vector with another one, for instance by providing heat either by a gas-fired boiler or by an electric HP ii) converting one energy vector to another one, for instance by converting surplus electricity into hydrogen via electrolysis or heat via electric HP iii) making use of multi-energy storage systems for temporal shift, for instance by charging a thermal energy storage via an electric HP and storing the heat until heat demand is needed. This electrical flexibility range of MESs at a given time instance can be quantified through operating envelopes and offered to external grid providers through certain ancillary services, e.g., load shifting, demand response or frequency-balancing services [97, 100] (see Chapter 5). In this chapter, dynamic flexibility is investigated, which can be applied to different markets by adjusting the market-specific techno-economic constraints as required.

4.1.2 Electrical flexibility of multi-energy systems

The operational flexibility provision of MESs has been investigated within various case studies. The real-time provision of electrical flexibility for a local energy community comprising residential households is demonstrated in [15, 101]. The individual buildings first serve their own individual objective, and second serve the wider grid of the LEC by increasing its self-consumption and self-sufficiency. Additionally, the LEC, supported by a community BESS, provides ancillary services to the external power grid by providing load flexibility and sharing battery capacity using model-predictive control (MPC). A framework for distributed MESs was developed to analyse the technical and economic potential of distributed MESs providing electrical flexibility and its monetisation. This framework was applied to a real innovative multi-energy district that provided its flexibility through various business cases with different price signals [14]. Similarly, the aggregation of bottom-up services provided by households through individualised, time-varying operating envelopes were analysed for more efficient short-term planning of distribution networks while ensuring network integrity [102]. It is important to note that internal energy networks can either enable greater flexibility by using them as an inherent storage system (thermal or gas networks) [103], or limit the aggregated flexibility due to their underlying constraints [97, 104]. Focusing on the role of multi-energy networks that enable or restrict flexibility, a comprehensive framework on the flexibility modelling, provision and application of distributed multi-energy systems is presented [3]. Further electrical flexibility for the power system can be enabled by integrating hydrogen into energy systems, e.g., by injecting it into existing natural gas networks, as hydrogen electrolysers can be operated as flexible loads [104]. Even though the operating conditions of the gas network can limit the flexibility contribution of hydrogen electrolysers, power-to-gas units such as electrolysers can significantly increase power system flexibility.

Besides energy communities comprising individual households or commercial buildings, non-residential entities such as the industry sector also incorporate multiple energy vectors. Therefore, they can be considered as MESs that can operate flexibly, e.g., shifting energy from high electricity periods to low electricity periods for cost minimisation [105–109]. On the one hand, this has been investigated within overarching studies, e.g., regarding general power-intensive process industry such as air separation, cement production or aluminium [106], or regarding the overall potential of energy-intensive industries to provide demand-side management (DSM) in electricity and balancing markets in 2030 [108]. On the other hand, studies looked at the the demand response potential of individual processes, e.g., specifically for the energy-intensive industrial copper process [107], as well as the demand-response flexibility of a cement production process that can be utilised to minimise bid cost in sequential energy markets [110]. Additionally, the impact of network tariffs and regulations on the demand response provision was investigated for the chlor-alkali process on day-ahead and reserve markets, finding that network tariffs on peak-demand are hindering new investments in flexibility [109].

Several studies have further developed advanced methodologies for assessing opera-

tional flexibility of both industrial processes and distributed MESs. For instance, [111] developed a flexibility assessment tool which quantifies the feasible operation regions of industrial processes for the provision of ancillary services during operation. Similarly, [112] evaluated the flexibility potential of distributed MESs comprising electricity, natural gas and heat in the process industry. Through a projection-based vertex enumeration method, integrated flexible regions are identified. Their findings demonstrate that accounting for energy conversion in the energy supply and production adjustments of the industrial loads enhances flexibility of the system, indicating the necessity of an integrated system approach for flexibility optimisation. Based on this study, uncertainty from production fluctuations, renewable variability and equipment failures was integrated into the flexibility assessment, which reduces the available flexibility by around 50 %. This demonstrates the importance of realistic, uncertainty-aware flexibility assessments [113]. Furthermore, time-coupling effects between multi-energy production processes and energy storage were captured within high-dimensional convex flexible regions, enabling improved multi-period dispatch strategies and market participation [114].

4.1.3 Integrated flexibility during design stage

Besides the presented studies above, which incorporate flexibility during operation, several works have already considered electrical flexibility during the design and planning stage. Typically, these studies focus on the economic feasibility of their investment and the subsequent operation of the system. For residential buildings, typical energy flexibility technologies were evaluated based on the levelized cost of energy flexibility index, which describes the total cost per unit of energy flexibility capacity during its lifetime at the design stage. According to their study of typical demand-side technologies providing grid services, heating, ventilation and air conditioning (HVAC) systems are the most cost-effective technologies for grid services [115]. In another study, the technical and commercial flexibility of a virtual power plant (VPP) was quantified, which simultaneously participates in multiple markets and provides grid services. As a further step to its operation, a sensitivity analysis was conducted regarding the sizes of a gas generator, a BESS and different price scenarios, which demonstrated the economic benefits of multi-market grid service participation of the VPP and the robustness to electricity price variations [116].

Within the industrial sector, there are several works that investigate economic investment decisions during the design stage for the subsequent flexibility provision at certain markets during operation. For an industrial plant, the economic potential of BESS and solar PV array investments was evaluated for several market streams and under different market conditions. The results indicate that BESS investment is attractive when a primary frequency market exists, whereas the PV investment depends on the solar irradiance [117]. The study concludes that future price developments and policy significantly impact the flexibility opportunities of industrial plants. [118] analysed the value of flexibility in decarbonising a manufacturing company with electricity and heat. Investments in energy

storage systems and utilising sector coupling enable flexibility and thus reduces decarbonisation costs and total annual costs. The study emphasises the importance of integrating flexibility at the design stage of MESs, and highlights inherent MES flexibility as a key factor for cost-effective decarbonisation. A system-wide study analysed whether flexibility investments driven by monetary aspects reduce the residual load in Germany, using a generic process model for load shifting [119]. Its findings indicate that existing price fluctuations do not incentivise investments in storage capabilities for bridging up to 24 h, which would be required to reduce the residual load. All these studies demonstrate the economic benefit of incorporating flexibility during the design stage, typically driven by arbitrage in market prices. However, these tools provide limited technical insights into how operational flexibility is impacted during the design phase. In particular, they do not quantitatively assess which components contribute how much flexibility, how changes in component sizes affect flexibility, or identify the interdependencies between individual components.

4.1.4 Summary

On the one hand, studies on the operational flexibility of both power systems and MESs define flexibility with respect to the current operating point. Technical feasibility regions are then calculated relative to this operating point, given certain ramping and duration limits. However, in industrial process plants and MESs with fluctuating demand and integrated variable RES, the operating schedule varies over time. Therefore, operational flexibility should rather be evaluated in relation to a *time-varying reference schedule*. This allows for constant marketable flexibility offers across multiple time steps, which is particularly important when the flexibility is offered within ancillary service markets. Therefore, the flexibility available for market participation must be evaluated against this time-varying reference schedule. On the other hand, existing studies on integrating operational flexibility within the design or retrofitting stage focus on specific use cases while assuming a fixed market framework for remunerating flexibility provision. As a result, their design decisions are heavily influenced by market prices and regulations. However, no study has systematically investigated how the design of individual components impacts the overall flexibility potential of an energy system from a technical perspective. Moreover, interdependencies between individual components and their effect on flexibility remain unexplored.

The contribution of Chapter 4 is twofold: First, a novel methodology that calculates operational flexibility in relation to a predetermined *time-varying* reference schedule is presented, which accommodates constant flexibility offers for a given duration. Second, the impact of individual component design on the provision of operational flexibility by MESs is quantified through a sensitivity analysis, and interdependencies between components are identified. The remainder of this chapter is structured as follows: Section 4.2 presents the integrated design and flexibility analysis framework, including the calculation of the flexibility in relation to a reference schedule. Section 4.3 outlines the case studies, while Section 4.4 presents the results. The chapter is concluded by the key remarks in Section 4.5.

4.2 Methodology

The methodology described in this chapter builds on the modelling framework for optimisation-based NOE for power systems, which was introduced in [97]. With this part of the thesis, this approach is further developed by integrating the assessment of flexibility into the design stage within MESs, thus investigating the impact of component design on operational flexibility. Moreover, this work investigates the provision of flexibility over multiple time steps relative to a predetermined reference schedule of the MES, while also incorporating intertemporal constraints of electrical and heat storage systems.

4.2.1 Integrated design and flexibility analysis framework

The flowchart for the proposed algorithm is depicted in Fig. 4.1, which consists of two main parts: the reference case and the sensitivity analysis. In the preprocessing phase, the input data is clustered into representative scenario days, which serve as the input for the reference case. Based on the representative days, investment costs, and the objective function, an integrated design and operational optimisation of the MES is performed. Given the operational schedule, the specified response time and flexibility duration, the maximum upward and downward active and reactive power values at the PCC at each time step are determined, respectively.

In the second stage, a sensitivity analysis is conducted by varying the design sizes of each component individually, while keeping the other component sizes fixed based on the reference case. Using the same method as for the reference case, the maximum upward and downward active and reactive power values are computed for the specified response time and duration for each time step. It is important to mention that these values are determined relative to the optimal schedule for the fixed design previously optimised in the respective iteration of the sensitivity analysis. The detailed flexibility calculation, which ensures constant flexibility provision over multiple time steps, is described in Section 4.2.2. In the post-processing stage, the determined flexibility values across all scenario days are aggregated for each component design variation. This aggregation enables a comprehensive analysis of the relationship between component sizing and achievable system flexibility.

Additionally, NOEs are derived to visualise the technically feasible ranges of active and reactive power at specific time steps. NOEs define safe operating regions through time-varying active and reactive power limits at the PCC, while incorporating constraints such as network limitations, response time, and flexibility duration [120]. For each time step, a separate NOE is calculated by iterating over the allowable reactive power values from the minimum to the maximum limits at the PCC, following the methodology in [97]. These reactive power values are fixed as constraints, and the corresponding minimum and maximum active power values at the PCC are determined, resulting in a two-dimensional NOEthat defines the feasible range of active and reactive power for each time step.

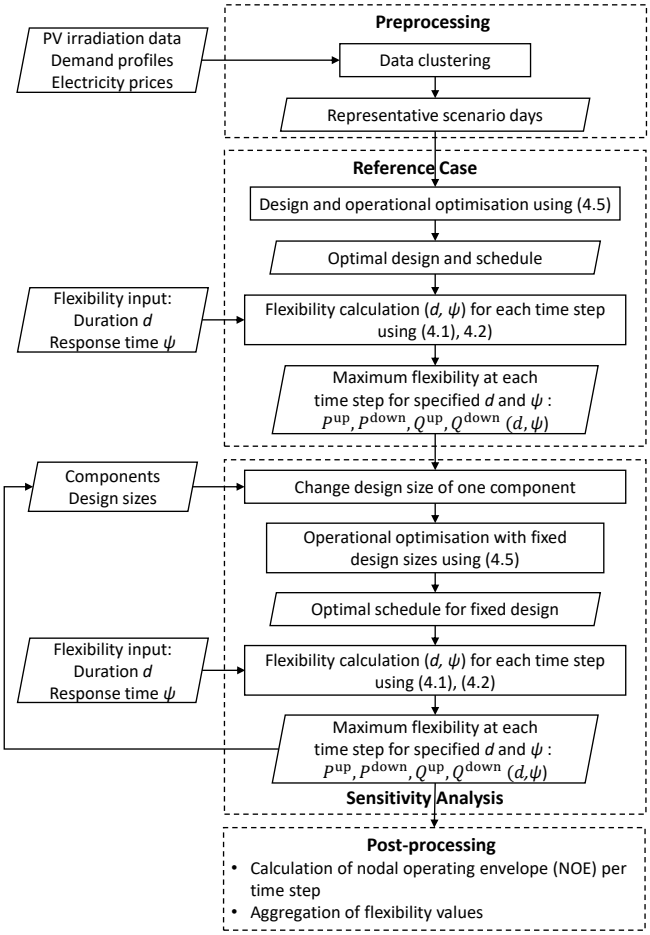

Fig. 4.1: Flowchart of the proposed framework that incorporates operational flexibility in the design stage while calculating flexibility in relation to a time-varying reference schedule.

4.2.2 Operational flexibility integration

Within this thesis, flexibility is referred to as the technical ability to dynamically adjust the operating point by effectively utilising interconnected energy carriers. Specifically, this is applied to electricity, which defines the technical capability of adjusting the active power and reactive power at the PCC of an energy system. Existing literature typically considers the transition from one operating point to another for a given response time and duration [97, 104, 111]. However, approaches assessing flexibility for an individual operating point do not take time-varying consumption or generation of energy systems into account. Subsequent time steps may deviate significantly from the current operating point due to variable loads or RES output. This is especially important for large actors like virtual power plant (VPP) or large energy systems, which are required to submit their op-

erational schedule one day ahead of delivery. In order to accurately estimate the technical flexibility potential over multiple time steps, this work defines flexibility in relation to a predetermined reference schedule, taking into account variable operational schedules.

4.2.2.1 Conceptual illustration of flexibility provision

The methodology of the constant flexibility provision over multiple time steps is illustrated in Fig. 4.2 for the example of active power. This illustration visualises the calculation of upward and downward flexibility, which is presented in detail in Section 4.2.2 for both upward flexibility (4.1) and downward flexibility (4.2). In Fig. 4.2, the predetermined reference active power schedule is represented by the black line, while the bars indicate the upward and downward active power flexibility over a required duration of four time steps. The flexibility provision available at time step t depends on the subsequent time steps τ within the required flexibility duration. In the presented example, it is assumed that the

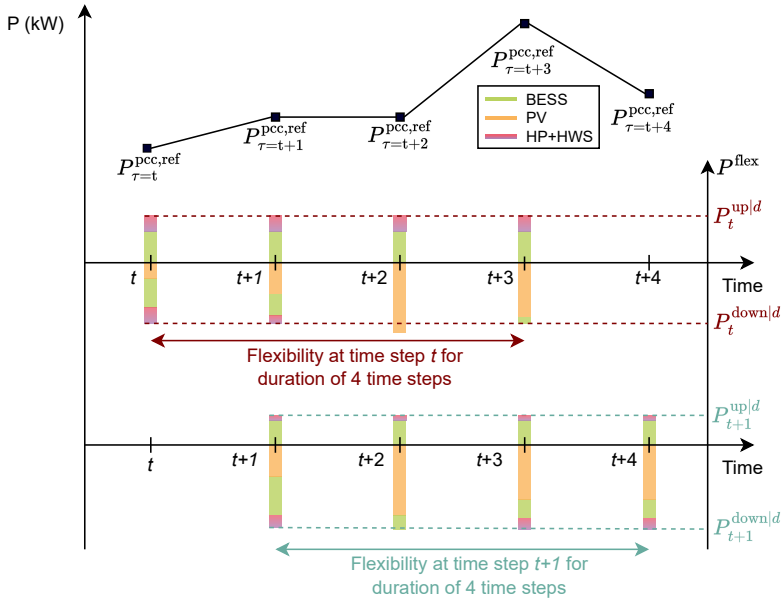

Fig. 4.2: Illustrative visualisation of the active power flexibility optimisation over multiple time steps. Based on a predetermined reference schedule, the bars indicate the available upward and downward active power flexibility at time step t and $t+1$, respectively, considering a flexibility duration of four time steps.

solar PV array is dispatched completely, thus the solar PV array does not contribute to upward flexibility. However, if the PV array were to be curtailed, it could also provide upward active power flexibility by increasing its active power generation. Only the BESS and the HP in combination with the HWS can provide upward active power flexibility. Since a constant flexibility provision is required for a specified duration, the flexibility potential is limited by the smallest flexibility value among all time steps over this duration. This is particularly important since the flexibility potential at each time step varies based on the operational schedule of the individual components. To maximise the constant flexibility

provision over the whole flexibility duration, the optimisation shifts the active power flexibility of storage systems to time steps with the lowest inherent flexibility potential. This flexibility potential shift of storage systems is particularly evident for downward flexibility in the illustrated example. For $\tau = t + 2$ and $\tau = t + 3$, potential PV curtailment enables large downward flexibility potential compared to $\tau = t$. Consequently, the optimisation of the maximum downward flexibility enhances the downward flexibility by charging the BESS and charging the HWS via the HP. Both of the storage systems enable an increased electricity consumption at $\tau = t$, and thus a larger constant downward flexibility potential over the specified duration.

4.2.2.2 Operational flexibility calculation

As outlined in Section 4.2.1, the flexibility calculation builds upon the previously determined system design and optimal operation of the MES. In this context, flexibility refers to the technical ability of the investigated energy system to adjust its operating point dynamically by effectively utilising interconnected energy carriers. Specifically, *upward flexibility* is defined as the capability to increase generation or decrease consumption of the flexibility vector relative to a predetermined reference schedule, while *downward flexibility* denotes a decrease in generation or an increase in consumption in relation to the reference schedule. The flexibility assessment is parameterised by the *response time* ψ, representing the time by which the adjusted operating point must be reached, and the *flexibility duration* d, which defines the time interval over which the operational deviation must be provided. Both upward and downward flexibility must be constant during the specified duration relative to the time-varying reference schedule.

For each time step t, two optimisation problems are solved to quantify the upward and downward flexibility provision at the PCC, which are subject to the given response time and flexibility duration. This flexibility calculation is applied to both the reference case and to all component size iterations of the sensitivity analysis. Note that these flexibility calculations require a predetermined operational schedule as an input, as shown in Fig. 4.1. While a general formulation for the flexibility vector is presented below, in the remainder of this thesis, the focus lies on active power flexibility. However, the methodology is equally applicable to other energy vectors, such as reactive power or heating power.

Upward flexibility

The upward flexibility for the flexibility vector f at each time step t of scenario day s is maximised as follows:

$$\max_{s\in\mathcal{S},t\in\mathcal{T}} \quad f_{s,t}^{\mathrm{up}\,|\,d} \tag{4.1a}$$

$$\text{s.t.} \quad f_{s,t}^{\mathrm{up}\,|\,d} \leq f_{s,\tau}^{\mathrm{flex}}, \qquad s \in \mathcal{S},\ t \in \mathcal{T},\ \tau \in \mathcal{T}_\tau(d), \tag{4.1b}$$

$$f_{s,\tau}^{\mathrm{flex}} = f_{s,\tau}^{\mathrm{pcc,ref}} - f_{s,\tau}^{\mathrm{pcc}}, \qquad s \in \mathcal{S},\ \tau \in \mathcal{T}_\tau(d), \tag{4.1c}$$

$$f_{s,\tau}^{\mathrm{pcc}} = \eta^{\mathrm{pcc}} \sum_{c\in\mathcal{C}} f_{s,\tau}^{c}, \qquad s \in \mathcal{S},\ \tau \in \mathcal{T}_\tau(d). \tag{4.1d}$$

Here, $f \in \mathcal{F} = \{P, Q\}$ denote the electrical flexibility vector, with $\mathcal{F} \subseteq \mathcal{V}$, where $\mathcal{V}$ is the set of the considered energy vectors. For a given flexibility duration d, the set of time steps for which the flexibility must be provided is $\mathcal{T}_\tau(d) \subseteq \mathcal{T}$, which is defined as $\tau \in [t, t+1, \ldots, t+n-1]$, with $d = n \cdot \Delta t$. Here, Δt is the time step size. The variable $f_{s,t}^{\text{up}|d}$ denotes the maximum feasible upward flexibility at the representative scenario s and time t for a given duration d. $f_{s,\tau}^{\text{pcc,ref}}$ is the value of the flexibility vector for the reference schedule, while $f_{s,\tau}^{\text{pcc}}$ denotes the energy vector variable at the PCC for scenario s and time τ, which is constrained by power flow equations presented in (2.10a) – (2.10f), or by the balancing-node equation of the energy vector given in (2.7). To account for electrical losses, an efficiency factor η^{pcc} is included in the proposed approach. Since internal building losses have a negligible impact on the system flexibility, a constant efficiency of one is assumed throughout this work.

In the presented formulation, the objective function in (4.1a) maximises upward flexibility at scenario day s and time step t for a given duration d. Constraint (4.1b) ensures that the upward flexibility at time t does not exceed the feasible flexibility at any time step τ during d. Constraint (4.1c) defines upward flexibility as the difference between the fixed reference value determined in the previous schedule optimisation, and the variable flexibility value at the PCC. The resulting upward flexibility at time step t equals the smallest maximum upward flexibility of all time steps across the duration d. Finally, (4.1d) enforces the balancing-node constraint of the flexibility vector by incorporating the constant efficiency factor.

It is important to differentiate between t and time steps $\tau \in \mathcal{T}_\tau$ over which the flexibility must be sustained. For example, for a specified flexibility duration of $d = 1\,\text{h}$ with a time step size $\Delta t = 0.25\,\text{h}$, then $\tau \in \mathcal{T}_\tau = [30, 31, 32, 33]$ for $t = 30$. Similarly, a new set of $\tau \in \mathcal{T}_\tau$ is determined for each time step t.

Downward flexibility

Similarly to the upward flexibility calculation, the downward flexibility formulation is as follows:

$$\min_{s \in \mathcal{S}, t \in \mathcal{T}} \quad f_{s,t}^{\text{down}|d} \tag{4.2a}$$

$$\text{s.t.} \quad f_{s,t}^{\text{down}|d} \geq f_{s,\tau}^{\text{flex}}, \qquad s \in \mathcal{S},\ t \in \mathcal{T},\ \tau \in \mathcal{T}_\tau(d), \tag{4.2b}$$

$$f_{s,\tau}^{\text{flex}} = f_{s,\tau}^{\text{pcc,ref}} - f_{s,\tau}^{\text{pcc}}, \qquad s \in \mathcal{S},\ \tau \in \mathcal{T}_\tau(d), \tag{4.2c}$$

$$f_{s,\tau}^{\text{pcc}} = \eta^{\text{pcc}} \sum_{c \in \mathcal{C}} f_{s,\tau}^{c}, \qquad s \in \mathcal{S},\ \tau \in \mathcal{T}_\tau(d). \tag{4.2d}$$

The calculation of downward flexibility differs from that of upward flexibility in that downward flexibility values are negative. Consequently, the objective function in (4.2a) is formulated as a minimisation problem, which reflects a decrease in power generation or an increase in consumption. Accordingly, the inequality constraint in (4.2b) is adjusted to a greater equality sign to reflect the reversed direction of flexibility provision.

4.2.2.3 Ex-post processing and visualisation

Flexibility value aggregation

To establish a connection between the calculated flexibility per time step as described above and the design choices for the components, the calculated flexibility values for all time steps across the entire operation are subsequently aggregated as follows:

$$f^{\mathrm{up}\,|\,d} = \frac{1}{|\mathcal{T}|} \sum_{s \in \mathcal{S}} w_s \sum_{t \in \mathcal{T}} f_{s,t}^{\mathrm{up}\,|\,d}, \tag{4.3}$$

$$f^{\mathrm{down}\,|\,d} = \frac{1}{|\mathcal{T}|} \sum_{s \in \mathcal{S}} w_s \sum_{t \in \mathcal{T}} f_{s,t}^{\mathrm{down}\,|\,d}. \tag{4.4}$$

This aggregated data set can be visualised in a box plot, and the mean over all time steps $\mathcal{T}$ weighted with the weight w_s of the respective scenario day quantifies the overall flexibility for a given system design, thus linking the system design and the overall operational flexibility. For the given energy system, the maximum upward and downward flexibility values can be calculated for the energy vectors *active power*, *heating power* and *reactive power* (not traditionally an energy vector). The focus in the remaining sections lies on the active power P, and to some extent on the reactive power Q, as there will be a reactive power market in the upcoming years in Germany [121, 122].

Nodal operating envelope calculation

For each time step, a NOE can be calculated to visualise the PQ-capability of the local MES at the PCC. The algorithm, which is based on [97], is briefly described here. First, the minimum and maximum values of active and reactive power at the PCC are calculated using Eq. (4.1) and Eq. (4.2). Then, the range of feasible reactive power values is discretised into K equidistant points. For each fixed discrete reactive power level $Q_{\mathrm{pcc},k}$ at the PCC, the corresponding minimum and maximum feasible active power values $P_{\mathrm{pcc},k}^{\mathrm{min}}$ and $P_{\mathrm{pcc},k}^{\mathrm{max}}$ at the PCC are determined via an optimisation. This algorithm generates $2K$ boundary points in the PQ−space. By linearly connecting these boundary points, the NOE represents the technically feasible region for the respective time step.

4.2.3 Objective functions

As this part requires several different optimisations (see Fig. 4.1), different objective functions apply. On the one hand, an integrated design and operational optimisation is carried out, aiming to minimise the TAC. Based on this operational schedule, four different optimisations are carried out to determine the active and reactive power flexibility at the PCC.

4.2.3.1 Design and operational objective

For the design and operational optimisation, the following objective applies:

$$\min \left\{ \sum_{c \in \mathcal{C}} \left(C_c^{\text{inv}} \cdot k_c^{\text{ann}} + \pi_c^{\text{fix}} \cdot C_c^{\text{inv}} \right) + \sum_{s \in \mathcal{S}} w_s \sum_{t \in \mathcal{T}} \pi_{s,t}^{\text{var}} \cdot o_{s,t} \cdot \Delta\tau \right\}, \tag{4.5a}$$

$$\text{with} \quad k_c^{\text{ann}} = \frac{(1+r)^{n_c} \cdot r}{(1+r)^{n_c} - 1}. \tag{4.5b}$$

Here, the total annualised cost (TAC) are minimised, accounting for the initial investment cost C_c^{inv} of all components $c \in \mathcal{C}$, their annual fixed costs π_c^{fix}, and their variable operational costs $\pi_{s,t}^{\text{var}}$. $o_{s,t}$ refers to an operational parameter value which has costs associated, e.g., the value of active power or heating power. The annualisation factor k_c^{ann} annualises the investment costs for the lifetime n_c of component c and interest rate r.

4.2.3.2 Flexibility objective

As described in Section 4.2.2, the operational flexibility is calculated based on the design and operation previously determined. Given this predetermined optimal schedule, for each time step t given a specified duration d and response time Ψ, the maximum upward and downward flexibility for both active and reactive power are calculated, respectively, leading to four different optimisations as follows:

- $P^{\text{up}|d}$: (4.1) with $f_{s,t} = P_{s,t}$.
- $P^{\text{down}|d}$: (4.2) with $f_{s,t} = P_{s,t}$.
- $Q^{\text{up}|d}$: (4.1) with $f_{s,t} = Q_{s,t}$.
- $Q^{\text{down}|d}$: (4.2) with $f_{s,t} = Q_{s,t}$.

This results in values for maximum upward and downward values for both active power and reactive power for each time step. If desired, this can be applied for different time durations and response times as well.

4.3 Case studies

To present the capabilities of the presented framework, two case studies are presented in the following, namely an individual building and a district-scale multi-energy system.

4.3.1 Individual building

The structure of the individual building is depicted in Fig. 4.3, which represents a residential or commercial building with both demands for electricity and heat, as well as

the components BESS, solar PV, HP and HWS which are to be sized. The BESS is integrated using (2.1), the solar PV array is modelled via (2.2), the linear HP model is implemented using (2.4), and the HWS using (2.6). Note that the energy vectors are internally balanced through (2.7).

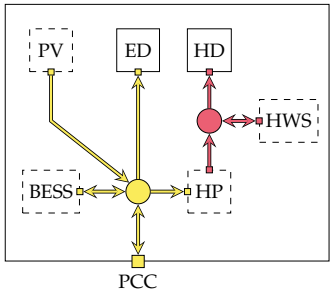

Fig. 4.3: Structure of the individual building case study, with electric demand (ED) and heat demand (HD), and the dashed-lined components to be sized battery energy storage system (BESS), solar photovoltaic (PV) array, heat pump (HP) and hot water storage (HWS).

4.3.2 District-scale multi-energy system

For simplicity reasons, it is assumed that the three buildings depicted in Fig. 4.4 are the same building as described in Section 4.3.1 with identical sizes, in order to illustrate the impact of the power grid on the flexibility of the district-scale MES at the PCC. Note that for a design optimisation where all components could be sized independently of each other, they would likely differ due to the impact of the internal grid constraints. Other factors, such as different demand data, also impact the optimal sizing. However, in this study, the focus lies on the impact of the internal grid on the flexibility provision. Therefore, the respective components of each building are sized identically to illustrate the effect of the internal power grid on the flexibility at the PCC when the component sizes are increased. The same model component constraints apply as above for each building. Additionally, the LinDistFlow equations are integrated using (2.10).

4.3.3 Input data

The input data for ED and HD is derived from a residential apartment building [123], while solar irradiation data is used for the year 2022 based on [124]. As described in Section 2.2.2, all time series were normalised, aggregated and clustered into four representative scenario days. For more information on the (error) duration curves of the time series aggregation, the reader is referred to Appendix C. A time step length of $\delta t = 15\,\text{min}$ is assumed. Furthermore, import and export prices for electricity are assumed constant, with a variable operating cost of $\mu^{var} = 0.30\,€/\text{kWh}$ for consuming active power at the PCC, and

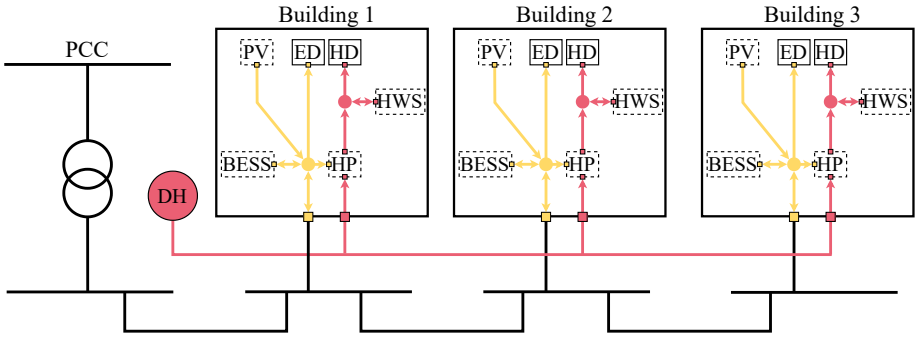

Fig. 4.4: Structure of the district-scale multi-energy case study, which includes an internal low-voltage power grid and a district heating (DH) network. The buildings are interconnected via 400 V electrical cables, while the point of common coupling (PCC) is at medium voltage of 10 kV. Note that components of the same type are identically sized across all buildings.

a remuneration of 0.05 €/kWh for exporting active power to the upstream power grid. For the district-scale energy system, all electrical cables are limited to an apparent power rating of 32 kVA, while the transformer between PCC and the low-voltage distribution grid has an apparent power limit of 40 kVA.

Tab. 4.1 lists the lower and upper limits of each design component, as well as their respective investment costs C^{inv} and relative maintenance costs π^{fix}.

Tab. 4.1: Techno-economic component parameter values for both case studies.

Parameter	2h-BESS	Heat pump	Solar PV array	HWS
Lower limit	4 kWh	6 kW_{th}	4 kWp	8 kWh
Upper limit	10 kWh	15 kW_{th}	12 kWp	20 kWh
Investment cost C^{inv}	909 €/kWh	1300 €/kW_{th}	941 €/kWp	97 €/kWh
Maintenance cost π^{fix}	2.5 %	1.1 %	1.0 %	1.0 %
Sources	[88, 125]	[125, 126]	[88]	[125, 127]

The flexibility capabilities of the electricity-consuming components in the PQ-space are illustrated in Fig. 4.5. The BESS is constrained by the thermal limit of its power inverter, while the solar PV array in combination with its inverter operates within its power factor limit of 0.9. The HP is modelled with a constant inductive power factor of 0.9. Although the internal compressor control might limit the ramping capability of the HP [128], a response time ψ of several minutes is assumed in this study. For the BESS and the solar PV system, a response time of a few seconds is assumed. Consequently, all electricity-consuming components are capable of fully ramping their active and reactive power output between minimum and maximum values within the considered 15 min time step.

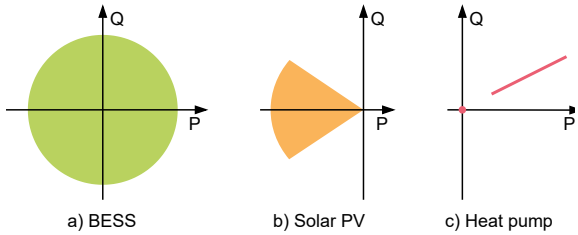

Fig. 4.5: Flexibility capabilities in the PQ-space of the considered electricity-consuming components: BESS, solar PV array, and HP. Negative values represent generation, while positive represent consumption.

4.4 Results

In this section, the impact of the design sizing of local MES components on the operational flexibility at the PCC is analysed. First, the results for the initial design and operational optimisation are presented in Section 4.4.1, followed by a quantified analysis on the impact of the thermal vector on the electrical flexibility of the local MES in Section 4.4.2. Afterwards, a sensitivity analysis of the individual component design is carried out in Section 4.4.3, which also compares the flexibility capabilities of air-to-water with water-to-water HP. Section 4.4.4 investigates the interdependency between HP and HWS, identifying an optimal ratio between their design sizes for electrical flexibility provision. As the focus of this investigation lies on gaining a better understanding of interdependencies and sizing sensitivities between MES components, the residential building is investigated as a simple case study for the aforementioned studies, i.e., no internal power grid is included. Finally, the impact of internal grid constraints is evaluated in Section 4.4.5 using a district-scale MES with an internal power grid.

4.4.1 Initial design and operation

An initial design and operational optimisation with the objective function Eq. (4.5a) is performed, determining the optimal design and reference schedule of the residential building by minimising the TAC of the building. The optimal design parameters are listed in Tab. 4.2, while the corresponding operational schedule is depicted in Fig. 4.6. The four representative scenario days represent different seasonal conditions, with the first day reflecting a typical winter day with high HD and low solar PV generation, while the last day corresponds to a typical summer day with low HD and high PV generation. Note that the SoC of both HWS and BESS are constrained to the same value at the beginning and the end of each representative day, which prevents energy shifting between representative days. Furthermore, the maximum and minimum active and reactive power values, respectively, are depicted at the PCC. Note that these values were calculated for each time step individually based on the predetermined operational schedule as described in Section 4.2.3.2,

Tab. 4.2: Component sizes for the reference optimisation.

Component	BESS	Heat pump	Solar PV array	HWS
Size	4 kWh	8.2 kW_{th}	12 kWp	10.8 kWh

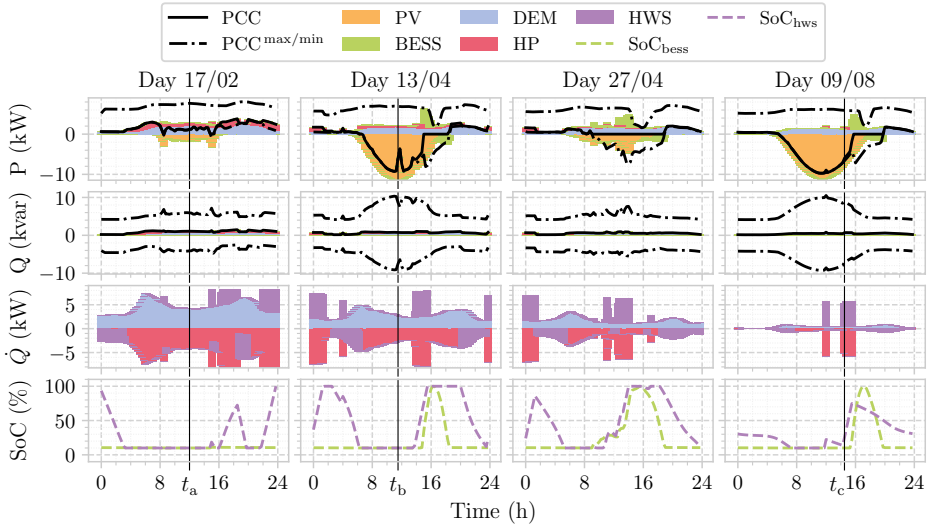

Fig. 4.6: Reference schedule of the individual building case study, displaying active power (top), reactive power (centre-top), heat (centre-bottom) and the SoC of the storage systems (bottom). Positive values indicate consumption, negative values denote generation. For the PCC, positive values represent electricity import and negative values electricity export. $PCC_{max/min}$ represents the maximum and minimum active and reactive power values for a given duration of 15 min. The electric demand (ED) and heat demand (HD) for both active and reactive power are referred to as demand (DEM).

for a duration of 15 min. The direction of flexibility is defined from the perspective of the upstream grid: *upward flexibility* refers to an increase in local generation or a demand reduction, while *downward flexibility* represents a decrease in generation or an increase in demand at the PCC.

It can be seen that during periods of discharged BESS and HWS, the local MES operates at its minimum active power limit, thus limiting its upward flexibility potential, as it is visible during the first representative day. Note that as power demand is denoted positive and generation negative, upward active power flexibility is the difference between P_{PCC}^{min} and P_{PCC}. Conversely, when solar PV generation exceeds the internal electricity demand, the excess renewable energy is used to charge both storage systems. As the energy system can later discharge the BESS or rely on stored thermal energy in the HWS instead of activating the HP to meet the heat demand, charged storage systems increased upward active power flexibility. Alternatively, during high solar PV generation periods, the system would be able to curtail its PV generation, thus increasing its downward flexibility.

4.4.2 Impact of the thermal vector on electrical flexibility

In the following, the impact of the thermal energy vector on active power flexibility at the PCC within the integrated MES is quantified. Unless stated otherwise, flexibility refers to *active power* flexibility. The thermal vector can provide downward flexibility by charging the HWS via an increased thermal output of the HP, thus increasing active power consumption. Conversely, upward flexibility can be provided by meeting the HD through the HWS rather than directly operating the HP, therefore reducing active power consumption if required. In order to quantify the impact of the thermal vector, the integrated multi-energy reference case as presented in Fig. 4.3 is compared to a similar system for which the HWS is removed, hereafter referred to as the *electricity-only* system. In the electricity-only system, the HP must meet the HD at all times, which eliminates its operational flexibility. Consequently, only the solar PV array and the BESS can provide electrical flexibility for the energy system.

The NOEs for three selected time steps are depicted in Fig. 4.7, considering flexibility durations of 15 min and 60 min. As expected, the NOE area decreases with increasing duration d, which reflects reduced constant flexibility provision over longer periods of time. When comparing the integrated multi-energy reference system with the electricity-only system without HWS, a smaller NOE can be observed for the electricity-only system across all examined time steps and flexibility durations. This visualisation outlines the contribution of the thermal energy vector to the electrical flexibility provision of the overall energy system. To quantify this contribution in electrical flexibility, the maximum upward and downward flexibility values were aggregated for all time steps across the operational schedule, e.g., t_a, t_b and t_c in Fig. 4.6 result in one maximum upward and downward flexibility value, respectively. On average, the integrated MES with explicit consideration of the thermal energy vector shows a 13.1 % increase in both upward and downward active power flexibility compared to the electricity-only system. These results demonstrate that assessing flexibility in an integrated multi-energy context is essential to identify its true technical flexibility potential, as the coupling of electricity and heat unlocks further inherent flexibility capabilities.

4.4.3 Sensitivity analysis of individual component sizing

Here, a sensitivity analysis of the individual component design is presented, focusing on the residential building without an internal power grid as a simple case study to better understand sizing sensitivities and interdependencies between components within a MES.

To compare the flexibility capabilities of the MES across different individual component designs, the maximum upward and downward flexibility values across all time steps are aggregated within one data set. For the given setup comprising four representative days and 15 min time steps, this results in a total of 384 flexibility values per design configuration. These values can be aggregated and visualised using box plots, which allow for

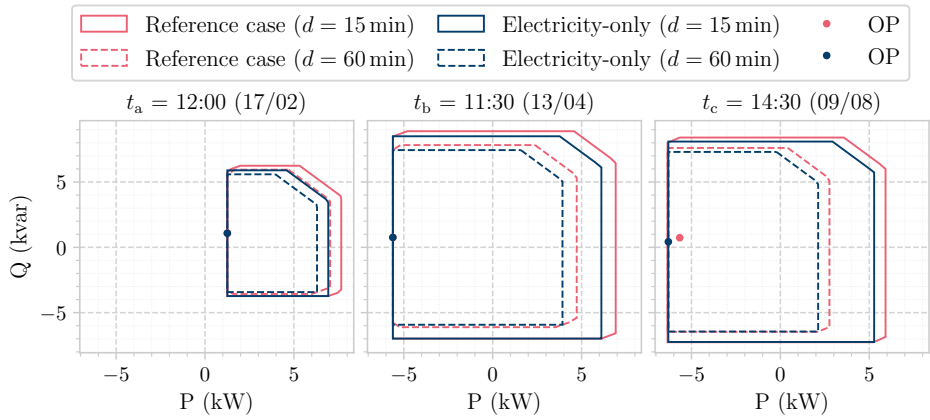

Fig. 4.7: Nodal operating envelope (NOE) of the individual building case study, illustrated for three representative scenario days and time steps, both for the multi-energy reference case and for the electricity-only system.

a comparative and quantifiable assessment of the distribution and average upward and downward flexibility values under different design configurations. Fig. 4.8 depicts these box plots for varying component sizes of the solar PV array, while all other components are kept at their reference size. providing insights into the impact of component sizing on overall system flexibility. Note that for each solar PV array size, a cost-optimal operational schedule is first determined, followed by the calculation of the maximum upward and downward flexibility values for every time step for the specified flexibility duration.

As the solar PV size increases, the available downward flexibility P^{down} increases significantly due to the higher potential for PV curtailment, while the upward flexibility P^{up} remains relatively stable. The widening interquartile range and the increase in outliers for downward flexibility with larger solar PV arrays indicate a greater variability in downward flexibility, which is primarily driven by solar availability as downward flexibility through solar PV curtailment is only available during daylight hours. While larger solar PV arrays offer more potential for downward active power flexibility during hours of solar irradiation, no flexibility can be provided during non-solar generation hours. This difference increases the variability in downward flexibility for increasing solar PV arrays.

The mean values of upward active power P^{up} and downward active power flexibility P^{down} for single component size variations, as indicated in Fig. 4.8 by the green dashed line for the solar PV array, are illustrated in Fig. 4.9 for all components. For each design combination, a new operational optimisation is performed, as outlined in the flowchart in Fig. 4.1. As each design combination leads to a different operational schedule, increasing component sizes could lead to a decrease in upward flexibility for some components. However, the respective larger increase in downward flexibility outweighs the reduction in upward flexibility, resulting in an overall increased NOE. One key observation is that increasing the size of the HP alone beyond a relative size of 1.5 does not result in additional flexibility. This saturation effect can be attributed to the interdependence between the HP

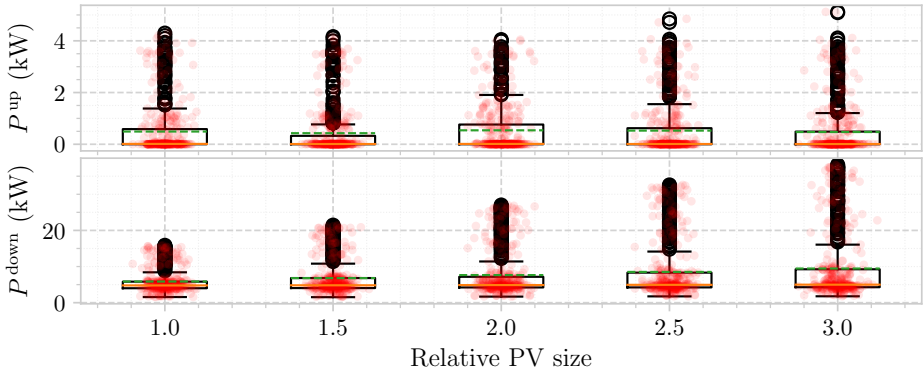

Fig. 4.8: Maximum active power flexibility of the multi-energy building for a duration of 60 min, varying the solar PV array size. Orange lines indicate the median, and green dashed lines represent the mean of the resulting dataset.

and HWS, where the fixed size of one component restricts the flexible utilisation of the other. Moreover, since the thermal inertia of the building is not explicitly modelled, the HP is required to meet the fixed heat demand profile and therefore cannot operate flexibly on its own. To overcome this identified constraint and better assess the coupled system flexibility, a combined sizing approach was implemented. By simultaneously increasing both the HP and the HWS, additional flexibility can be unlocked, especially in the downward direction, as shown in the right-hand column of Fig. 4.9.

The associated additional investment and total annualised costs, relative to the reference system in per unit, are shown in Fig. 4.10. It is evident that due to the relatively low investment cost of the HWS, jointly scaling both HWS and HP significantly enhances the flexibility provision of the overall system while maintaining cost efficiency.

4.4.3.1 Air-to-water vs. water-to-water heat pump

As the HP is the linchpin coupling component between electricity and heat in MESs, the impact of different HP technologies on the electrical flexibility provision is of interest. Therefore, an air-to-water HP is compared to a water-to-water HP in terms of their electrical flexibility provision. Fig. 4.11 depicts the mean upward and downward flexibility values for individual component variations when using an air-to-water HP. For comparability, the results are shown as per-unit values relative to the flexibility of the energy system with a water-to-water HP, while using identical component sizes. For the reference configuration with relative component sizes equal to one, the system with the air-to-water HP shows higher upward and downward flexibility values compared to the system with water-to-water HP depicted in Fig. 4.9, with a combined increase in flexibility of 9.0 %. Moreover, the flexibility advantage of the air-to-water HP becomes more evident when jointly increasing the HP and the HWS, for which the system flexibility increases by 20.8 % compared to the system with the water-to-water HP. The larger electrical flexibility potential of air-to-water HPs can be attributed to their lower COP due to the lower temperature at the evaporator,

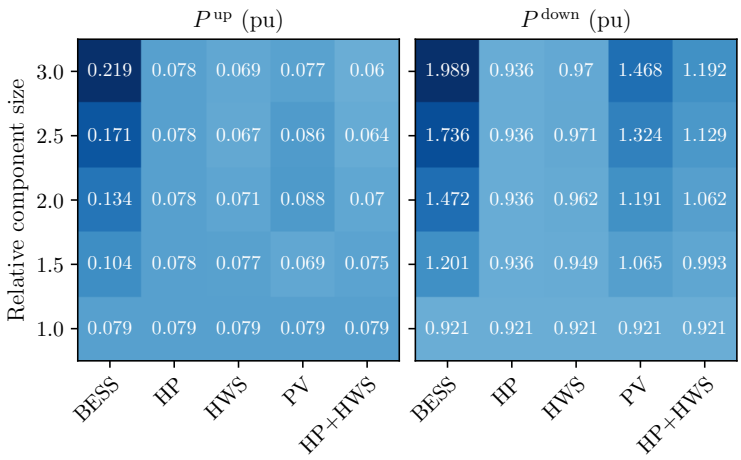

Fig. 4.9: Mean maximum active power flexibility of the multi-energy building relative to the reference case for a duration of 60 min, varying one component size at a time. Flexibility per unit is defined as the sum of the mean upward and downward flexibility in the reference case.

which results in larger electricity consumption for a given thermal output. This increased electric demand is less cost-efficient, but it increases the capability of the system to shift or curtail more electric load, which expands the active power flexibility potential at the PCC.

4.4.4 Interdependency between hot water storage and heat pump

In addition to the individual analysis of each component, this section explores interdependencies that influence the flexibility provision within the MES by varying two components at a time. Understanding these interdependencies in integrated MESs could avoid over- or under-dimensioning of individual components, thus avoiding inefficient resource expansion. In particular, as the storage capabilities of the HWS enable the flexible operation of the HP, it is of specific interest to understand and quantify their interdependency, which is therefore investigated in the following.

Fig. 4.12 illustrates the mean upward and downward flexibility values when varying the sizes of both the HP and HWS simultaneously. As previously noted, increasing the size of the HP beyond 150 % of its reference size does not enhance the flexibility of the MES when the HWS size is fixed. However, once the size of the HWS increases, further flexibility gains can be achieved by subsequently increasing the HP size up to a point. Beyond a certain threshold, the system flexibility reaches a plateau, indicating that additional investment in a larger HP does not result in greater flexibility unless accompanied by a corresponding increase in HWS capacity. This threshold can be identified as the ratio of the maximum thermal output power of the HP $\bar{\dot{Q}}_{\text{hp,out}}$ to the thermal capacity of the HWS $C^{\text{des}}_{\text{hws}}$. From Fig. 4.12, it becomes evident that – for this case study – both upward and downward active power flexibility remain unchanged when the HP size increases beyond a relative ratio

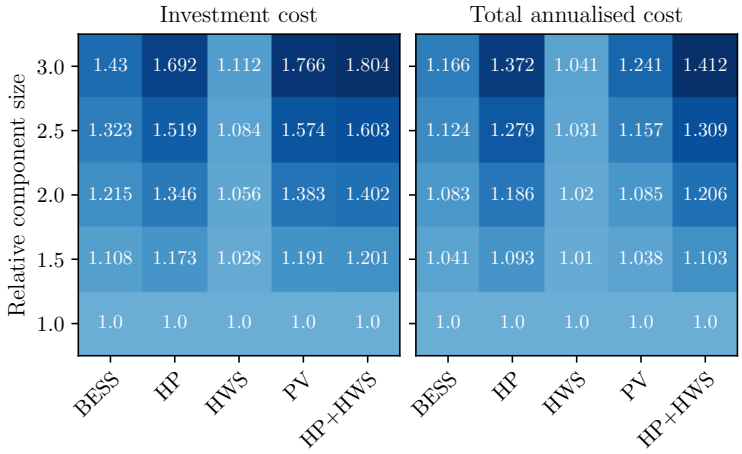

Fig. 4.10: Investment cost and total annualised cost of the multi-energy building relative to the respective cost of the reference case, varying one component size at a time. Note that the total annualised cost does not include remuneration for flexibility provision.

of 1.5, as highlighted by the red boxes. This confirms that increasing the HP size alone, i.e., moving vertically within a column of a fixed HWS size, does not improve the system flexibility further.

By applying linear regression to the identified threshold component sizes indicated by the red boxes, a linear relation between the thermal capacity of the HWS and the thermal output of the HP can be derived as follows:

$$\bar{Q}^{\text{thr}}_{\text{hp,out}} = 5.89 + 0.56\, C^{\text{des}}_{\text{hws}}\ [\text{kW}_{\text{th}}].$$

This means that increasing the size of the HP above this threshold will not result in any flexibility gain, thus requiring investments in a larger HWS capacity. For instance, for the given case study, if the HWS has a capacity of 27 kWh, a HP with a maximum thermal output above 20.5 kW_{th} does not increase the system flexibility. This can be confirmed by the reference case, where a relative HWS size of 2.5 combined with HP sizes above 20.5 kW_{th} shows no improvement in system flexibility. These findings highlight the critical role of thermal storage in enhancing the flexibility of MESs. Therefore, the sizing of HWS must be carefully coordinated with the sizing of the HP to unlock their full active power flexibility potential.

For a more detailed visualisation, Fig. 4.13 presents the total active power flexibility, i.e., the sum of the mean upward flexibility P^{up} and downward flexibility P^{down} values, for varying sizes of HP and HWS using a higher level of granularity. This figure reveals clear plateaus in flexibility for each fixed HWS capacity, beyond which an increase in HP size no longer improves the system flexibility. These plateaus underline the importance of thermal storage capabilities in enabling electrical flexibility of HP.

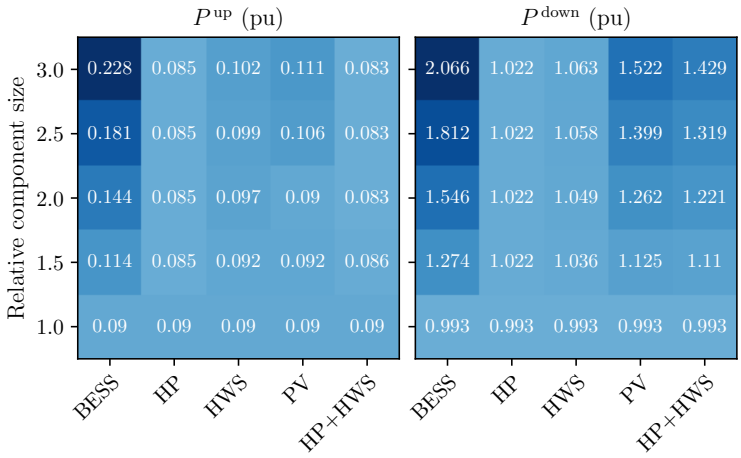

Fig. 4.11: Mean maximum active power flexibility of the multi-energy building relative to the reference case for a duration of 60 min, varying one component size at a time for the *air-to-water HP*. Flexibility per unit is defined as the sum of the mean upward and downward flexibility in the reference case with the *water-to-water heat pump*.

4.4.5 Impact of internal power grid constraints

So far, the analysis has focused on the residential building as a simple case study where internal power grid modelling was omitted due to negligible electrical losses. This allowed for a clear understanding of interdependencies between components in the MES. However, larger entities such as local districts that offer flexibility to the upstream power grid have an underlying power grid, which could significantly affect the technical flexibility potential at the PCC due to voltage constraints or apparent power limits. Therefore, the following investigation introduces the district-scale MES as the second case study, which allows for assessing the impact of the internal power grid on the system flexibility provision. This case study also demonstrates the capabilities of the proposed framework to incorporate and handle internal energy network constraints in the flexibility assessment. Note that to ensure comparability with the residential case study, each building in the district-scale MES uses the same input data and component sizes as the single-building setup presented in Tab. 4.2.

Fig. 4.14 illustrates the impact of increasing the BESS capacity on both the operation and the NOE of the district-scale MES across several time steps. For instance, at $t_{\text{b}} = 346$, different BESS sizes lead to different operating points (OP), which reflect the newly optimised schedules for each design configuration. Moreover, at $t_{\text{a}} = 48$, it can be seen that the maximum active power consumption is limited at 32 kW. This thermal cable limit is reached with a BESS capacity twice that of the reference case. Further increases in the BESS capacity do not result in additional active power consumption. Similarly, the reactive power provision of the system is also constrained by the apparent power limits of the cables, which is represented by the diagonal line at 32 kVA. For comparison, the dashed line

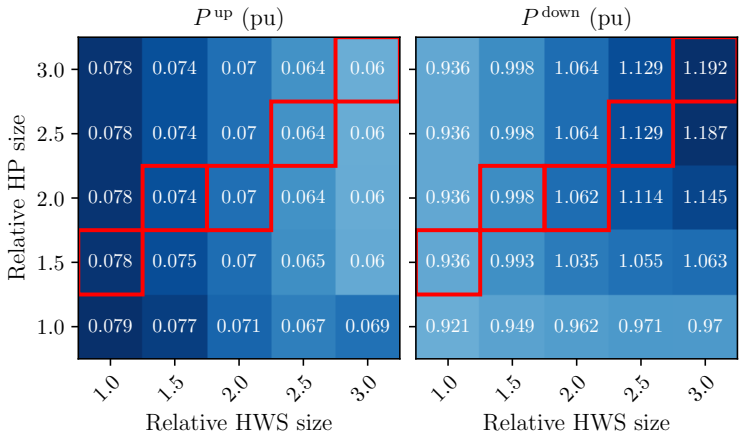

Fig. 4.12: Mean maximum active power flexibility of the multi-energy building relative to the reference case for a duration of 60 min, varying the component sizes of heat pump (HP) and hot water storage (HWS). The red boxes highlight the highest mean flexibility values for each HWS size.

indicates the NOE without internal power grid constraints, which is significantly larger than the internally constrained one. These results clearly show how the underlying electricity network restricts the achievable flexibility at the PCC due to apparent power limits or voltage magnitude limits. This highlights the necessity of incorporating the internal power flow constraints to evaluate the technical electrical flexibility potential at the PCC accurately.

4.4.6 Key findings & discussion

This section investigated the electrical system flexibility of local MESs embedded during the design phase. Through a comprehensive sensitivity analysis, the impact of individual component sizing on the overall system flexibility was quantified, which enables the identification of key components that enhance or hinder operational flexibility. A novel method for calculating flexibility over multiple time steps was introduced, which is dependent on a predetermined reference schedule. This allows for constant flexibility provision and variable durations, which is especially relevant for large consumers who need to submit their schedule one day in advance. One of the key findings is that coupled flexibility from the thermal vector significantly increases active power flexibility, positioning the HP as a linchpin coupling component between electricity and heat in local MESs. A major limiting factor remains the underlying electricity network, due to limits on apparent power and voltage magnitude. In addition to individual components, the interdependence between the size of the HP and the thermal capacity of the HWS tank was quantified through a linear threshold relation, beyond which further increasing the HP size does not improve system flexibility.

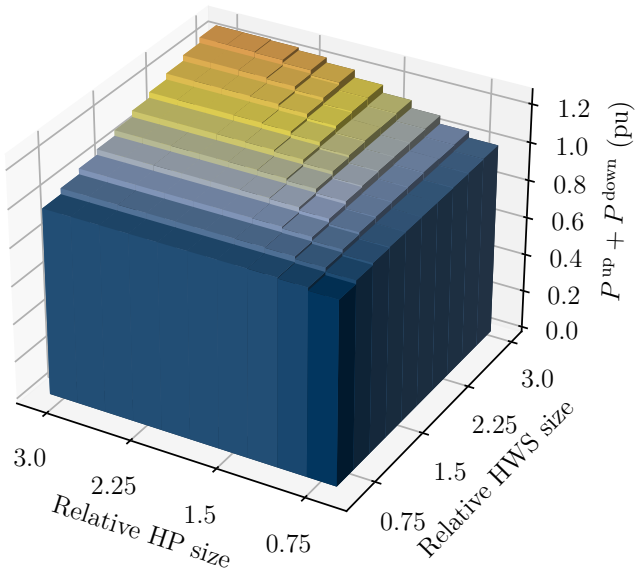

Fig. 4.13: Mean maximum active power flexibility of the multi-energy building relative to the reference case for a duration of 60 min in 3D, varying component sizes of both heat pump (HP) and hot water storage (HWS). Flexibility per unit is defined as the sum of the mean upward and downward flexibility in the reference case.

The presented framework allows for the estimation of the flexibility potential of local MESs at the design stage in relation to a predetermined reference schedule. The identification of technical constraints and component interdependencies is highly relevant for the formulation of technically feasible market bids. To ensure that the identified flexibility is monetised effectively, the specific regulations and technical requirements of suitable markets must be taken into account. This allows for a more informed assessment of economic investment feasibility during the design phase. For instance, active power flexibility could be provided to frequency reserve markets, while reactive power flexibility might be remunerated in emerging reactive power markets. However, if flexibility is monetised through market participation, the reference schedule will change upon activation. As a result, the flexibility potential in subsequent time steps changes, introducing a short-term changing system schedule that is not captured by the current framework. Therefore, while this framework focuses on design-phase flexibility assessment, real-time operational decisions, including activation of tendered flexibility bids, should be addressed in a separate optimisation. For instance, a multi-stage scheduling model accounting for possible market activations and further uncertainty could focus on real-time scheduling optimisation.

Finally, it is important to acknowledge the influence of user behaviour on the flexibility potential of buildings. Variations in occupancy patterns, daily routines, comfort expectations and the willingness to participate in a flexible operation can significantly affect the realisable flexibility potential [129]. Additionally, the current study does not account for thermal building inertia, which could significantly affect the optimal threshold between HP and HWS. By enabling inertia-based control strategies, thermal inertia allows for ad-

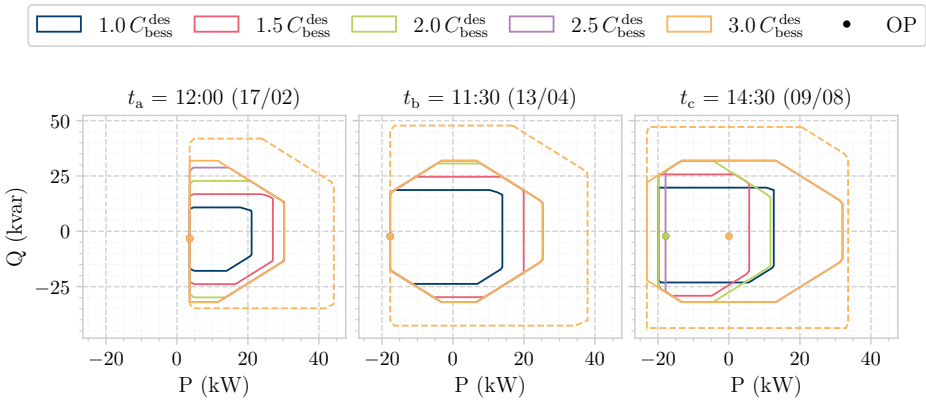

Fig. 4.14: Nodal operating envelope (NOE) at the PCC of the district-scale energy system for a duration of 60 min, illustrated for three representative scenario days and time steps. The BESS capacity is varied relative to its reference size $C_{\text{bess}}^{\text{des}}$. The operating points (OP) correspond to the NOE with the respective BESS size colour, while the dashed line represents the NOE without internal power grid constraints.

ditional thermal load shifting, which could reduce the required HWS capacity. Future research should address these limitations by incorporating user behaviour modelling and thermal inertia analysis.

4.5 Chapter summary

This chapter presented a technical framework to quantify the impact of component design choices on the flexibility provision of local multi-energy systems. By embedding operational flexibility into the design stage, a comprehensive technical understanding of interactions between multi-energy components can be gained, and components that hinder or enable system flexibility can be identified. Moreover, ideal ratios between components can be identified, which can serve as a guideline for flexibility potential assessment during the planning stage. The proposed framework further allows for a quantified flexibility analysis over multiple time steps that is dependent on a predetermined reference schedule while considering different durations of flexibility, which is crucial for large energy systems that participate in the energy market and provide ancillary services. Another trait of the framework is the seamless integration of network constraints, which is crucial for an accurate flexibility estimation at the PCC with the upstream power grid. In order to highlight the capabilities of the framework, two case studies are deployed, both representing local MESs comprising electricity and heat. The results show the importance of explicitly integrating the coupled thermal vector and internal power grid constraints for a realistic flexibility determination of multi-energy systems.

CHAPTER 5

Assessment of local multi-energy systems design under participation in multiple markets

This chapter demonstrates how the explicit consideration of ancillary service provision already in the design phase impacts optimal sizing decisions within local MESs. By accounting for varying future market conditions within a scenario-based uncertainty-aware design analysis, the proposed framework supports identifying the most reliable design choices under multiple scenarios. Besides an energy market, the primary and secondary frequency reserve markets in Germany are explicitly considered, as well as a potential future reactive power market. While the proposed approach is set up to apply within the German market setup; the general concept and modelling approach is widely applicable to other regions or market setups. The presented framework is applied to a district-scale MES as the case study, which illustrates that incorporating these additional revenue streams within the design stage significantly impacts the optimal design of local MESs. Additionally, the influence of future scenarios is assessed via parameter variations, highlighting the importance of uncertainty-aware planning to ensure optimal MES investment decisions.

5.1 Introduction

Energy storage systems are widely viewed as key components that could address certain grid challenges. In particular, concerning the power system, BESSs could be one of the solutions to lift the burden of temporary lines and transformers congestion, dampen the renewable forecast error or provide fast frequency support in low-inertia systems [54]. Besides individual BESSs, local MESs have the technical capability to provide operational flexibility, as demonstrated in Chapter 4. When equipped with appropriate control and communication capabilities, local MESs can provide their operational flexibility to the upstream power grid in ancillary service markets [14–16]. While incorporating these market

revenues improves the economic use case, they could further be a key factor for investment decisions during the design stage of local MESs.

This section is structured as follows: Section 5.1.1 outlines existing literature regarding simultaneous market participation of BESSs, followed by multi-market optimisation studies of MESs in Section 5.1.2. Finally, a summary of the existing literature and the identified gap is presented in Section 5.1.3.

5.1.1 BESS market participation

BESS applications can be distinguished between behind-the-meter (BTM) and front-of-meter (FOM) configurations. BTM systems are typically owned and operated by consumers and primarily used for self-consumption or local flexibility. In contrast, FOM systems are connected directly to the grid and participate in wholesale energy and ancillary service markets [130]. Besides the advantages of BTM BESSs within energy communities as discussed in Section 3.1.1, individual FOM BESSs have gained recent attention in existing literature. These BESSs are increasingly deployed to provide flexibility services across multiple electricity markets due to their inherent technical capabilities [131].

Several studies investigated short-term bidding strategies of FOM BESSs to stack revenues across energy and frequency-balancing markets in an optimal manner, using robust optimisation, stochastic optimisation or model predictive control approaches to incorporate various price and signal uncertainties [132–135]. In commercial applications, BESSs can reduce electricity costs by providing peak shaving and frequency regulation while accounting for capacity degradation [133, 134]. At the distribution grid level, BESSs can support voltage regulation, relieve local congestion, and reduce overall system losses through dynamic pricing schemes [136]. In combination with a solar PV array, the BESS can reduce both economic costs and emissions through a joint energy and frequency-balancing markets bidding strategy [137]. Recently, hybrid BESS configurations that combine BTM and FOM revenue streams have received increased attention. This hybrid setup was investigated for the European market setup with multiple market participation in [138], while [139] proposed a hybrid structure of a community-scale BESS for the Australian market, which further provided hedging against the risk of low market prices. However, these studies focus on the short-term operational benefits without investigating the long-term sizing impact on the BESS.

Besides the operational optimisation by stacking multiple revenues, the sizing and placement of BESSs under market participation has gained recent attention. These studies investigate optimal investment and sizing decisions of BESSs while factoring in multiple revenue streams, degradation, replacement costs and optimal power-to-energy ratios [140–142]. For instance, it was shown that frequency regulation accelerates BESS degradation but improves its profitability, while peak shaving improves grid performance but offers limited economic return [141]. In another study on BTM BESSs providing multiple grid services, a BESS power-to-energy ratio of 1:2 was identified as the optimal ratio to max-

imise revenue in frequency regulation markets [142]. All the above studies show that both FOM and BTM BESSs can economically benefit from accessing revenue streams from multiple markets. However, while these studies investigate the techno-economic benefits of BESSs participating in multiple markets, they typically consider isolated systems rather than BESSs embedded in larger local MES with additional components and coupled energy vectors.

5.1.2 Multi-energy system market participation

While considerable research has been conducted on the optimal operation of local MESs for self-consumption and cost minimisation, such energy systems can also provide flexibility to the upstream power grid, e.g., through participation in ancillary service markets. Recent studies have increasingly explored optimal bidding strategies that enable local MES to minimise operational costs and carbon emissions while offering grid services. These operational strategies under multiple market participation schemes were investigated for various configurations. These include a multi-energy system comprising wind, thermal units and energy storage systems [143], energy-intensive production-inventory planning [110], and industrial prosumers such as manufacturing companies [118] and general industrial electricity consumers [144], as well as for VPPs under uncertainty [145]. In another study, the techno-economic assessment of a university campus operating as an urban VPP in Australia was evaluated, which participated in energy, reserve, demand response and hedging contract markets. The study demonstrates that the participation in ancillary service markets can significantly improve the economic feasibility of distributed DER investments, which can further lead to fast payback periods [146].

Besides focusing on the optimal operation within multiple markets, these additional revenue streams can further be a key factor for investment decisions. This has been demonstrated in multi-energy industrial parks and microgrids [147–150]. For instance, it was shown that participation in frequency-balancing markets has economic benefits for industrial parks [148], while investments in thermal energy storage for frequency-balancing market participation can achieve cost savings of up to 17 % for an industrial MES [149]. These studies demonstrate that revenue streams from ancillary service provision are not only economically beneficial during operation, but can also affect the optimal sizing and selection of energy assets, such as BESS or thermal energy storage. Participation in frequency-balancing markets or responding to real-time pricing signals can economically justify larger storage capacity investments or the deployment of additional flexible components. Consequently, these findings highlight the importance of explicitly incorporating ancillary service markets into the system design phase. By stacking multiple revenue streams from various markets, local MES can identify cost-optimal configurations and thus improve the overall economic performance of system design and operation.

5.1.3 Summary

While existing literature either focuses on the short-term operational scheduling of individual BESSs or embedded MESs, or the design of local energy systems under economic or environmental aspects, a knowledge gap exists in the detailed assessment of potential market revenues during the design phase of local MESs. Specifically, a detailed design analysis for electricity and heat components under reserve market participation has not yet been explored. Moreover, a detailed uncertainty-aware design analysis considering several future market price scenarios to ensure optimal investment decisions has not been investigated. To bridge these gaps, this work presents a design optimisation study that explicitly integrates both energy and reserve markets during the design phase of local MESs comprising BESSs, solar PV arrays, HPs and HWSs. In contrast to prior work, several future market price scenarios are incorporated to assess the most robust design of the local MES, which ensures optimal investment decision-making under uncertainty. Moreover, to highlight the capabilities of the presented framework, the potential impact of a future reactive power market on the optimal local MES design is investigated.

The remainder of this chapter is as follows: Section 5.2 gives an overview of the German market setup, including both spot markets, frequency-balancing reserve markets and a potential future reactive power market. Section 5.3 presents the methodology of the market integration into the design stage, including the scenario-based uncertainty-aware design analysis and the respective constraints. In Section 5.4, the case study is presented. Section 5.5 presents the results for an uncertainty-aware assessment of participating in existing frequency reserve markets on the MES design. Then, Section 5.6 investigates the impact of a potential reactive power market participation. Section 5.7 concludes the chapter.

5.2 Theoretical background on German electricity markets

This section provides a general overview of the German market setup in Section 5.2.1, covering day-ahead (DA) and intraday (ID) spot markets in Section 5.2.2, the frequency containment reserve (FCR) market in Section 5.2.3, the automatic frequency restoration reserve (aFRR) market in Section 5.2.4, and a potential future reactive power market in Section 5.2.5.

5.2.1 General overview

Electricity markets have been designed to facilitate an efficient allocation of production, distribution and consumption of electrical energy. They consist of various sub-markets and include long-term contracts and over-the-counter trades outside of power exchanges. These trades are common among conventional power plants to mitigate their financial

risks due to fluctuating short-term spot market prices. Their prices are constant for periods up to several years, roughly based on expectations of the future spot-market prices. The short-term spot markets, i.e. the day-ahead market and the intraday market, are essential for balancing power generation and demand on short notice. Their time-varying electricity prices incentivise flexible power consumption [151]. Another tool within electricity markets to compensate for sudden imbalances between power generation and demand is frequency-balancing markets, which respond to fluctuations within seconds or minutes to ensure a constant frequency of around 50 Hz.

An overview of the spot markets and frequency reserve markets in Germany is presented in Tab. 5.1, while the gate closure times for the respective markets are illustrated in Fig. 5.1.

Tab. 5.1: Specifications of the intraday (ID), the day-ahead (DA), the frequency containment reserve (FCR) and the automatic frequency restoration reserve (aFRR) capacity and energy markets.

	Intraday	Day-ahead	FCR	aFRR (capacity)	aFRR (energy)
Gate closure time	t - 5 min	12 p.m. (d-1)	8 a.m. (d-1)	9 a.m. (d-1)	d - 25 min
Payment	pay-as-bid (cont.)	pay-as-clear	pay-as-clear	pay-as-bid	pay-as-clear
Block duration	15 min	60 min	4 h	4 h	15 min
Activation time	-	-	30 s	5 min	5 min
Symmetry	-	-	symmetric	up & down	up & down

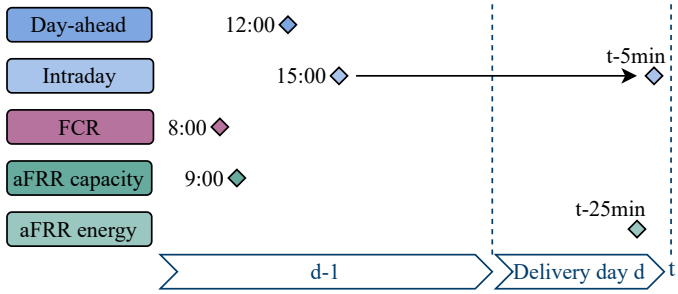

Fig. 5.1: Gate closure times in the day-ahead market, continuous intraday market, FCR and aFRR capacity and energy markets within the German market setup.

Note that the presented study is based on the German electricity market, the proposed framework is versatile and can be applied to other regions and market structures. The considered day-ahead (DA) and intraday (ID) markets as well as the frequency reserve and reactive power markets exist in various countries and electricity systems, even though their specific products and rules might differ. Nevertheless, the methodology with its inherent constraints for sizing, operation and market participation can be adapted to these electricity systems with similar market mechanisms. This highlights the versatility and the broader relevance of the presented framework. In the following, the markets and their respective specifications are described in detail.

5.2.2 Spot markets

Two electricity spot markets are central to short-term trading in Germany: the DA and ID markets. The DA market is the largest electricity trading platform in Europe, accounting for approximately 75 % of the traded electricity volumes on the European Power Exchange (EPEX) spot market [152]. Trading in the DA market is organised in hourly blocks with gate closure at 12 p.m. on the day prior to physical delivery. The DA market is cleared under a uniform pay-as-clear pricing mechanism, i.e., all accepted bids below the marginal clearing price are remunerated at the clearing price [153].

The ID market complements the DA market by enabling continuous trading of 15 min products up to 25 min before delivery. This allows market participants to respond to updated forecasts and accommodate short-term adjustments. Unlike the DA market, the ID market is based on bilateral pay-as-bid transactions without a uniform clearing price. A widely used reference price is the ID3 price, which represents the volume-weighted average price of all trades executed within the three hours before delivery [153].

5.2.3 Frequency containment reserve market

The FCR market is the primary mechanism for frequency-balancing reserve, which is activated when system frequency deviates beyond the deadband of 49.99 Hz and 50.01 Hz. Activation of FCR is fully automatic, non-selective and proportional among all participants within the synchronous FCR cooperation area [151]. Each participating unit must be capable of deploying its contracted reserve capacity fully within 30 s for up to 15 min. The compensation is based on the reserved capacity, with no remuneration for delivered energy. The FCR market is symmetric, which means that bids must include equal upward and downward reserve [154]. Although the standard bid duration time is 4 h, energy-limited assets such as BESS are excepted. While these energy storage assets must remain available for the whole bidding period during which they can be called multiple times, they only need to be able to deliver frequency reserve for at least 1 h consecutively. Moreover, their maximum bid is capped at 80 % of their rated output power to ensure sufficient margin for internal energy storage management [155].

5.2.4 Automatic frequency restoration reserve

The aFRR market serves as the secondary frequency-balancing reserve, which gradually replaces FCR after 30 s, with full activation required within 5 min. The aFRR market is split into a capacity market and an energy market. Participating bids that were accepted in the aFRR capacity market must also submit corresponding bids in the aFRR energy market for at least the awarded amount of the capacity market. However, energy-only market bids

without awarded capacity bids are also allowed, which enables short-term flexibility among market participants [156]. The aFRR capacity market is based on a pay-as-bid remuneration scheme, with BESS typically receiving around 75 % of the maximum accepted price [157].

In contrast to FCR, the aFRR market is not energy-neutral, but separate products exist for upward and downward frequency response. Participants must start ramping up within 30 s and reach full activation within 5 min. After a defined recovery time, they must be capable of repeating the activation cycle. The aFRR capacity auction is cleared once per day and divided into six four-hour blocks. In contrast, the energy market operates on 15 min intervals, with real-time dispatch signals issued every four seconds. Although the activated energy differs every four seconds, a single uniform clearing price per 15 min interval is determined ex-post based on the aggregated activated energy volume.

5.2.5 Reactive power market

Conventional generators can vary their power factor to locally supply reactive power for voltage stability. As the number of conventional generators will decrease in the future, a growing need for reactive power is expected to maintain voltage levels within acceptable limits [158]. To address this, market-based mechanisms for reactive power are planned and introduced, e.g., a remuneration scheme targeting the high-voltage grid in Germany [159, 160]. The market-based procurement of reactive power began in April 2025 in Northeast Germany, led by 50 Hertz and divided into five regions [161]. The tendering process concluded in March 2025, with successful offers agreeing to contracts that compensate for reactive power provision exceeding standard grid connection requirements [162]. As transporting reactive power over long distances causes higher losses, and voltage stability is inherently a local phenomenon, decentralised solutions are needed for reactive power provision [163]. Local MESs could play a key role in providing reactive power locally. Several studies explored how active distribution networks can support upstream grids through reactive power provision [16, 17]. In addition to technical capabilities, local reactive power markets could reduce the need for dedicated compensation devices by leveraging existing systems to provide reactive power.

5.3 Methodology

In this section, the methodology of market integration is outlined. First, Section 5.3.1 presents the framework of the scenario-based uncertainty-aware design analysis. Second, the detailed constraints for frequency reserve market participation are outlined in Section 5.3.2. Third, the generation of spot market and frequency reserve market price scenarios is outlined in Section 5.3.3, followed by the integration of the future reactive power market in Section 5.3.4. Finally, the objective function is presented in Section 5.3.6.

5.3.1 Scenario-based uncertainty-aware design analysis

The scenario-based uncertainty-aware design analysis, illustrated in Fig. 5.2, is described in the following. In Fig. 5.2 (a), a set of key input parameter combinations is defined, and their values are systematically varied (for more information on the chosen parameters and their values, see Tab. 5.4). These parameter combinations represent plausible future scenarios with uncertain market conditions, such as electricity prices or achievable revenues limited by forecasting. For each future scenario, which is characterised by one unique parameter set, a two-stage stochastic optimisation is performed to jointly determine the optimal system design and operational decisions.

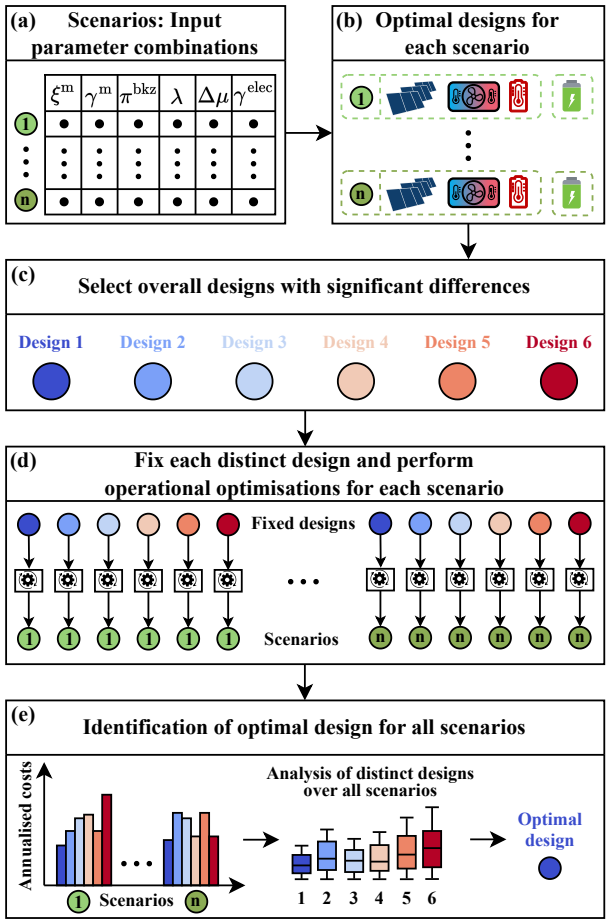

Fig. 5.2: Flowchart of the uncertainty-aware design analysis. The revenue factor ξ^m, the frequency reserve price γ^m, the building cost subsidy π^{bkz}, the volatility factor λ, the afternoon price shift $\Delta\mu$ and the electricity price factor γ^{elec} as the input parameters for the future scenarios are explained in Section 5.5.1.2.

Each optimisation results in a scenario-specific optimal design for all sizing components of the local MES (first stage), as shown in Fig. 5.2 (b). For example, 144 parameter combinations result in 144 distinct optimisation problems, each of which produces building-specific component sizes and one shared community BESS, and the corresponding operational schedules. Since some of these designs are similar in component sizes and cost performance, a representative subset of *distinct designs* is selected in Fig. 5.2 (c), based on maximal pairwise distances in the design space to ensure a diverse representation. Each selected design corresponds to the optimal solution of a particular future scenario.

In the next step, depicted in Fig. 5.2 (d), the operational performance of each distinct design is evaluated across all future scenarios. By fixing the design and re-optimising only the operational variables for each scenario, this systematic evaluation reveals how well each distinct design performs when future conditions differ from those it was originally optimised for. This step is critical to assess the performance of different designs under deep uncertainty where the likelihood of future scenarios is unknown. Finally, Fig. 5.2 (e) visualises the annualised costs for each design across all future scenarios using boxplots. This allows for a comparative assessment of economic performance across all future scenarios and identifies the optimal design based on different objectives, e.g., minimising the expected cost or the worst-case cost.

This framework enables an uncertainty-aware evaluation of optimal component sizing, while capturing sensitivities of component sizing decisions to varying market assumptions and future uncertainty. The analysis framework further supports decision-making under different risk preferences, such as risk-neutral expected cost minimisation or risk-averse worst-cost minimisation.

5.3.2 Frequency reserve market constraints

In this section, the governing equations and underlying constraints for participating in the frequency reserve (FR) markets are presented. In the following, the following sign convention applies: Positive values for the active power P_c of component c represent generation, while negative values represent demand. Similarly, upward services $P_c^{\uparrow}$, which correspond to increasing generation or decreasing demand, are represented as positive values, whereas downward services $P_c^{\downarrow}$, which reflect decreasing generation or increasing demand, are denoted as negative values.

5.3.2.1 Component participation constraints

Given the activation time τ_m, the duration d_m of market m, as well as the classified markets $m \in \mathcal{M}$ for each component $c \in \mathcal{C}$ as listed in Tab. 5.3, the following constraints for

market-participating components apply:

$$P^{\uparrow}_{c,s,t} = \sum_{m \in \mathcal{M}} P^{\uparrow}_{c,m,s,t} \,, \qquad c \in \mathcal{C},\ s \in \mathcal{S},\ t \in \mathcal{T}, \tag{5.1}$$

$$P^{\downarrow}_{c,s,t} = \sum_{m \in \mathcal{M}} P^{\downarrow}_{c,m,s,t} \,, \qquad c \in \mathcal{C},\ s \in \mathcal{S},\ t \in \mathcal{T}. \tag{5.2}$$

$$P^{\text{base}}_{c,s,t} = P_{c,s,t} + \sum_{m \in \mathcal{M}} P^{\uparrow,\text{act}}_{m,s,t} + P^{\downarrow,\text{act}}_{m,s,t} \,, \qquad c \in \mathcal{C},\ s \in \mathcal{S},\ t \in \mathcal{T}, \tag{5.3}$$

$$P^{\uparrow}_{c,s,t} \leq P^{\text{max}}_{c} - P^{\text{base}}_{c,s,t} \,, \qquad c \in \mathcal{C},\ s \in \mathcal{S},\ t \in \mathcal{T}, \tag{5.4}$$

$$P^{\downarrow}_{c,s,t} \geq P^{\text{min}}_{c} - P^{\text{base}}_{c,s,t} \,, \qquad c \in \mathcal{C},\ s \in \mathcal{S},\ t \in \mathcal{T}, \tag{5.5}$$

$$P^{\uparrow}_{c,s,t} \leq \left(1 - \gamma_{\text{p}}\right) P^{\text{max}}_{c} \,, \qquad c \in \mathcal{C},\ s \in \mathcal{S},\ t \in \mathcal{T}, \tag{5.6}$$

$$P^{\downarrow}_{c,s,t} \geq \left(1 - \gamma_{\text{p}}\right) P^{\text{min}}_{c} \,, \qquad c \in \mathcal{C},\ s \in \mathcal{S},\ t \in \mathcal{T}, \tag{5.7}$$

$$\text{with } \left[P^{\uparrow}_{c,s,t}, P^{\uparrow}_{c,m,s,t}\right] \geq 0 \,, \qquad m \in \mathcal{M},\ c \in \mathcal{C},\ s \in \mathcal{S},\ t \in \mathcal{T}, \tag{5.8}$$

$$\text{with } \left[P^{\downarrow}_{c,s,t}, P^{\downarrow}_{c,m,s,t}\right] \leq 0 \,, \qquad m \in \mathcal{M},\ c \in \mathcal{C},\ s \in \mathcal{S},\ t \in \mathcal{T}. \tag{5.9}$$

As the HP charges the HWS, both components participate jointly in the FR markets, since their flexible operation is inherently coupled, as shown in Section 4.4.4. $P^{\uparrow}_{c}$ and $P^{\downarrow}_{c}$ denote the total upward and downward bids submitted to markets in which component c is participating. The parameter P^{min}_{c} defines the minimum active power and thus the maximum absolute power consumption, while P^{max}_{c} defines the maximum active power generation. P^{base}_{c} represents the nominal baseline operation of component c without any reserve market participation, for instance, a BESS that charges and discharges solely based on internal energy system needs and prices. Equations (5.1) and (5.2) define the total aggregated upward and downward market bids. The resulting total active power of each component, accounting for activation in energy markets, e.g., aFRR energy market, is expressed in (5.3). The aggregated upward and downward bids across all markets are constrained by the physical power limits of the component via (5.4) and (5.5). A security margin γ_{p} is incorporated into constraints (5.6) and (5.7), aligning with the German regulatory requirements, stating that market bids may not exceed 80 % of the rated power of energy storage systems. This margin ensures operational headroom for energy management measures during activations [155], thus $\gamma_{\text{p}} = 20\,\%$. The notation defined in (5.8) and (5.9) requires upward bids to be expressed as positive values, and downward bids as negative values.

Furthermore, for reserve markets with a bidding duration longer than the model time step Δt, it must be assured that the market bids are uniform throughout the bidding period k. Let $\mathcal{T}_k \subseteq \mathcal{T}$ denote the set of time steps associated with bidding period k of market m, then the following constraint applies:

$$P^{\uparrow}_{\text{pcc},m,s,t_k} = P^{\uparrow}_{\text{pcc},m,s,k} \,, \qquad m \in \mathcal{M},\ k \in \mathcal{K}_m,\ s \in \mathcal{S},\ t_k \in \mathcal{T}_k, \tag{5.10}$$

$$P^{\downarrow}_{\text{pcc},m,s,t_k} = P^{\downarrow}_{\text{pcc},m,s,k} \,, \qquad m \in \mathcal{M},\ k \in \mathcal{K}_m,\ s \in \mathcal{S},\ t_k \in \mathcal{T}_k. \tag{5.11}$$

Under the current market structure, both the FCR and aFRR capacity markets operate based on bidding blocks of 4 h. With a model time step length of $\Delta t = 0.25\,\text{h}$, each bid-

ding block k corresponds to a set of time steps $\mathcal{T}_k \subseteq \mathcal{T}$, for instance, $\mathcal{T}_1 = \{1,2,...,16\}$. It is important to distinguish between the market bids of individual components and the aggregated market bid of the overall MES at the PCC. While individual component can vary their bids within the bidding period, e.g., due to operational constraints or availability, the aggregated bid submitted by the MES must remain constant throughout the full duration of each bidding block. Furthermore, in line with German prequalification requirements, units offering FCR or aFRR with limited energy capacity, such as BESS, must be capable of continuously providing the contracted reserve power for at least 1 h within each 4 h bidding block [155]. This requirement allows storage systems access to frequency reserve markets while effectively utilising their active power capabilities.

5.3.2.2 Storage system constraints

In this section, additional constraints for energy storage systems that participate in multiple markets simultaneously are presented. To ensure reliable operation, energy storage systems must maintain their SoC within specified upper and lower bounds during activation and avoid over-committing with market bids. Therefore, the following additional constraints apply:

$$\sum_{m\in\mathcal{M}} P^{\uparrow}_{c,m,s,t}\, d_m + P^{\text{base}}_{c,s,t}\,\Delta t \leq \left(\text{SoC}_{c,s,t} - \text{SoC}^{\min}_{c}\right)\left(1-\gamma^{\text{soc}}_{c}\right), \quad c\in\mathcal{C}_{\text{st}},\, s\in\mathcal{S},\, t\in\mathcal{T}, \tag{5.12}$$

$$\sum_{m\in\mathcal{M}} P^{\downarrow}_{c,m,s,t}\, d_m + P^{\text{base}}_{c,s,t}\,\Delta t \geq \left(\text{SoC}^{\max}_{c} - \text{SoC}_{c,s,t}\right)\left(1-\gamma^{\text{soc}}_{c}\right), \quad c\in\mathcal{C}_{\text{st}},\, s\in\mathcal{S},\, t\in\mathcal{T}. \tag{5.13}$$

Here, d_m denotes the maximum duration within a bidding period in market m that the active power deviation must be maintained. The parameter γ^{soc}_{c} defines the relative security margin at the upper and lower SoC limits, which are constrained by $0 \leq \gamma^{\text{soc}}_{c} \leq 1$, and set to be $\gamma^{\text{soc}}_{c} = 10\,\%$.

To limit BESS degradation, a daily cycle limit is incorporated. Since the representative scenarios days $s \in \mathcal{S}$ are assumed to be cyclic, i.e., the SoC at the beginning of the day equals the SoC at the end, only the charging energy is counted towards the cycle limit. To account for energy throughput from FCR provision, a heuristic ratio $\xi^{\text{act}}_{\text{fcr}}$ is introduced, which represents the expected relationship between FCR activation energy and tendered FCR capacity. This heuristic factor, predetermined based on historical data, approximates the expected energy associated with FCR activations:

$$\begin{aligned}&\sum_{t\in\mathcal{T}}\left(\frac{1}{\eta^{\text{out}}_{\text{bess}}} P^{\text{out}}_{\text{bess},s,t} + \kappa_{\text{bess}}\,\text{SoC}_{\text{bess},s,t} + \xi^{\text{act}}_{\text{fcr}}\, P^{\uparrow}_{\text{fcr},s,t}\right)\Delta t \\ &\leq N^{\text{lim}}_{\text{cyc}}\left(\text{SoC}^{\max}_{\text{bess}} - \text{SoC}^{\min}_{\text{bess}}\right),\end{aligned} \tag{5.14}$$

which applies to all representative scenario days $s \in \mathcal{S}$.

5.3.2.3 Internal power grid constraints

The aggregated bids of each building must be constrained to account for the thermal limits of the power grid. Let $\mathcal{L}_{\text{tr}}$ denote the set of transformers, and C_{bd} represent the set of components located at each building connected to transformer ik. The apparent power rating S_{ik}^{rate} of the connecting transformer ik at each building limits the sum of all corresponding bids as follows:

$$\sum_{c \in \mathcal{C}_{\text{bd}}} P_{c,s,t}^{\text{base}} - P_{c,s,t}^{\uparrow} \leq S_{ik}^{\text{rate}}, \qquad ik \in \mathcal{L}_{\text{tr}},\ s \in \mathcal{S},\ t \in \mathcal{T}, \tag{5.15}$$

$$\sum_{c \in \mathcal{C}_{\text{bd}}} P_{c,s,t}^{\text{base}} - P_{c,s,t}^{\uparrow} \geq -S_{ik}^{\text{rate}}, \qquad ik \in \mathcal{L}_{\text{tr}},\ s \in \mathcal{S},\ t \in \mathcal{T}, \tag{5.16}$$

$$\sum_{c \in \mathcal{C}_{\text{bd}}} P_{c,s,t}^{\text{base}} + P_{c,s,t}^{\downarrow} \leq S_{ik}^{\text{rate}}, \qquad ik \in \mathcal{L}_{\text{tr}},\ s \in \mathcal{S},\ t \in \mathcal{T}, \tag{5.17}$$

$$\sum_{c \in \mathcal{C}_{\text{bd}}} P_{c,s,t}^{\text{base}} + P_{c,s,t}^{\downarrow} \geq -S_{ik}^{\text{rate}}, \qquad ik \in \mathcal{L}_{\text{tr}},\ s \in \mathcal{S},\ t \in \mathcal{T}, \tag{5.18}$$

Additionally, in a radial distribution grid, both the aggregated market bids and the baseline active power contributions of all components connected to the buses downstream of each branch must be considered to ensure that their thermal limits are not exceeded. Let $\mathcal{L}$ be the set of all branches, and let $c \in \mathcal{C}_{\text{ds},ik}$ denote the set of all components located downstream of branch ik, then the thermal limit of each branch is enforced by the following constraints:

$$\sum_{c \in \mathcal{C}_{\text{ds},ik}} P_{c,s,t}^{\text{base}} - P_{c,s,t}^{\uparrow} \leq S_{ik}^{\text{rate}}, \qquad ik \in \mathcal{L},\ s \in \mathcal{S},\ t \in \mathcal{T}, \tag{5.19}$$

$$\sum_{c \in \mathcal{C}_{\text{ds},ik}} P_{c,s,t}^{\text{base}} - P_{c,s,t}^{\uparrow} \geq -S_{ik}^{\text{rate}}, \qquad ik \in \mathcal{L},\ s \in \mathcal{S},\ t \in \mathcal{T}, \tag{5.20}$$

$$\sum_{c \in \mathcal{C}_{\text{ds},ik}} P_{c,s,t}^{\text{base}} + P_{c,s,t}^{\downarrow} \leq S_{ik}^{\text{rate}}, \qquad ik \in \mathcal{L},\ s \in \mathcal{S},\ t \in \mathcal{T}, \tag{5.21}$$

$$\sum_{c \in \mathcal{C}_{\text{ds},ik}} P_{c,s,t}^{\text{base}} + P_{c,s,t}^{\downarrow} \geq -S_{ik}^{\text{rate}}, \qquad ik \in \mathcal{L},\ s \in \mathcal{S},\ t \in \mathcal{T}. \tag{5.22}$$

5.3.3 Future price scenario generation

This section outlines the generation of future price scenarios for both frequency reserve markets and the spot market. To assess the effect of potential future price developments on the optimal design of local MES, multiple future scenarios are considered that aim to capture the uncertainty of future revenue streams. The following presents the methodology used to derive volatile wholesale electricity prices and adjusted frequency reserve prices. All future scenarios are based on a reference price year derived from historical data.

5.3.3.1 Spot market price scenarios

With the increasing penetration of RES, particularly solar PV, spot market prices are expected to become more volatile, in particular with negative prices during midday peak solar generation and higher prices during morning and evening demand peaks (the so-called *duck-curve*). This trend is already observable in Australia [164, 165] and Europe [10, 166], and is expected to becoming more pronounced to the the continuous adoption of RES.

To reflect this development, the future time series of the spot market prices incorporate an increased volatility factor and a downward shift in prices during solar peak hours (10 a.m. to 4 p.m.), which is modelled using a parabolic function. The electricity price for each future scenario $\omega \in \Omega$ is then defined as follows:

$$\begin{aligned} \pi_{\mathrm{el},s,t}^{\mathrm{buy},\omega} = \gamma^{\mathrm{elec}} \overline{\pi}_{\mathrm{el},s}^{\mathrm{ref}} + \lambda(\pi_{\mathrm{el},s,t} - \overline{\pi}_{\mathrm{el},s}^{\mathrm{ref}}) \\ + b_{\mathrm{ps}} \cdot \xi_{s,t} \cdot \Delta\pi \cdot Y, \quad s \in \mathcal{S},\ t \in \mathcal{T}. \end{aligned} \tag{5.23}$$

Here, $\pi_{\mathrm{el},s,t}^{\mathrm{buy},\omega}$ denotes the variable electricity price for each representative scenario day s and time step t in future price scenario ω. $\overline{\pi}_{\mathrm{el},s}^{\mathrm{ref}}$ refers to the mean electricity price of the reference year for representative scenario day s, which can be uniformly decreased or increased using the electricity price factor γ^{elec}. The volatility factor λ scales the standard deviation of the price signal, with values $\lambda > 1$ representing increased price variability. The binary variable b_{ps} equals one during peak solar hours (10 a.m. to 4 p.m.) and zero otherwise. $\xi_{s,t}$ is a parabolic function applied during these peak solar hours to represent the impact of solar generation. Additionally, the stochastic term $Y \sim \mathcal{N}(1, 0.1^2)$ introduces normally distributed randomness around the base level, representing further market uncertainty. The resulting spot market price time series used in the scenario analysis is illustrated in Fig. 5.5 in Section 5.5.1.

5.3.3.2 Frequency reserve price scenarios

Due to the increasing penetration of BESSs in the power system and their accompanying participation in FR markets, the prices for FCR and aFRR markets are expected to decline in the coming years as a result of market saturation [167]. In contrast to the wholesale electricity prices, which show a clear trend towards increased volatility and the duck-curve pattern, the potential average reduction in FR market prices is captured using a simple scaling factor:

$$\pi_{s,t}^{m,\omega} = \gamma^{m} \cdot \pi_{s,t}^{m,\mathrm{ref}}, + b_{\mathrm{ps}} \cdot \xi_{s,t} \cdot \Delta\pi \cdot Y, \qquad s \in \mathcal{S},\ t \in \mathcal{T}, \tag{5.24}$$

where γ^{m} represents the FR price factor to decrease or increase the mean reference price $\pi_{s,t}^{m,\mathrm{ref}}$.

5.3.4 Reactive power market

5.3.4.1 Potential future market-based procurement

Despite current plans for a reactive power market in Germany, no standardised price signals are available in the literature yet. While the remuneration for the market-based procurement in the Northeast of Germany is capped at 0.7 ct/kvarh [168], no detailed data is available regarding the actual market outcome. Existing bilateral agreements range from 0.08 ct/kvarh to 0.227 ct/kvarh [169]. To account for potential future price developments, an assumed price range between 0.1 ct/kvarh and 0.7 ct/kvarh is adopted.

This work adapts a time-dependent reactive power requirement through a local signal, indicating periods during which reactive power absorption or injection is required. During peak solar hours (11 a.m. - 3 p.m.), over-voltage issues could be mitigated by absorbing reactive power [16], while voltage drops during peak demand evening hours could be mitigated by reactive power injection. The applied reactive power signal is depicted in Fig. 5.11. Note that due to the lack of publicly available data, the reactive power signal is arbitrarily chosen. This signal could be based on local voltage measurements and enforced through an automatic voltage-control scheme, which may be coordinated by the transmission system operator (TSO).

5.3.4.2 Reactive power capabilities

The reactive power capabilities of the electricity-consuming components are shown in Fig. 5.3. It is assumed that the three electricity-consuming components BESS, solar PV, and HP are equipped with power converters, which can adjust their reactive power capabilities. The BESS has full four-quadrant capabilities, while the solar PV array is assumed to adjust its reactive power within its power factor limits of $\cos\varphi \geq 0.9$, while the heat pumps' power factor limit is set to $\cos\varphi \geq 0.95$, with an implemented relative part-load limit of $P_{\text{min}} = 20\,\%$ of the maximum active power output.

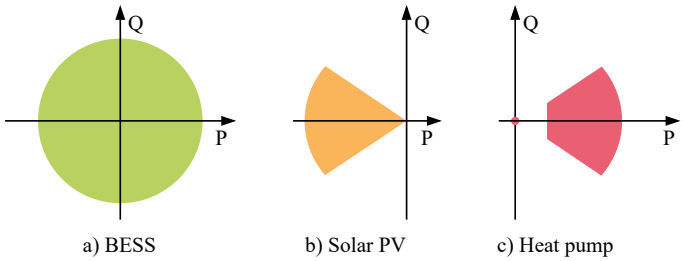

Fig. 5.3: Active power (P) and reactive power (Q) capabilities of the considered electricity-consuming components: BESS, solar PV and HP. Negative values indicate generation, and positive values indicate consumption.

5.3.5 Iterative second-order cone program algorithm

The introduced SOCP formulation in Section 2.1.7.2 relaxes the current magnitude constraint in (2.9h), which incentivises increased non-physical currents for negative active or reactive power prices, leading to non-exact solutions [170]. To address this issue, an iterative second-order cone program (ISOCP) algorithm first introduced in [171] is deployed. The ISOCP algorithm successively reduces the relaxation error e_{ik}, which represents the difference between the two sides of the inequality constraint presented in (2.9h), defined as follows:

$$e_{ik} = p_{ik}^2 + q_{ik}^2 - \lambda_{ik} W_i \,. \tag{5.25}$$

Note that the relaxation error is smaller or equal zero. First, the initial problem with the conventional SOCP formulation is solved, for which the absolute value of the exactness error across all branches within the local MES is calculated. If the maximum absolute value across all branches exceeds the predefined tolerance value $tol = 0.001$, the iterative algorithm as described in Algorithm 5.1 starts. With each iteration, the error is moving closer to zero based on (5.26), with $\gamma \leq 1$ determining the convergence speed [172]. The power flow solution at $(n+1)^{th}$ iteration is obtained by a change of variable in (5.27), linking the decision variables of the prior iteration x^n with the results from the current iteration x^{n+1}.

$$e_{ik}^{n+1} \geq \gamma e_{ik}^{n}, \tag{5.26}$$

$$x^{n+1} = x^n + \alpha \Delta x^{n+1}. \tag{5.27}$$

Here, the acceleration factor α is set to 1, and Δx^{n+1} represents the decision variables determined at the current iteration.

Algorithm 5.1: ISOCP algorithm

Data: Power grid model, grid constraints, component constraints, representative input data, $tol = 0.001$, $\alpha = 1.0$, $\gamma = 0.85$
Output: Active and reactive power dispatch
Init: Iteration count, $n = 1$
Calculate: Optimal design and operation of original problem using (2.9), (5.29), component constraints
Calculate: $e_{ik}, \forall ik \in \mathcal{L}_k$ using (5.25)
while $\max(|e_{ik}|) \geq tol$ **do**
  Update iteration counter: $n = n + 1$
  Obtain linearised constraints using (5.28)
  Solve (n+1)$^{\text{th}}$ iteration of original problem using (2.9), (5.29), component constraints and (5.28) for Δx^{n+1}
  Update problem variables: $x^{n+1} = x^n + \alpha \Delta x^{n+1}$
  Calculate $e_{ik}^{n+1}, \forall ik \in \mathcal{L}_k$
  Calculate $\max(|e_{ik}^{n+1}|)$
end

As the error defined in (5.26) is nonlinear, it is linearised using first-order Taylor series approximation in (5.28), resulting in the following linear constraints:

$$2p_{ik}^{(n)}\Delta p_{ik}^{(n+1)} + 2q_{ik}\Delta q_{ik}^{(n+1)} - \Lambda_{ik}^{(n)}\Delta w_i^{(n+1)} - w_i^n \Delta\Lambda_{ik}^{(n+1)} \geq (\gamma - 1)e_{ij}^n. \tag{5.28}$$

These constraints are incorporated in the original problem formulation. The details of the algorithm are presented in Algorithm 5.1. For more information and further analysis on the proof of convergence, see [171, 172].

5.3.6 Objective function

The objective function of the framework is to minimise the TAC, with positive values representing costs, and negative values corresponding to revenues. The objective function accounts for the initial investment cost for the components to be sized and their corresponding maintenance costs (first line), costs for buying electricity and revenue for selling electricity (second line) at the wholesale energy market, revenues from participating in the reserve markets (third line), as well as revenues from reactive power provision (fourth line). Subject to the above-listed constraints in (5.1)–(5.24), as well as the respective component constraints as presented in Section 2.1, the objective function of the model is to be minimised as follows:

$$\begin{aligned}
\min \Bigg\{ & \sum_{c\in\mathcal{C}} \left(C_c^{\text{inv}} \cdot k_c^{\text{ann}} + \pi_c^{\text{fix}} \cdot C_c^{\text{inv}} \right) \\
& + \sum_{s\in\mathcal{S}} w_s \sum_{t\in\mathcal{T}} \left(\pi_{\text{el},s,t}^{\text{buy}} \cdot P_{\text{pcc},s,t}^{\text{in}} - \pi_{\text{el},s,t}^{\text{sell}} \cdot P_{\text{pcc},s,t}^{\text{out}} \right) \Delta t \\
& - \sum_{s\in\mathcal{S}} w_s \sum_{t\in\mathcal{T}} \sum_{m\in\mathcal{M}} \xi^m \cdot \cdot P_{\text{pcc},s,t}^m \cdot \Delta t \\
& - \sum_{s\in\mathcal{S}} w_s \sum_{t\in\mathcal{T}} \pi_{s,t}^{\text{q}} Q_{\text{pcc},s,t} \Delta t \Bigg\},
\end{aligned} \tag{5.29}$$

$$\text{with} \quad k_c^{\text{ann}} = \frac{(1+r)_c^n \cdot r}{(1+r)_c^n - 1}. \tag{5.30}$$

Here, $\mathcal{S}$ denotes the set of representative scenario days, while $\mathcal{T}$ represents the set of time steps with a specified time step length of Δt in hours. The set of reserve markets the local MES can participate in is denoted by $\mathcal{M}$. Each representative scenario day $s \in \mathcal{S}$ has a corresponding weighting factor w_s which reflects its statistical occurrence over the year. The investment cost of each component C_c^{inv} is annualised using the factor k_c^{ann}, which accounts for the interest rate r and the component lifetime n_c, resulting in equal annual payments over the investment period. The annual fixed cost π_c^{fix}, which includes maintenance and service, is assumed to be a fraction of the overall investment cost C_c^{inv} of the respective component. All the aforementioned component-specific parameters are given in Tab. 5.2.

The variable cost of buying electrical energy, denoted by $P_{\text{pcc}}^{\text{in}} \Delta t$, is priced at $\pi_{\text{el}}^{\text{buy}}$, while

the revenue for selling electrical energy, denoted as $P_{\text{pcc}}^{\text{out}} \Delta t$, is determined by $\pi_{\text{el}}^{\text{sell}}$. Both buying and selling electricity are carried out at the wholesale spot market. Participation in reserve markets is modelled through the tendered bid $P_{\text{pcc},s,t}^{m}$ at market m. The corresponding revenue is determined by the market price $\pi_{s,t}^{m}$ for the respective market product. To account for imperfect foresight in forecasting market prices and activation volumes, a heuristic reduction factor ξ^{m} is applied. This factor incorporates the expected share of the theoretical market revenue that is realised, with $\xi^{m} = 1$ representing perfect foresight, and lower values reflecting smaller market revenues due to forecast uncertainty. Additionally, the framework includes potential remuneration for reactive power provision through the reactive power exchanged at the PCC $Q_{\text{pcc},s,t}$, and the corresponding price signal $\pi_{s,t}^{\text{q}}$. Further details on the two-stage stochastic problem formulation and its mathematical implementation can be found in [40].

5.4 Case study: Local multi-energy system

This section presents the local district-scale MES comprising electricity and heat as energy carriers, which is adopted as the case study. The single-phase representation of the internal power grid, the district heating and the overall structure of the case study are illustrated in Fig. 5.4, together with the internal structure of each building.

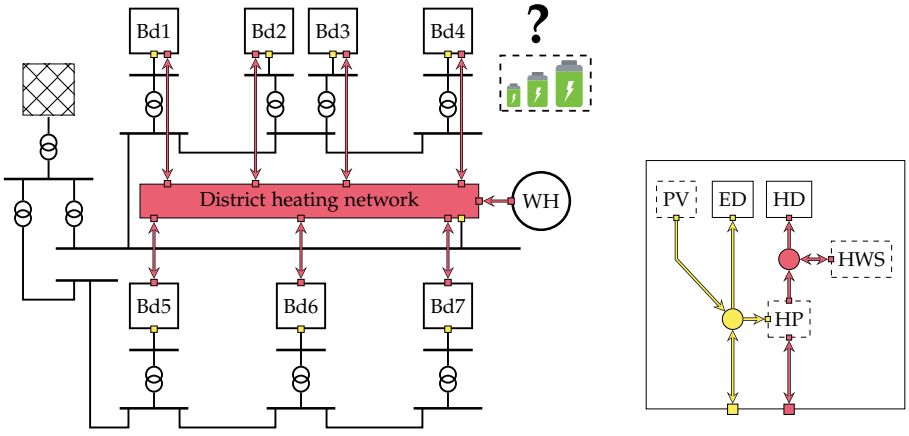

(a) Local multi-energy system **(b)** Internal building structure

Fig. 5.4: Local multi-energy system (a) with seven buildings (Bd) which are interconnected through an internal power grid and a district heating network supplied by waste heat (WH). The electric demand (ED) of each building is supplied by the grid supply and the rooftop solar PV array. The heat demand (HD) is supplied by the heat pump (HP) and supported by the hot water storage (HWS). The components outlined with dashed lines are to be sized. A shared community BESS is to be sized and installed at one of the bus bars of the buildings.

The PCC with the upstream power grid is connected to the local MES at the 110 kV level. The voltage is transformed to 10 kV and distributed via two feeders, each supplying

several buildings. Within each building, the solar rooftop PV array, HP and HWS are sized, as illustrated in Fig. 5.4b by the dashed lines. Furthermore, a shared community BESS is sized and allocated to one of the seven buses of the connected buildings. The buildings comprise a mix of office and laboratory spaces, reflecting diverse load profiles.

The component-specific parameters and assumed lifetimes are listed in Tab. 5.2. In the following, the presented case study is applied to two different applications. The input data specific to each case study application is given at the beginning for the respective application section, in Section 5.5.1 and Section 5.6.1. Note that the aforementioned data and parameters apply to both applications within this chapter. The first case study application investigates the impact of frequency reserve market participation, including an uncertainty-aware design analysis. In order to assess potential future market revenues, the second case study application analyses the impact of a reactive power market on the optimal design of local MESs. These two applications demonstrate the capabilities of the proposed methodology, which can be applied to any market setup, such as a different market structure based on other regulations or a future market, such as an inertia market or a locational flexibility market at the distribution level.

Tab. 5.2: Techno-economic component parameter values for investment costs C^{inv}, relative fixed costs π^{fix} and lifetime n.

Parameter	Symbol	2h-BESS	Heat pump	Solar PV array	HWS
Investment cost	C^{inv}	457 €/kWh	1300 €/kW_{th}	941 €/kWp	97 €/kWh
Annual fixed cost	π^{fix}	2.5 %	1.1 %	1.0 %	1.0 %
Lifetime	n	10 a	25 a	25 a	10 a
Sources	-	[88, 125]	[125, 126]	[88]	[125, 127]

For the remainder of this chapter, the following component models from Chapter 2 are used: The BESS is modelled via (2.1), the solar PV array is integrated using (2.2), the linear HP model is implemented using (2.4) with a minimum relative part-load of 20 %, the HWS is modelled via (2.6), and the heating network is modelled via the energy vector balance equations (2.7). While the internal power grid in Section 5.5 is represented by the LinDistFlow approximation using (2.10), the ISOCP algorithm from Algorithm 5.1 is deployed within Section 5.6.

5.5 Application 1: Impact of frequency reserve markets

This section assesses the sizing of the local MES under DA and reserve markets (FCR, aFRR capacity) participation. Section 5.5.1 outlines the input data and key assumptions. In Section 5.5.2, the optimal component designs and their operation are presented, followed by a sensitivity analysis regarding spot market and reserve market prices and frequency reserve market participation in Section 5.5.3. Section 5.5.4 investigates an uncertainty-aware design assessment of components across various future scenarios, which was presented in Section 5.3.1. Finally, the key findings and a brief discussion are presented in Section 5.5.5.

5.5.1 Input data & assumptions

Tab. 5.3 provides the classification of components concerning their eligibility and capability to participate in the considered markets. The FCR market is symmetric, and thus participating units must offer the same amount of both upward and downward frequency regulation. This symmetry must be upheld at the PCC, i.e., while individual components might only offer one direction of flexibility, the aggregated provision must be symmetric. In contrast, the aFRR capacity and energy markets have separate upward and downward products, although the component classifications listed in Tab. 5.3 apply to both directions identically. The following sections provide application-specific input parameters and assumptions used in the case study.

Tab. 5.3: Classification of each component for market participation.

	Day-ahead	FCR	aFRR (capacity)
BESS	✓	✓	✓
PV array	✓		
HP & HWS	✓	✓	✓

5.5.1.1 Energy and frequency reserve market prices

The market prices for the representative scenario days of the frequency reserve market application, based on data from the year 2023, are presented in Fig. 5.5. The DA prices are based on [173], the prices for FCR and aFRR are based on [156], while data on activation of tendered offers is obtained from [174]. In addition to historical DA prices, two future price scenarios are shown in the top row of Fig. 5.5, to account for increased price volatility and potential negative prices during peak solar hours, as implemented in (5.23). It is important to note that the DA price reflects the price for selling electrical energy. In contrast, the effective price for purchasing electrical energy includes taxes, levies and surcharges, which amounts to 2.83 €/kWh for medium-sized consumers [31]. The probability of activation in the FCR market, based on historical activation data in 2023 and 2024, is $\xi_{\text{fcr}}^{\text{act}} = 9\,\%$.

5.5.1.2 Scenario input parameters

This section presents the five key input parameters that represent the future uncertainty scenarios, as depicted in Fig. 5.2 (a). Each parameter is varied across a realistic range, as defined in Tab. 5.4, to evaluate its influence on system design and economic performance. Notably, the volatility factor λ and the afternoon price shift $\Delta\mu$ are treated as paired values.

- *Frequency reserve (FR) revenue factor* ξ^{m}: Captures reductions in expected market revenues due to imperfect foresight in operational scheduling, price forecasting, and unforeseen maintenance downtimes. It adjusts the realised revenue relative to perfect foresight from participating in frequency reserve markets.

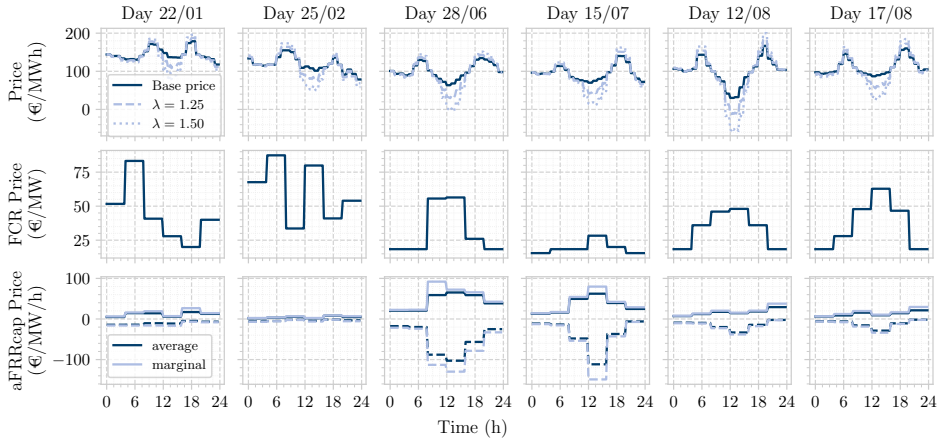

Fig. 5.5: Input data for the market prices, including future price scenarios $\omega \in \Omega$ of the day-ahead (DA) electricity market characterised by larger volatility (top), the frequency containment reserve (FCR) market, and the upward and downward (dashed) automatic frequency restoration reserve capacity (aFRRcap) market. The base price of the DA market reflects historical prices, while the future scenarios with $\lambda = 1.25$ and $\lambda = 1.50$ represent increased price volatility by 25 % and 50 %, respectively. The future scenarios further include a systematic afternoon price reduction, which is implemented via $\Delta\mu = -25\,€/\mathrm{MWh}$ and $\Delta\mu = -50\,€/\mathrm{MWh}$, respectively, as described in (5.23).

- *FR price factor* γ^m: Models an expected reduction in average FR market prices, resulting from increased competition and market saturation due to growing BESS deployment and FR market participation.
- *Building cost subsidy*: Represents a grid connection fee charged on BESS installations to partly compensate for required network reinforcements. The fee ranges from 0 €/kW to 180 €/kW, based on regional regulations and the voltage level [175].
- *Volatility factor* λ: Increases the standard deviation of electricity prices to account for a higher volatility due to a growing solar PV penetration, reflecting larger midday price dips associated with the *duck curve* phenomenon (see (5.23) for more details).
- *Afternoon price shift* $\Delta\mu$: Introduces a downward price shift in electricity prices during solar peak hours (10 a.m. – 4 p.m.) to account for price pattern changes due to excess renewable generation (see (5.23) for more details).
- *Electricity price factor* γ^{elec}: Accounts for a decrease or increase in the mean electricity price.

5.5.1.3 Assumptions and key aspects

As local MESs are typically small players in electricity and FR markets, they are considered *price takers*, i.e., their bidding behaviour does not influence the market-clearing price [176, 177]. Furthermore, the minimum bid size of 1 MW does not apply in this context, as the local MES participates in the markets as part of a VPP. The FCR market is assumed to be an energy-neutral market, i.e., the activations for upward and downward FCR over

Tab. 5.4: Iterable input parameter values for the future scenarios ω, as applied in Section 5.5.4, resulting in a total of 288 scenarios.

Parameter	Symbol	Values	Unit
FR revenue factor	ξ^m	[50, 60, 80]	%
FR price factor	γ^m	[50, 65, 85, 100]	%
BESS building cost subsidy	π^{bkz}	[0, 80]	€/kW
Volatility factor	λ	[100, 125, 150, 175]	%
Afternoon price shift	$\Delta\mu$	[0, 25, 50, 70]	€/kWh
Electricity price factor	γ^{elec}	[80, 100, 120]	%

time roughly balance out. As a result, no additional cost or revenue from FCR activation is considered [178]. The aFRR energy market is excluded from this study due to the high uncertainty with its energy activations, which lies beyond the scope of this design-focused analysis [179, 180]. Furthermore, this study considers the DA market as the representative spot market. Although ID trading represents a relevant revenue stream in reality, its explicit modelling would require sequential scheduling [110, 181] to avoid unrealistic arbitrage effects under perfect foresight. Nevertheless, it is assumed that the local MES has access to the ID continuous spot market to trade short-term imbalances resulting from FR activation. This short-term flexibility is especially important for the operation and energy management of storage systems.

5.5.2 Optimal design and operation

For the analysis in this section, the default values of the input parameters are applied: the FR revenue factor is set to $\xi^m = 80\,\%$, the FR price factor to $\gamma = 100\,\%$, the building cost subsidy for the BESS to $\pi^{\text{bkz}} = 80\,€/\text{kW}$, and the volatility factor to $\lambda = 100\,\%$ with no afternoon price shift $\Delta\mu$ and an electricity price factor $\gamma^{\text{elec}} = 100\,\%$. The optimal sizing of all components for each building within the local MES, as well as the sizing and placement of the community BESS, are presented in Tab. 5.5. The BESS is installed at the bus bar of Bd1, located at the top of the feeder. The operational schedule shown in Fig. 5.6 corresponds to this optimal system design. All values presented in this figure are aggregated over all buildings, except for the community BESS.

The results show that the majority of the BESS capacity is reserved for the provision of frequency-balancing reserve in the FCR and aFRR capacity markets. The SoC is maintained around 55 %, representing the midpoint of the usable SoC range, given $\text{SoC}^{\text{min}}_{\text{bess}} = 10\,\%$. This enables the BESS to provide symmetric FCR bidding, and offer both upward and downward aFRR capacity provision. In response to high upward aFRR capacity prices and low FCR at the end of representative days 22/01, 25/02 and 17/08, the reserve capacity is shifted from FCR to aFRR capacity. A similar trend is observed across the entire days of 28/06 and 15/07. The SoC profile, which does not utilise the full energy capacity of the BESS, indicates that energy arbitrage in the DA or ID markets does not significantly complement participation in the reserve capacity markets. This is mainly because providing

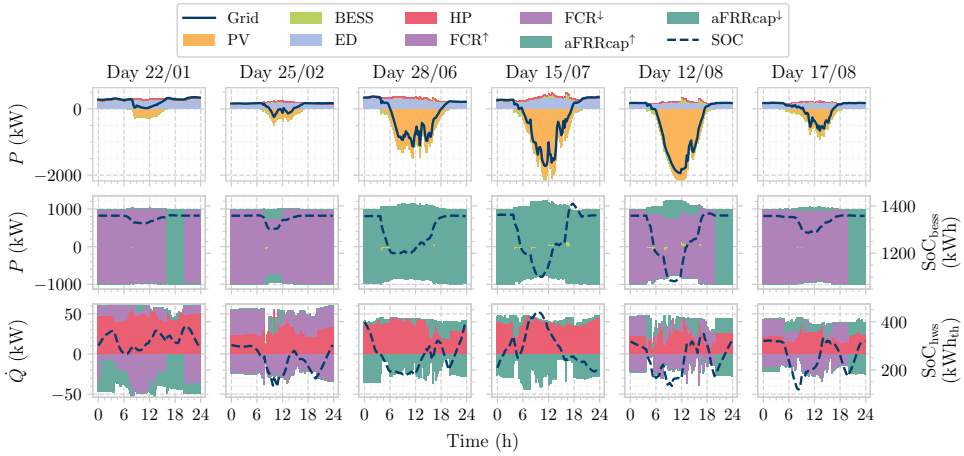

Fig. 5.6: Operation of the local district-scale MES and its participation in frequency reserve markets, with the total aggregated electric demand (ED) and generation (top), the operation of the BESS and its SoC (centre), and the thermal output of the HP alongside the SoC of the HWS (bottom).

symmetrical frequency reserve, which is required by regulation for FCR and typically cost-optimal for aFRR, requires the SoC to be kept near 50 %. This operational strategy ensures availability for both upward and downward flexibility, but limits the depth of charging and discharging for energy arbitrage. For the considered prices, the operational strategy of the BESS prioritises FR provision over energy arbitrage to maximise its revenue. These findings align with the revenue streams for a real BESS in operation participating in the aFRR market [157].

Tab. 5.5: Optimal component sizes for the reference local multi-energy system.

Location	BESS	Heat pump	Solar rooftop PV	Hot water storage
Bd1	2465 kWh	15 kW_{th}	320 kWp	31 kWh_{th}
Bd2	-	37 kW_{th}	320 kWp	37 kWh_{th}
Bd3	-	42 kW_{th}	213 kWp	45 kWh_{th}
Bd4	-	35 kW_{th}	400 kWp	35 kWh_{th}
Bd5	-	24 kW_{th}	320 kWp	24 kWh_{th}
Bd6	-	141 kW_{th}	600 kWp	245 kWh_{th}
Bd7	-	31 kW_{th}	320 kWp	63 kWh_{th}
$\sum$	2465 kWh	326 kW_{th}	2493 kWp	481 kWh_{th}

During representative days with high rooftop solar PV generation, excess electricity is exported to the upstream power grid. The BESS is typically discharged in the morning to profit from high DA prices and recharged in the afternoon with rooftop solar PV. Additionally, it is evident that the HP in combination with the HWS, can contribute to withholding reserve capacity for both the FCR and aFRR markets, which introduces an additional revenue stream from the heating sector in the FR markets.

5.5.3 Impact of price uncertainty and market participation

To assess the influence of reserve market participation, electricity price volatility and reserve market price uncertainty on optimal component sizing, a comprehensive sensitivity analysis is performed. The analysis further explores the impact of explicitly considering individual FR markets during the design phase. Throughout this investigation, a building cost subsidy for the BESS of $\pi^{\text{bkz}} = 0\,€/\text{kW}$, a FR revenue factor $\xi^{m} = 80\,\%$, and an electricity price factor $\gamma^{\text{elec}} = 100\,\%$ are assumed. The resulting aggregated component designs are visualised in Fig. 5.7 within a heatmap. Each cell in the heatmap corresponds to the outcome of a distinct design and operational optimisation, for a specified input combination of electricity price volatility, FR market prices, and FR market participation options.

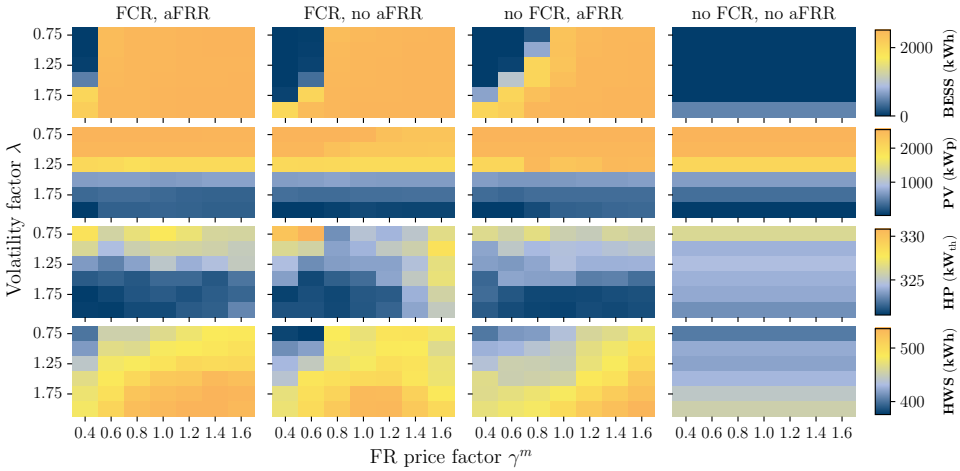

Fig. 5.7: Optimal component sizes for variations in electricity price volatility (y-axis) and frequency reserve price (x-axis) under different frequency market participation settings. The resulting sizes for the community BESS (top row), aggregated solar rooftop PV arrays (top-centre row), aggregated HP (bottom-centre row) and the aggregated HWS (bottom row) are shown.

The first row reveals that BESS sizing is mainly driven by access to frequency reserve revenues. The FCR market has a slightly stronger influence than the aFRR capacity market, which can be attributed to the higher remuneration prices of FCR provision. If FR market participation is excluded during the design phase, i.e., neither FCR nor aFRR markets, the optimal community-scale BESS capacity is either relatively small for high electricity price volatility, or not built at all. Although energy arbitrage in the DA market is allowed, the existing price spreads are too small to outweigh the investment in a largeBESS without complementary FR revenue streams. This finding is consistent with recent studies on the limited profitability of DA spot market arbitrage under current market conditions [182].

The second row indicates that rooftop solar PV sizing is predominantly shaped by electricity prices and their volatility. As price volatility increases, primarily due to larger system-level PV adoption, the optimal solar PV capacity within the local MES declines. The reduced PV sizes are caused by the increasing number of hours of low or negative

electricity prices typically coinciding with high solar irradiance periods, which reduces the marginal market value of solar PV generation [10, 183]. Since rooftop solar PV does not participate in FR markets, its optimal sizing remains largely unaffected by the explicit reserve market consideration.

The third and fourth rows depict the optimal sizing outcomes for the HPs and the HWSs, respectively. The HP sizes vary only marginally independent of FR participation and price dynamics, indicating that the thermal load requirements primarily determine their sizing. Moreover, high investment costs further restrict the economic feasibility of HP oversizing for potential FR market participation. In contrast, the HWS sizes show a higher sensitivity to both electricity price volatility and FR revenues. Mainly due to lower investment costs and their critical role in enabling temporal decoupling and thus providing flexibility, the HWS capacities are oversized by over 35 % in scenarios of high volatility and FR market participation. This shows that the combined system of HP and HWS can offer additional operational flexibility, which is remunerated through FR markets. These findings show that moderate oversizing of thermal storage is economically feasible, as the thermal vector enables additional flexibility, which improves the business case of local MES through reserve market revenues or real-time energy arbitrage.

5.5.4 Scenario-based uncertainty-aware design analysis

This section presents a scenario-based uncertainty-aware design analysis of the local MES, focusing on its performance across a range of future scenarios. As illustrated in Fig. 5.2 (a) and presented in detail in Tab. 5.4 of Section 5.5.1.2, a total of 288 future scenarios are defined based on different combinations of input parameters. For each future scenario, a separate optimal system design is obtained. From these 288 system designs, a representative subset of six distinct designs is selected for further analysis, as presented in Section 5.5.4.1. Subsequently, these distinct designs are fixed and an operational optimisation is performed across all considered future scenarios, as described in Section 5.5.4.2. This enables the evaluation of the economic performance of each distinct design and the identification of the most suitable system design under uncertainty.

5.5.4.1 Optimal distinct designs

Fig. 5.8 presents the selected subset of representative designs and their corresponding input parameter values as listed in Tab. 5.6. It is important to note that these results are not directly comparable to those shown in Fig. 5.7, since this analysis includes the participation in both FR markets, and a wider range of input parameter values.

Significant variations in the sizing of the BESS and the solar PV arrays can be observed across the distinct designs. For instance, designs 5 and 6 feature relatively small BESSs, which correspond to scenarios with high building cost subsidies or reduced revenues from the FR markets due to forecast inaccuracy or lower FR prices. As it can be seen for design 3, 4 and 6, the solar PV arrays are sized smaller with a higher electricity price volatility

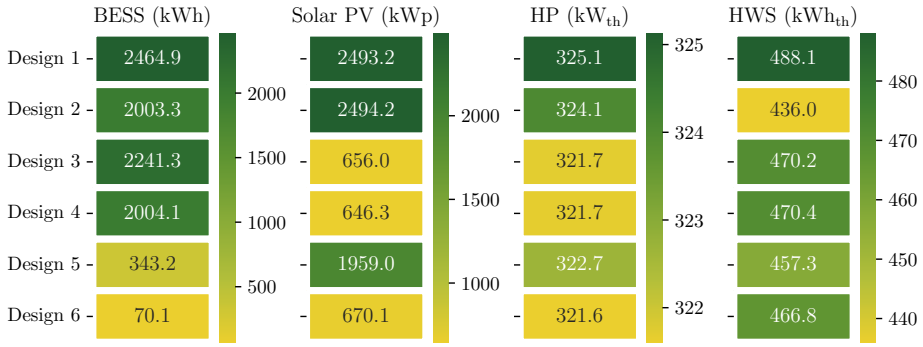

Fig. 5.8: Representative subset of distinct designs for the uncertainty-aware design analysis, based on the optimal design for the future scenarios as listed in Tab. 5.6.

and the accompanying negative or low prices during peak solar hours. This confirms the strong impact of electricity price volatility on optimal solar PV sizing as shown before in Section 5.5.3.

The sizing of the HPs remains largely unaffected across future scenarios, confirming the findings from Section 5.5.3 that HP capacity is primarily driven by the thermal demand requirements. In contrast, the HWS capacities show greater variation due to their lower investment costs compared to the HP, leading to an increasing operational flexibility of the integrated heating system.

5.5.4.2 Uncertainty-aware design analysis results

This section presents the results of the uncertainty-aware design analysis. The six evaluated designs are selected as a representative subset of distinct system designs resulting from all considered future scenarios. As illustrated in Fig. 5.2 (d), these design configurations are fixed and their operation is optimised across all future scenarios to assess their economic performance under uncertainty.

Fig. 5.9a presents the distribution of TAC of the six distinct design sets across 144 future scenarios for two building cost subsidies, respectively. Designs 1 – 4 result in similar expected cost levels, though the large tails of their cost distribution show significant risk

Tab. 5.6: Future scenario parameter values for the subset of distinct designs for frequency reserve revenue factor ξ^m, the frequency reserve price factor γ^m, the building cost subsidy π^{bkz}, the energy price volatility factor λ, the corresponding afternoon price shift $\Delta\mu$, and the electricity price factor γ^{elec}.

Design	ξ^m	γ^m	π^{bkz}	λ	$\Delta\mu$	γ^{elec}
Design 1	80 %	100 %	0 €/kW	100 %	0 €/kWh	100 %
Design 2	80 %	50 %	0 €/kW	100 %	0 €/kWh	100 %
Design 3	80 %	50 %	0 €/kW	150 %	−50 €/kWh	100 %
Design 4	80 %	50 %	80 €/kW	150 %	−50 €/kWh	100 %
Design 5	80 %	50 %	80 €/kW	125 %	−25 €/kWh	100 %
Design 6	60 %	50 %	0 €/kW	150 %	−50 €/kWh	100 %

exposure. Designs 5 and 6, characterised by the smallest BESS capacities, show the highest TAC expected costs for both considered building cost subsidies. However, the tails on either side of their cost distribution are much smaller than for the designs 1 – 4. This is further underlined by Fig. 5.9b, which depicts Conditional Value-at-Risk (CVaR) with various confidence levels for the distinct designs. For instance, despite design 5 having the second highest expected TAC, its CVaR for confidence levels $\alpha \geq 0.8$ is the lowest across all designs. Conversely, design 3 has the second-lowest expected TAC, but this design results in the highest values for $\text{CVaR}_{0.9}$, which represents the most expensive 10 % of all scenarios. Moreover, the impact of solar PV array sizing on risk assessment becomes apparent when comparing designs 2 and 4, which have almost identical component sizes except for the substantial difference in solar PV capacity. While the expected TAC of both designs is nearly identical, design 4 has a higher CVaR compared to design 2 for various confidence levels. This indicates that larger solar PV arrays combined with a large BESS capacity mitigate tail risk exposure more effectively than systems with smaller solar PV arrays and an equally large BESS capacity.

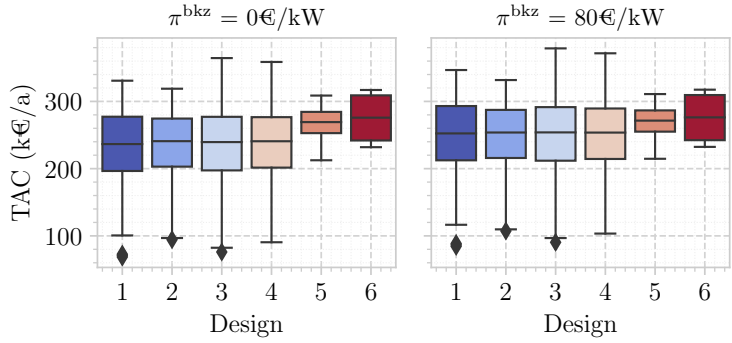

(a) Total annualised cost.

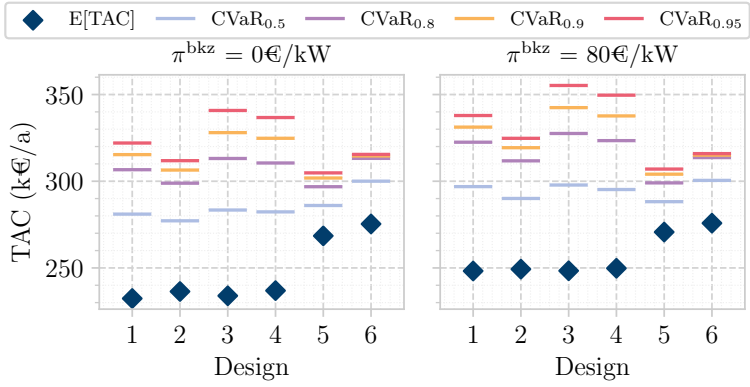

(b) Conditional Value-at-Risk (CVaR) and expected total annualised cost $\mathbb{E}$[TAC].

Fig. 5.9: Boxplot for the total annualised cost (TAC), and CVaR_{α} for different confidence levels α for the six distinct design sets as presented in Fig. 5.8 across 144 scenarios for two different building cost subsidies π^{bkz}, respectively, as indicated in Tab. 5.4.

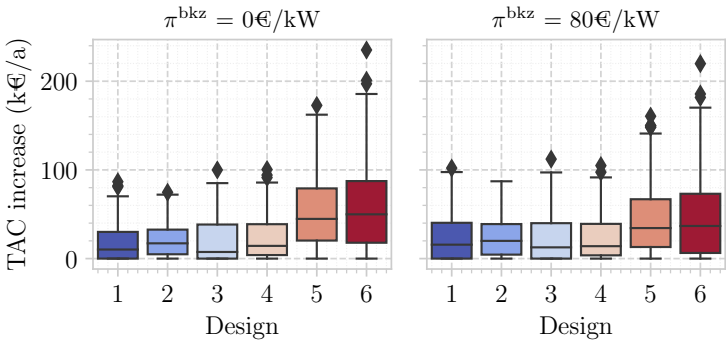

Fig. 5.10: Increase in total annualised cost (TAC) compared to the cost-optimal design for the six design choices as presented in Fig. 5.8 across 144 scenarios for two different building cost subsidies π^{bkz}, respectively, as listed in Tab. 5.4.

These results underline that the risk position of investors plays an important role in investment decisions within local MES. On the one hand, a risk-neutral position aiming to minimise the expected (average) TAC over all scenarios would favour design 1, which exhibits the lowest expected TAC. On the other hand, an investor with a risk-averse position who aims to minimise CVaR would prefer design 5 with the lowest $CVaR_{\alpha \geq 0.8}$. Alternatively, a balanced trade-off that minimises expected costs while reducing exposure to high-cost tail risks may favour design 2, which achieves comparable expected TAC to design 1 but with significantly lower tail risks, as evident by its lower CVaR.

Besides mitigating tail risks by minimising CVaR or minimising expected costs across all scenarios, the least worst regret (LWR) evaluates decisions under uncertainty relative to the ex-post optimal choice [184], i.e., the design with the lowest TAC in each scenario of this study. Therefore, to assess the LWR of the considered designs, Fig. 5.10 presents the distribution of TAC increases relative to each scenario-specific cost-optimal design. Design combinations with the smallest BESS capacity (designs 5 and 6) have the largest TAC increase in most scenarios. While design 3 leads to the smallest regret of TAC increase across all scenarios, design 2 has the lowest maximum TAC increase. These results underline the importance of risk preference for investment decisions under uncertainty, which can be incorporated and assessed with the proposed design analysis framework.

Comparing the results of LWR with mitigating tail risks through CVaR analysis, it is notable that smaller BESS capacities lead to large regrets for many scenarios, but result in lower CVaR values. The contrary applies for large BESS capacities, which reduce expected TAC but expose the system to the highest TAC in extreme cases. These results show that there is not a single optimal design combination due to its techno-economic performance, but the decision-making is significantly impacted by the risk position of investors and system planners. Therefore, different risk metrics such as CVaR or worst-regret should be taken into account for an uncertainty-aware design investment that allows decision-makers to control their desired risk position.

5.5.5 Key findings & discussion

The impact of explicitly considering ancillary services within the design phase on local MES sizing was demonstrated through an uncertainty-aware design analysis. The presented results have several key takeaways for local MES planning under uncertain market conditions. First, solar PV arrays are highly susceptible to volatile electricity prices with low or negative prices during peak solar hours, which is likely to increase with larger penetration of RES. Therefore, coupling solar PV with BESS effectively mitigates this economic risk by storing excess solar energy during low-price hours for usage during high-price evening hours. Second, the investment in large community BESS capacity is economically prudent for the considered market price scenarios. The BESS can serve both the internal energy needs of the local MES, and participate in external energy and frequency reserve markets, thus stacking multiple revenue streams. Third, the HP is sized primarily based on the thermal demand requirements, while any oversizing aimed at enhancing electricity market participation is economically not feasible. However, modest oversizing of HWS can be economically prudent due to its low investment cost and the additional operational flexibility it provides, which can unlock further revenue streams in electricity markets. Finally, the results confirm that optimal design decisions depend on the risk position of the investor. Risk-neutral positions aiming to minimise expected cost favour large BESS capacities and solar PV arrays, while risk-averse positions prefer smaller BESS to limit high-cost tail risks under uncertainty. Regardless of the objective, the proposed framework provides a structured approach to evaluate economic trade-offs and risks under uncertainty, thus supporting informed investment decisions during the design of local MESs that account for different risk preferences.

Despite the valuable insights presented in this study, several limitations must be acknowledged. First, the analysis only considers participation in the aFRR capacity market, while the aFRR energy market is excluded. Future research could explore heuristic methods to estimate revenues from aFRR energy provision and assess their potential influence on investment decisions. Second, only the DA market was considered as a spot market, which simplifies the real-world setup with both DA and ID markets. However, the focus of this study is on system design rather than detailed operational scheduling. Real-time operation of a local MES would require more detailed scheduling optimisation to coordinate multi-market participation, which would complement the presented design framework. Third, a heuristic factor accounting for imperfect foresight was incorporated within the market participation. The aforementioned operational scheduling optimisation could quantify this parameter more precisely. Fourth, the future scenario generation focused on a few key parameters such as market prices and volatility, which are considered to be most relevant for investment feasibility. Additional uncertainties, e.g., future regulatory changes such as the participation of solar PV in reserve markets, evolving technology costs or shifts in demand patterns, should be explored in future studies to cover a wider range of uncertainty and enable more informed decision-making.

5.6 Application 2: Impact of reactive power market

For a realistic revenue assessment over the operational lifetime, potential future market revenues should be considered at the planning stage, even if such markets are not yet available or fully established. To illustrate this, the impact of the planned reactive power market in Germany on the optimal design of local MESs is investigated as an exemplary case study, demonstrating the ability of the framework to include reactive power provision. Besides the reactive power market, an energy spot market and the FCR market is considered. In the following, Section 5.6.2 depicts the operation of the local MES under the aforementioned assumptions, while Section 5.6.3 analyses the impact of different reactive power prices on the optimal component design. Section 5.6.4 discusses the presented findings.

5.6.1 Input data

Fig. 5.11 depicts the input prices for the day-ahead market (top) and for the reactive power market (bottom). For the DA market, a future scenario with more volatile prices is assumed, with negative prices during peak solar hours and higher prices during load peak hours. For the reactive power market, a time-dependent local requirement is assumed, with inductive reactive power during peak solar hours and capacitive reactive power during peak demand hours. The price magnitude, assumed in this figure to be 0.5 ct/kvarh, can be adjusted. Note that all components can participate in the reactive power market, with the HP and the HWS participating jointly. Moreover, due to the price signal of the reactive power market remunerating (inductive) reactive power consumption, the SOCP formulation may result in non-physical solutions due to its relaxed ampacity constraint as described in Section 5.3.5. Therefore, the ISOCP algorithm is deployed to ensure exact solutions for the power flow of the internal grid.

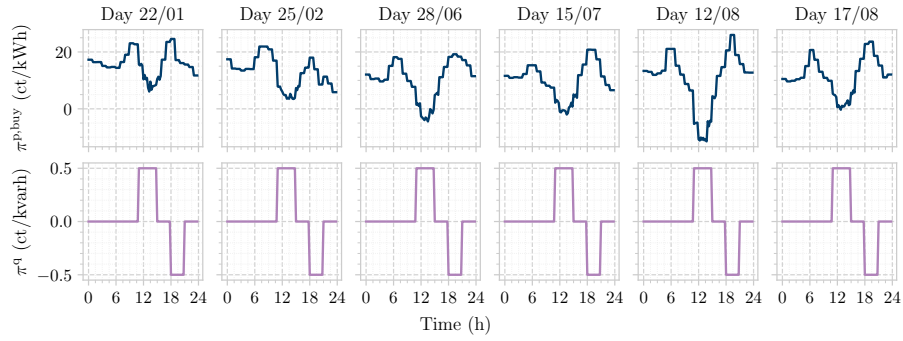

Fig. 5.11: Input data for the day-ahead market price and an exemplary signal for the reactive power market. Note that the price of $\pi^{\mathrm{q}} = 0.5\,\mathrm{ct/kvarh}$ can be adjusted. The electricity price represents a future high volatile scenario with $\lambda = 1.75$ and a price afternoon shift of $\Delta\mu = 70\,€/\mathrm{MWh}$ (see (5.23)).

5.6.2 Operational results

Fig. 5.12 shows the active power (a) and the reactive power (b) when considering reactive power market participation. It can be seen that the reactive power at the PCC follows the price signal, with reactive power consumption during peak solar hours and injection in the evening during high-demand hours. All electricity-consuming components (BESS, solar PV and HP) contribute reactive power when the price signal indicates local requirement. In addition, the reactive power at the PCC is roughly equal to the sum of the individual components within the MES, indicating low reactive power losses within the internal power grid.

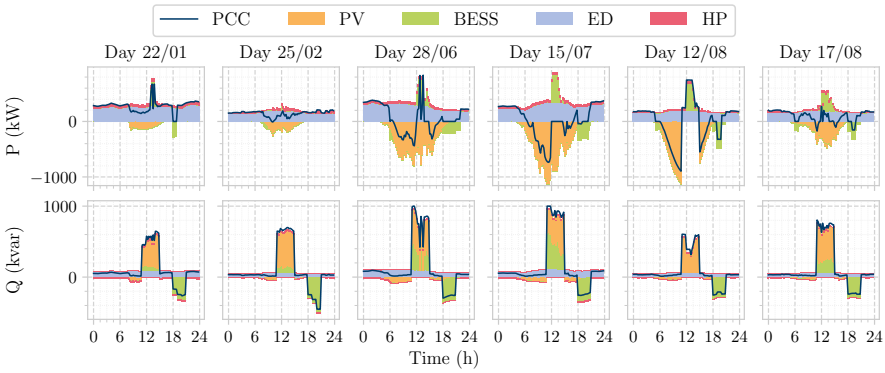

Fig. 5.12: Aggregated operational results for active power (top) and reactive power (bottom) under reactive power market participation with a remuneration of $\pi^{\mathrm{q}} = 0.5\,\mathrm{ct/kvarh}$. Active and reactive power are depicted at the PCC, for the solar PV arrays, the community BESS, the ED and the HP.

5.6.3 Design results

Fig. 5.13 depicts the optimal design results for the aggregated building components and the community BESS. Independent of the reactive power remuneration, the community BESS is always placed at the head of the feeder at building 1. It can be seen that with increasing reactive power prices, the optimal size of the community BESS increases. For an assumed price of 0.7 ct/kWh, representing the maximum price limit in Northeast Germany [168], the optimal BESS capacity increases by 22.2 % compared to not considering reactive power provision as an upstream grid service. Similarly, the aggregated solar PV arrays increase by 8.0 %. The thermal components, in particular the HP as an electricity-consuming component, remain at their original sizes. This indicates that the reactive power market remuneration is not sufficient to oversize the HP, despite its reactive power provision.

Fig. 5.14 depicts the annualised cost for design, operational cost and revenue from the energy market, revenue from the FCR market and reactive power market, as well as the TAC across different reactive power remuneration levels. It can be seen that the increase

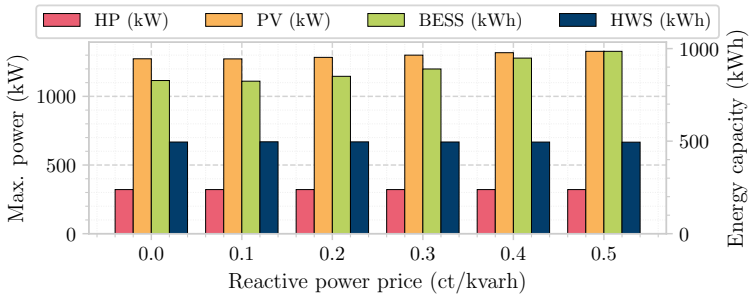

Fig. 5.13: Design results for the community BESS and the aggregated components for varying reactive power prices. Note that the HP and the solar PV refer to the left y-axis, while the community BESS and the aggregated HWS sizes refer to the right y-axis.

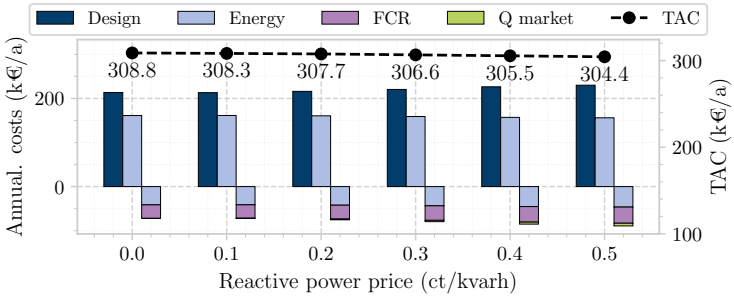

Fig. 5.14: Annualised costs for design and operation, FCR and reactive power revenues (left y-axis), for varying reactive power prices. Note that the total annualised cost (TAC), representing the overall sum of costs and revenues, is depicted on the right y-axis.

in reactive power market revenue, driven by higher prices and increased BESS capacity, is relatively small compared to the TAC. Nevertheless, the additional revenue from the reactive power market combined with the FCR and energy market revenues, outweigh the higher investment cost in a larger community BESS and solar PV arrays, resulting in lower operational costs. Overall, the reduction in TAC resulting from higher reactive power prices remains modest, with up to 2 % for an assumed reactive power remuneration of 0.7 ct/kvarh. This indicates that the solution space is quite flat, i.e., small additional remuneration can shift investment decisions.

5.6.4 Key findings & discussion

To illustrate the impact of a future reactive power market on optimal local MES design, a time-dependent signal indicating either provision or consumption of reactive power was assumed, for which the remuneration was varied within an estimated range. The presented results show that investing in a larger BESS capacity and to some extent solar PV arrays is economically feasible when additional remuneration from reactive power provision is

considered. However, the HWS and the HP sizes did not change for the considered prices, indicating that the additional revenue streams do not outweigh their investment costs.

While the presented work offers valuable insights into the impact of future reactive power markets on local MES design, several limitations and opportunities remain for further research. The inherent uncertainty of prices, particularly for local services such as reactive power provision, makes it challenging to estimate potential market remuneration accurately. However, after this work had been conducted, the market-based procurement of reactive power began in Northeast Germany, which was divided into five regions [161]. Two reactive power provision schemes exist, both remunerating reactive power exceeding the current grid connection requirements [162]. Secured provision must be continuously available at the contractually agreed level and is compensated via a standby price, while unsecured provision is not continuously available and is remunerated based on the delivered reactive power. Even though the exact remuneration of accepted bids is not available, the techno-economic insights of this real-world setup should be incorporated within the presented framework in future work. Nevertheless, the presented work demonstrates the relevance of local MES as potential players in such markets, which should be considered during the design stage of local MES.

Within this work, the sole impact of a reactive power market is considered. In reality, the BESS (and to some extent other flexible electricity-consuming components) could create further revenue by participating in frequency-balancing markets or exploiting short-term price differences within the ID market. Lastly, instead of a time-dependent requirement for reactive power provision as adopted in this work, a capacity-based market would be possible where the availability of reactive power provision is remunerated. A constant remuneration for availability could impact the optimal component design even further, and thus should be investigated.

5.7 Chapter summary

This chapter presented a techno-economic framework for investigating the optimal design of local MES under participation in multiple energy markets. The framework supports uncertainty-aware component sizing across a range of future scenarios, illustrating how uncertain parameters affect optimal investment decisions, which can be adapted based on the availability or desired uncertainty focus. This was demonstrated in the first case study, which focused on participation in energy and reserve markets. The second case study showcased how potential future markets, such as a reactive power market, can be further integrated within the presented framework. While both case studies were applied to current German market regulations, the proposed framework is versatile and can be applied to different regions and market structures. The presented findings highlight the importance of incorporating potential market revenues and scenario uncertainty during the early-planning stage of local MES to ensure uncertainty-aware and economically optimal investment decisions.

CHAPTER 6

Conclusions

Therefore, there is an increasing need to develop models to gain a deeper understanding of the technical interdependencies and the economic potential of local multi-energy systems (MESs) with electricity and heat, especially at the design stage.

The central focus of this work was the development of a techno-economic framework for the optimal design of local MESs comprising electricity and heat. The two-stage stochastic optimisation framework incorporated different models for individual components, the internal power grid and the heating network, enabling a comprehensive analysis of modelling choice within a local electricity-heat energy system. Furthermore, investment costs for component sizing, as well as the technical constraints and the potential revenue streams from participating in energy, frequency reserve or reactive power markets were integrated. Moreover, a novel flexibility calculation approach ensuring constant flexibility provision related to a time-varying reference schedule was developed to quantify the impact of individual component sizing and interdependencies between components on the electrical flexibility potential. Finally, the modelling was extended to include uncertainty based on future scenarios, enabling informed decision-making at the design stage of local MESs.

The case study applications for the modelling choice impact on the design of electrical storage showed that neglecting the thermal vector significantly oversizes the battery energy storage system (BESS) and increases overall costs, thus highlighting the importance of modelling coupled energy carriers already during the design stage. Moreover, the internal power grid formulation plays a key role in the optimal sizing of BESSs, both in terms of modelling accuracy and computational workload. While a time-varying electricity tariff incentivises larger investment in BESS capacity and results in lower annualised cost compared to a constant tariff, high solar irradiance years lead to larger BESS sizes, reduced cost and lower annual emissions. Overall, this framework provided practical modelling guidelines for design studies of integrated electricity-heat systems. Moreover, a deeper technical understanding of the impact of individual sizing of components and their interdependencies was gained by embedding system flexibility potential into the design stage.

The thermal vector not only impacts the optimal BESS capacity, but also provides substantial active power flexibility, which can further be enhanced by identifying an optimal ratio between heat pump and thermal storage in terms of overall system flexibility.

Beyond internal renewable energy sources (RES) utilisation and efficiency optimisation, ancillary service markets present an important revenue opportunity for local MESs. Their controllable assets in combination with storage systems can adjust their active power to participate in frequency-balancing reserve markets, while capacitive or inductive reactive power provision contributes to stabilising local voltage magnitudes. By developing a framework that incorporated ancillary service markets with their inherent revenue streams, valuable insights into key investment drivers and economic opportunities within local MESs were gained. The case study demonstrated that including revenue stream from energy and frequency reserve markets significantly affects optimal component sizing, even determining whether a community BESS was built. Moreover, future scenarios were incorporated that account for varying future market conditions, ensuring optimal investment decision-making under uncertainty. An expected increasing electricity price volatility worsens the business case of solar photovoltaic (PV), but its combination with a community BESS remains profitable across all evaluated scenarios.

The presented thesis contributes to a deeper understanding of designing local MESs with electricity and heat, and identifies and quantifies key investment drivers and their interactions. In the following, the key novelties and contributions are described.

6.1 Research novelty and contributions

This thesis presented research on the optimal design of local MESs comprising electricity and heat beyond the state of the art. The following sections summarise the novelty of this work, present the key findings, and further draw conclusions.

6.1.1 Comprehensive analysis of modelling impact in multi-energy systems

The computational burden of explicitly modelling integrated MESs typically leads to simplifications on coupled energy carrier models, particularly during design studies. To address this, a comprehensive analysis was developed to investigate the impact of different component modelling choices on the design of BESSs and their computational implications within an integrated electricity-heat system. The key contributions can be summarised below:

(i) A comprehensive design analysis was developed, which analysed the impact on the optimal BESS sizing of several models within a local multi-energy system: heat pump, thermal building representation, heating network and internal power grid.

(ii) By deploying different model formulations for the optimal BESS sizing in local MESs,

relevant and novel insights were gained. First, the coupled thermal vector is crucial for optimal BESS sizing, as its inherent thermal storage avoids electrical storage oversizing and reduces overall system costs. Second, a constant heat pump efficiency model proves to be sufficient for electrical storage design studies. Third, the second-order cone program approximation for the internal power represents a suitable trade-off between computational tractability and modelling accuracy, while the solution with the exact AC optimal power flow (AC OPF) equations is not tractable. Fourth, while the explicit modelling of the internal heating network slightly decreases the optimal BESS capacity, it significantly increases the computational burden. Finally, a time-varying electricity tariff not only incentivises larger BESS investment, but also reduces costs and CO_2 emissions, especially for high solar irradiance years.

(iii) Practical modelling guidelines, representing an optimal trade-off between modelling accuracy and computational tractability, were presented for the design of electrical storage systems in multi-energy systems.

6.1.2 Flexibility assessment in relation to time-varying reference schedule

For the participation in ancillary service markets, active or reactive power at the point of common coupling with the upstream power grid must be reduced or increased for a given duration. To ensure a constant provision of upward or downward flexibility for market participation, it is important to calculate the potential for reduction or increase in relation to a reference schedule. This work expanded the state-of-the-art flexibility calculation by including a predetermined schedule as a reference, ensuring constant flexibility over several time steps. The key contributions can be summarised as follows:

(i) A technical framework was developed, which calculates the maximum constant flexibility in relation to a time-varying predetermined reference schedule. By considering variable load patterns and time-varying RES generation, the framework enables energy system operators to quantify and ensure constant flexibility bids over multiple time steps. This novel calculation of electrical flexibility is especially important for participation in ancillary service markets, where their tendered bids for upward or downward deviations from the planned schedule must remain constant. This allows energy system operators to reliably size their flexibility bids and reduce the risk of non-delivery penalties in the real-world implementation.

(ii) While the presented framework was applied to active power flexibility, it is adaptable to assess the flexibility of reactive power, heat or other energy vectors. It further incorporates a delivery duration and response time, which are required by market regulations. This adaptability allows the assessment of various flexibility products under different market regulations and across energy vectors, thus translating technical capabilities of local MESs into market-compliant bids.

6.1.3 Framework of operational flexibility assessment within design phase

Operational flexibility is essential within low-carbon power grids. To fully leverage the flexibility potential of MESs, a deeper technical understanding of operational flexibility during the sizing process is required. Therefore, a technical framework was developed that analysed the impact of individual component sizing and interdependencies on electrical system flexibility. The framework can further incorporate network constraints, different durations and response times of flexibility, making it adaptable to any market requirements. The key contributions can be summarised as follows:

(i) A technical flexibility framework was presented to quantify the impact of component sizing on the flexibility potential in MESs during the design phase. The framework allows for a systematic impact assessment of individual component design choices and further identifies threshold ratios between components that constrain overall system flexibility.

(ii) The key insights provided by this framework are the following: First, the thermal vector significantly contributes to electrical system flexibility, and therefore should be included for enhancing electrical flexibility. Second, the BESS is the most significant flexibility provider, while downward flexibility (curtailment) of the solar PV array is temporarily limited to solar availability, which underlines the benefits of combining solar PV with electrical storage. Third, an optimal ratio between the heat pump and its thermal storage was identified, above which increasing the heat pump capacity did not provide additional flexibility. This quantitative assessment can provide clear design guidelines to avoid component oversizing and allocate investment efficiently. Finally, internal networks must be considered for a realistic system flexibility assessment, as their constraints limit the flexibility potential at the point of common coupling (PCC) with the upstream power grid.

(iii) The presented framework enables a deeper understanding of the complex interdependencies within electricity-heat systems, which can assist investment stakeholders in making more informed decisions when facing long-term uncertainties in prices or demand forecasts.

6.1.4 Uncertainty-aware design analysis under market participation

Besides optimising self-efficiency and self-consumption within local MESs, its investment decisions are also affected by the participation in electricity wholesale markets. This part of the work incorporated energy, frequency-balancing reserve, and future reactive power markets to investigate their impact on the optimal component sizing of local MESs, while future scenarios were considered for an uncertainty-aware decision-making. The key contributions of the uncertainty-aware design analysis under market participation are as

follows:

(i) A techno-economic design optimisation model was developed that jointly optimised electricity and thermal components (BESS, solar PV, heat pump (HP), thermal storage) within local MESs under energy and reserve market participation for the German electricity market.

(ii) A detailed sensitivity analysis was conducted to quantify the impact of market participation, with several key insights. First, frequency reserve market participation for some cases determines whether a community BESS was built, which highlights the importance of market revenue integration during the design phase. Second, declining frequency reserve prices combined with increasing electricity price volatility shift the economic value of BESSs from reserve provision to energy arbitrage, thus increasing the attractiveness of longer-duration BESS. Third, even though solar PV are highly susceptible to volatile prices, its combination with a BESS remains profitable. Finally, while the heat pump was solely driven by the heat demand, modest oversizing of the hot water storage was proven to be economically prudent under the assessed electricity market conditions, suggesting that thermal storage should be considered to increase system flexibility. These insights imply that system planners should explicitly account for all potential market revenues during the design, and hybrid PV-BESS systems represent an adaptive and robust investment for cost-effective flexible local MES, which can be further enhanced by modestly oversizing thermal storage.

(iii) A novel scenario-based uncertainty-aware design analysis was developed, which considers future variations in market prices and forecast uncertainty. Its findings highlight that optimal design depends on the risk preference of investors. While risk-averse positions favour larger solar PV with smaller BESS to limit low-revenue tail risks under declining frequency-balancing prices, risk-neutral positions prefer larger BESS to minimise expected costs across all scenarios. This systematic analysis evaluates economic risks and trade-offs under uncertainty, supporting informed decision-making at the design stage of local MESs.

(iv) The revenue from a potential future reactive power market was further analysed, which makes investment in larger BESS and slightly larger solar PV economically prudent, as the additional revenue stream combined with improved energy arbitrage and frequency-balancing market revenues outweighs the higher investment costs. However, the economic viability of these investments depends on the reactive power capabilities of the components, the reactive power prices, the temporal and locational requirements, competing revenues from other markets, and potentially limiting internal grid constraints. All of these aspects must be considered during the design stage, and require further study on their precise implications on component sizing.

6.2 Future Work and Outlook

Besides the presented work and contributions on the optimal design of local multi-energy systems, there are open questions and areas of research that could be further explored. In the following sections, several topics are discussed that could improve and extend the presented work.

6.2.1 Integration of further energy carriers within multi-energy systems

Expanding upon the presented research of electricity-heat systems, further energy carriers could be integrated into the local MES, and their impact on the electrical domain investigated. In addition to the thermal vector, cooling demand is becoming more important, particularly in warmer climate regions. The fifth generation of district heating and cooling network, equipped with decentralised HPs, can serve both heating and cooling demands by utilising bidirectional flows at low temperatures. Moreover, these networks can be used as thermal energy storage, both for short-term buffering and long-term seasonal balancing. This functionality, in combination with additional cooling demand, introduces new aspects for the sector coupling with the electrical domain, which should be systematically investigated within the presented frameworks.

Transportation is another rapidly growing energy vector, driven by technological advances in electric vehicles (EVs), which bring both challenges and opportunities. On the one hand, high-power EV charging increases the stress on local distribution networks. On the other hand, bidirectional charging enables EVs to provide vehicle-to-grid services, such as shaving peak demands, frequency-balancing, or storing excess energy of RES. Therefore, the impact of EVs within local MESs is worth investigating in future studies, both in terms of their interaction with other coupled energy carriers and regarding flexibility provision through ancillary services.

6.2.2 Electrical storage degradation

The presented research established community BESSs as a cornerstone in the design of local MESs. An important aspect of Li-ion BESSs is its degradation over time, causing the usable capacity to gradually decline. To mitigate this effect, a daily cycle limit was implemented in this work. However, the cycle limit does not capture key ageing mechanisms such as high (dis)charging currents, deep discharging cycles or calendar ageing, all of which are the main contributors to capacity degradation. Incorporating a detailed degradation model could affect optimal sizing, operational flexibility, and long-term economic decisions of storage systems. Therefore, such a degradation model should be integrated into design studies to ensure optimal investment decisions over the operational lifetime.

6.2.3 Additional market considerations

The design analysis under energy and reserve market integration underlined the importance of integrating relevant possible revenue streams during the design stage. Therefore, further work should extend the presented analysis by incorporating the automatic frequency restoration reserve (aFRR) energy market, which was excluded in this thesis. Its short gate closure time of up to 25 min before delivery and duration bids of 15 min should allow for fairly accurate forecasts, which in turn unlocks additional revenue streams and thus has a significant impact on solar PV sizing. Even though solar PV is not eligible to participate in frequency-balancing markets on its own, the combination with a BESS could become more profitable with aFRR energy market participation. Heuristic methods for a rough revenue estimation could enable the integration of the aFRR energy market into the presented design framework computationally efficiently.

While this work investigated reactive power remuneration, the new secured and unsecured remuneration schemes compensating beyond grid connection requirements in Germany were not considered. Future work should explore how these remuneration schemes affect the design of local MESs, including whether it is economically feasible to potentially oversize inverters separately for permanent reactive power provision.

6.2.4 Real-time integration of local energy systems providing services to the upstream grid

The presented research outlined the capability of local MESs to provide frequency-balancing service and reactive power for voltage stability. As the next step, future studies could explore how the ancillary service provision of multiple local MESs can support the stability of a regional distribution or transmission grid. Within a simulation model of the power grid, the flexibility potential could be embedded via nodal operating envelopes in the PQ-space, which could enable a dynamic active or reactive power response. Such a simulation-based analysis could provide valuable insights into the required scale of decentralised flexibility from local MESs, as well as the technical challenges and the limitations of such an integration.

APPENDIX A

District-scale case study parameters

This section presents additional information on the district-scale MES which was investigated in Chapter 3 and Chapter 5. In particular, the internal power grid and the parameter values of the individual buildings are listed in the following.

A.1 Internal power grid

The internal power grid of the district-scale multi-energy case study is presented in Tab. A.1, applying to both Chapter 3 and Chapter 5.

Tab. A.1: Branch parameters and apparent power limits for the internal power grid of the district-scale MES considered in Chapter 3 and Chapter 5.

Bus (i)	Bus (k)	r_{ik} (p.u.)	x_{ik} (p.u.)	b_{ik}^{sh} (p.u.)	S_{ik}^{rate} (p.u.)	Type
B_PCC	B_35	1.25e-05	3.592e-04	0	80	Transformer
B_35	B_BB1	2.00e-04	0.003294	0	30	Transformer
B_35	B_BB2	1.667e-04	0.003363	0	30	Transformer
B_BB1	B_B1	0.02000	0.00540	0.02764	1.5	Cable
B_B1	B_Bd1	0.02000	0.07700	0	1.0	Transformer
B_B1	B_B2	0.02604	0.00414	0.02073	1.0	Cable
B_B2	B_Bd2	0.02000	0.07700	0	0.4	Transformer
B_B2	B_Bd3	0.02000	0.07700	0	0.12	Transformer
B_B2	B_B4	0.02000	0.00540	0.02764	0.7	Cable
B_B4	B_Bd4	0.02000	0.07700	0	0.4	Transformer
B_BB2	B_B5	0.02000	0.00540	0.02764	1.5	Cable
B_B5	B_Bd5	0.03000	0.11300	0	1.0	Transformer
B_B5	B_B6	0.01000	0.00270	0.01382	1.0	Cable
B_B6	B_Bd6	0.03000	0.11300	0	0.7	Transformer
B_B6	B_B7	0.02000	0.00540	0.02764	0.7	Cable
B_B7	B_Bd7	0.04000	0.15500	0	0.4	Transformer

A.2 Building parameters

Tab. A.2 presents the component parameters for the individual buildings within the real-world MES case study. The values for the thermal building inertia K_{bd} stem from the dwellings and the hot water storage of the respective building. Note that while the whole table applies to Chapter 3, only the first part applies also to Chapter 5, as the solar PV arrays, the HPs and the hot water storage (HWS) are sized in this chapter.

Tab. A.2: Detailed input parameters for the district-scale case study, which are based on the real-world MES. The values of the heat demand and electric demand are based on historical measurement data. Bd represents the respective building, whereas BB1 represents the upper bus bar to which the central PV array is connected. Note that that the first part applies to the district-scale MES in both Chapter 3 and Chapter 5, while the second part only applies to Chapter 3.

Component	Symbol	Unit	Bd1	Bd2	Bd3	Bd4	Bd5	Bd6	Bd7	BB1
Building	$T_{\mathrm{hp}}^{\mathrm{con,max}}$	[°C]	85	70	85	70	70	70	70	-
Heat demand	$\dot{Q}_{\mathrm{hd}}^{\mathrm{max}}$	[$\mathrm{kW_{th}}$]	92.8	14.6	134.9	64.8	70.2	265.8	36.5	-
	$\dot{Q}_{\mathrm{hd}}^{\mathrm{mean}}$	[$\mathrm{kW_{th}}$]	38.8	5.3	49.3	23.7	25.7	52.1	15.2	-
Electric demand	$P_{\mathrm{ed}}^{\mathrm{max}}$	[$\mathrm{kW_{el}}$]	24.9	39.9	45.0	25.4	27.4	197.1	49.7	-
	$P_{\mathrm{ed}}^{\mathrm{mean}}$	[$\mathrm{kW_{el}}$]	8.4	34.5	33.0	23.3	14.7	70.2	16.8	-
PV array	$P_{\mathrm{pv}}^{\mathrm{max}}$	[kWp]	80	80	80	100	80	150	80	1000
Heat pump	$\dot{Q}_{\mathrm{hp}}^{\mathrm{max}}$	[$\mathrm{kW_{th}}$]	350	90	500	90	110	550	130	-
Building	K_{bd}	[kWh/°C]	300	100	600	100	100	600	200	-

APPENDIX B

Additional information to Chapter 3

B.1 Additional results to the individual building study

In Chapter 3, Section 3.4.1 investigates the optimal design of a BESS within an individual building. Tab. B.1 presents the detailed sizing results of the BESS for time-varying and constant electricity tariffs, different HP and thermal building models, as well as the respective total annualised cost (TAC) and global warming impact (GWI).

Tab. B.1: Optimal BESS capacity, total annualised cost (TAC) and global warming impact (GWI) emissions for time-varying and constant electricity tariffs, different heat pump (HP) models, as well as the multi-energy and the *all-electric* building model, respectively.

Electricity tariff	HP model	Building model	BESS capacity	TAC	GWI
Time-varying	Detailed	Multi-energy	33.7 kWh	16.4 k€/a	30.0 t_{CO_2}/a
	Linear (with PL)	Multi-energy	30.9 kWh	16.4 k€/a	30.5 t_{CO_2}/a
	Linear (no PL)	Multi-energy	30.9 kWh	16.4 k€/a	30.4 t_{CO_2}/a
	Linear (with PL)	*All-electric*	52.4 kWh	18.6 k€/a	31.0 t_{CO_2}/a
	-	No heat demand	39.4 kWh	12.8 k€/a	22.8 t_{CO_2}/a
Constant	Detailed	Multi-energy	2.5 kWh	17.2 k€/a	35.2 t_{CO_2}/a
	Linear (with PL)	Multi-energy	2.5 kWh	17.3 k€/a	35.3 t_{CO_2}/a
	Linear (no PL)	Multi-energy	2.5 kWh	17.3 k€/a	35.2 t_{CO_2}/a
	Linear (with PL)	*All-electric*	5.5 kWh	19.6 k€/a	38.9 t_{CO_2}/a
	-	No heat demand	14.5 kWh	13.3 k€/a	27.0 t_{CO_2}/a

APPENDIX C

Additional information to Chapter 4

C.1 Duration curves of input data for Chapter 4

In Section 2.2.2, the time series aggregation of the input data was presented, showcased at the example of Chapter 3. The duration curves in Fig. C.1 show the input data and the aggregated time series for Chapter 4. It can be seen that the error duration curve for the heat demand slightly increases for four representative days. Such reduced accuracy for an individual data set can occur to better capture the overall variability, as the time series aggregation optimises the weighted sum of Euclidean distances across all data sets. This can be seen in the continuous reduction of the clustering objective value depicted on the right side of the figure. While six representative days would provide a more accurate approximation, four representative days are chosen to limit the computational requirements, since the focus of Chapter 4 lies on demonstrating the technical feasibility of the proposed methodology rather than maximising time series aggregation accuracy.

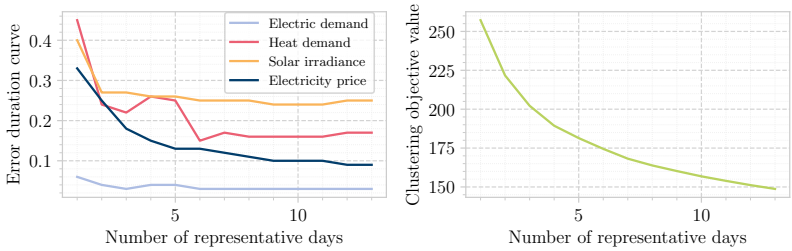

Fig. C.1: Error duration curves (left) and objective value of k-medoids clustering optimisation (right) depending on the number of representative days for the building case study in Chapter 4.

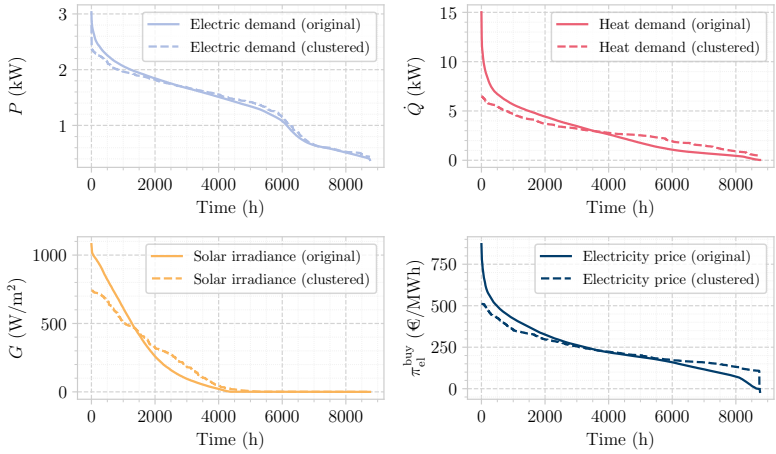

Fig. C.2: Duration curves for the building case study in Chapter 4 for four representative clustering days, with the non-dashed line representing the original data set, while the dashed lines depict the duration curves of the clustered data set.

C.2 Individual sensitivity analysis

Section 4.4.3 presents a sensitivity analysis of individual component design, with a boxplot for size variations of the solar PV array. In the following, the maximum active power flexibility values of the overall MES for design variations of the components BESS, HP and HWS are presented.

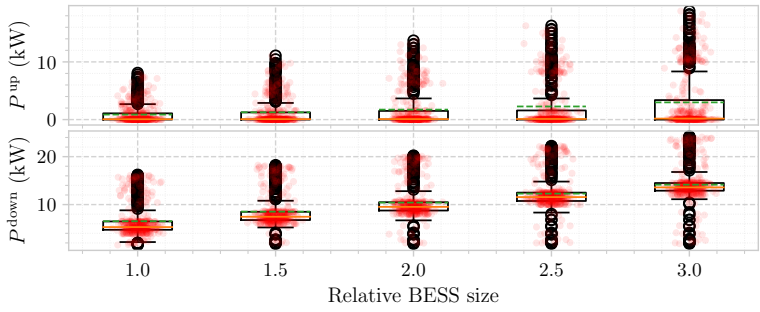

(a) T = 15 min

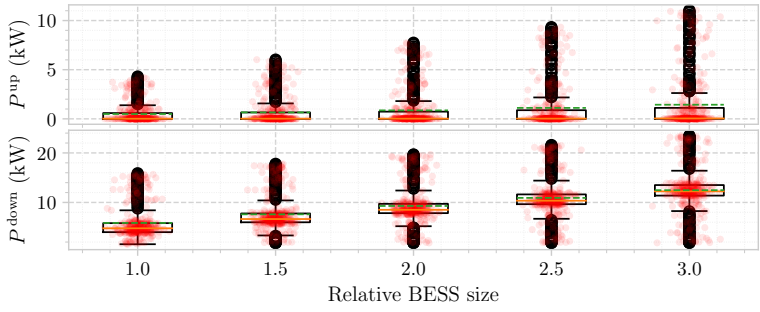

(b) T = 60 min

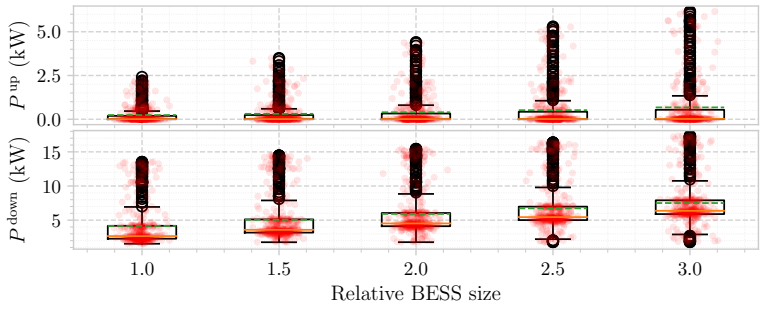

(c) T = 120 min

Fig. C.3: Maximum active power flexibility of the multi-energy building for BESS size variations relative to its reference design. Orange lines indicate the median, and green dashed lines represent the mean of the resulting dataset.

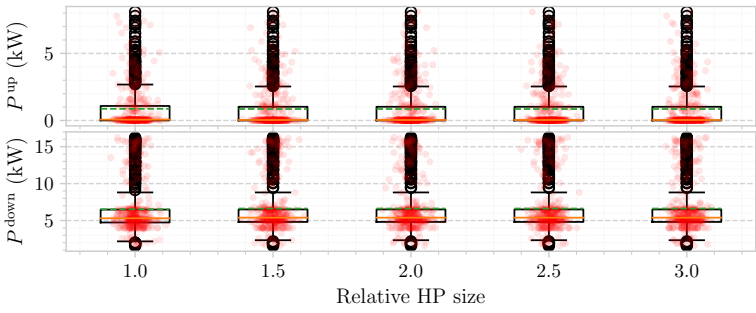

(a) T = 15 min

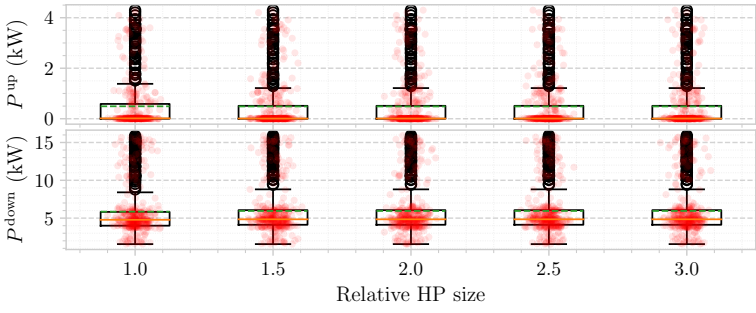

(b) T = 60 min

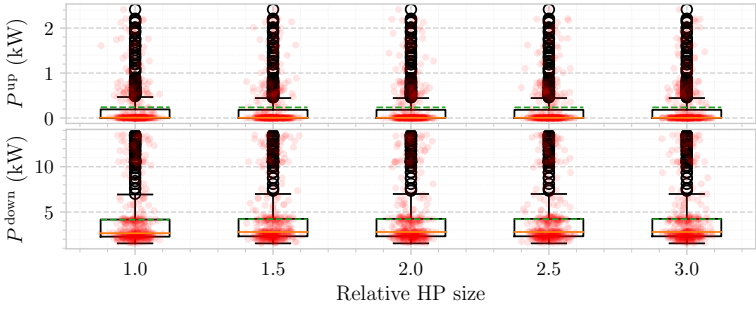

(c) T = 120 min

Fig. C.4: Maximum active power flexibility of the multi-energy building for HP size variations relative to its reference design. Orange lines indicate the median, and green dashed lines represent the mean of the resulting dataset.

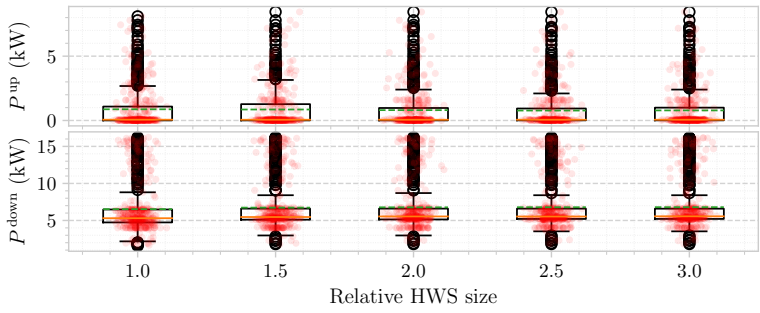

(a) T = 15 min

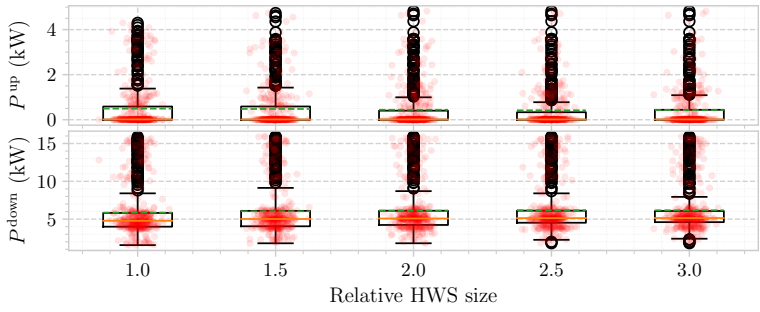

(b) T = 60 min

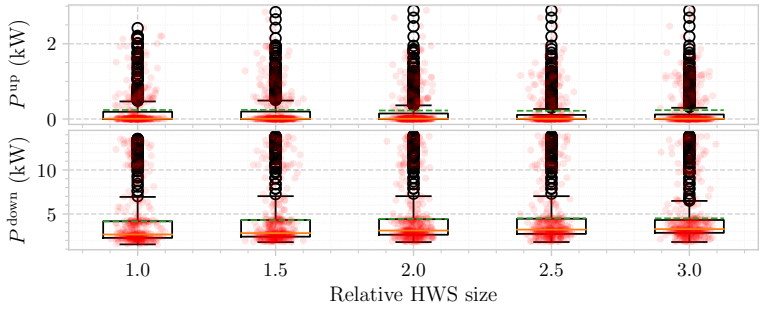

(c) T = 120 min

Fig. C.5: Maximum active power flexibility of the multi-energy building for HWS size variations relative to its reference design. Orange lines indicate the median, and green dashed lines represent the mean of the resulting dataset.

C.3 Active power flexibility for different durations

The mean of maximum active power flexibility values can be investigated for different flexibility durations. Fig. C.6 presents the heatmaps of varying one component at a time for different durations, highlighting the decreasing flexibility capability for larger flexibility durations, independent of the individual component. The per-unit flexibility values are referred to the flexibility values of the reference case for a duration of 60 min.

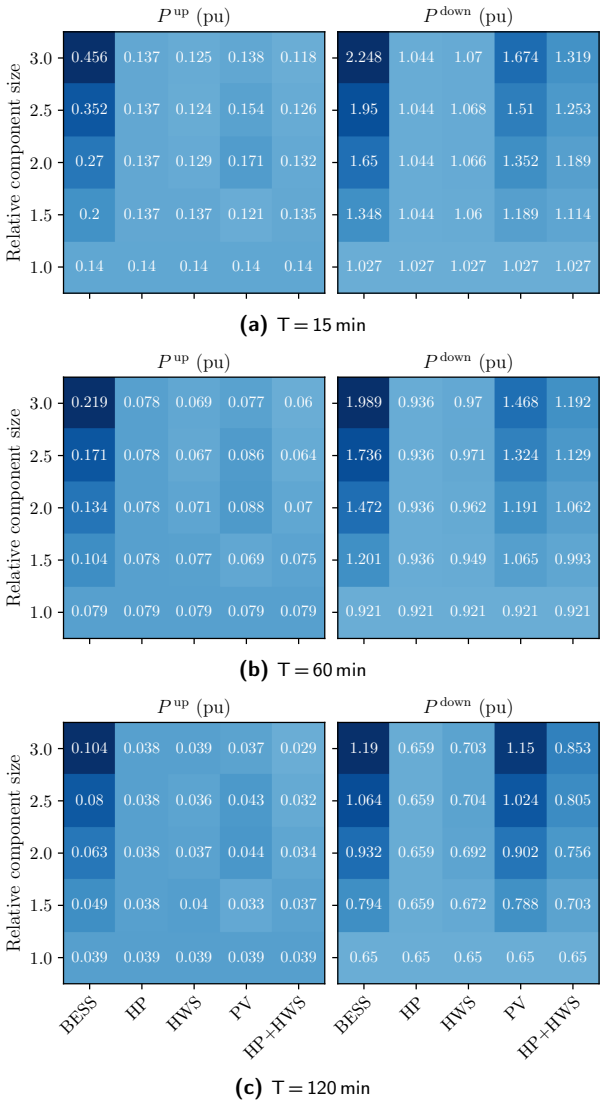

Fig. C.6: Mean maximum active power flexibility of the multi-energy building relative to the reference case, varying one component size at a time for different durations. Flexibility per unit is defined as the sum of the mean upward and downward flexibility in the reference case for a duration of 60 min.

C.4 Interdependency between PV array and BESS

Section 4.4.4 investigated the interdependency between HP and HWS for electrical flexibility provision, showcasing a tight interdependence with a saturating flexibility provision above a certain sizing ratio. In contrast, the interdependency between solar PV array and BESS is more decoupled in terms of electrical flexibility provision, as it is depicted in Fig. C.7. There is no optimal ratio above which no further gains in flexibility provision can be achieved, as both components can contribute to active power flexibility individually. While the BESS capacity increases, both upward and downward flexibility are enhanced, the contribution of increasing the solar PV size is evident for the downward flexibility, i.e., curtailing the PV generation.

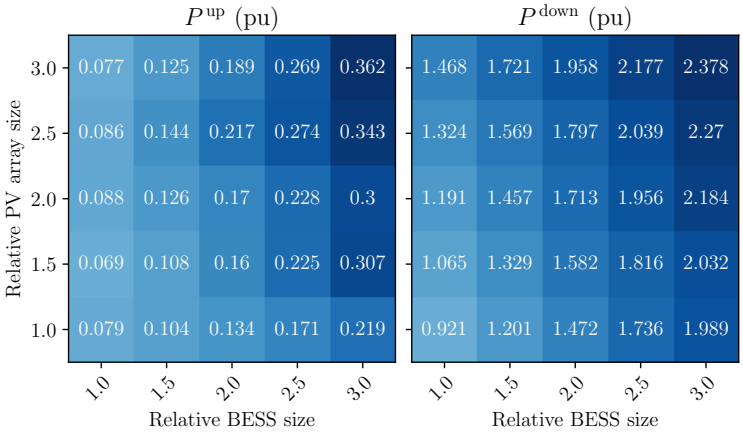

Fig. C.7: Mean maximum active power flexibility of the multi-energy building relative to the reference case for a duration of 60 min, varying component sizes of solar PV array and BESS.

APPENDIX D

Additional information to Chapter 5

D.1 Duration curves of input data for Chapter 5

In Section 2.2.2, the time series aggregation of the input data was presented, showcased at the example of Chapter 3. The following duration curves present the input data and the time series aggregation for Chapter 5, with six representative days being chosen as a compromise between accuracy and computational workload.

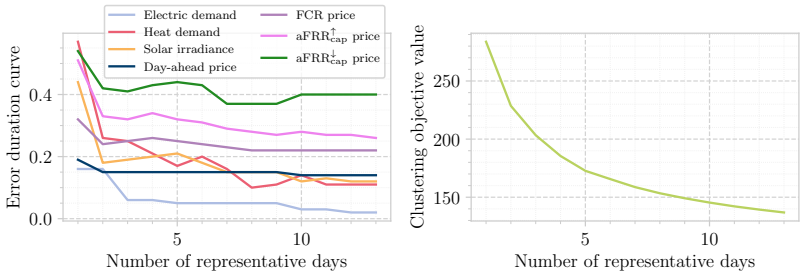

Fig. D.1: Error duration curves (left) and objective value of k-medoids clustering optimisation (right) depending on the number of representative days for the district-scale case study in Chapter 5.

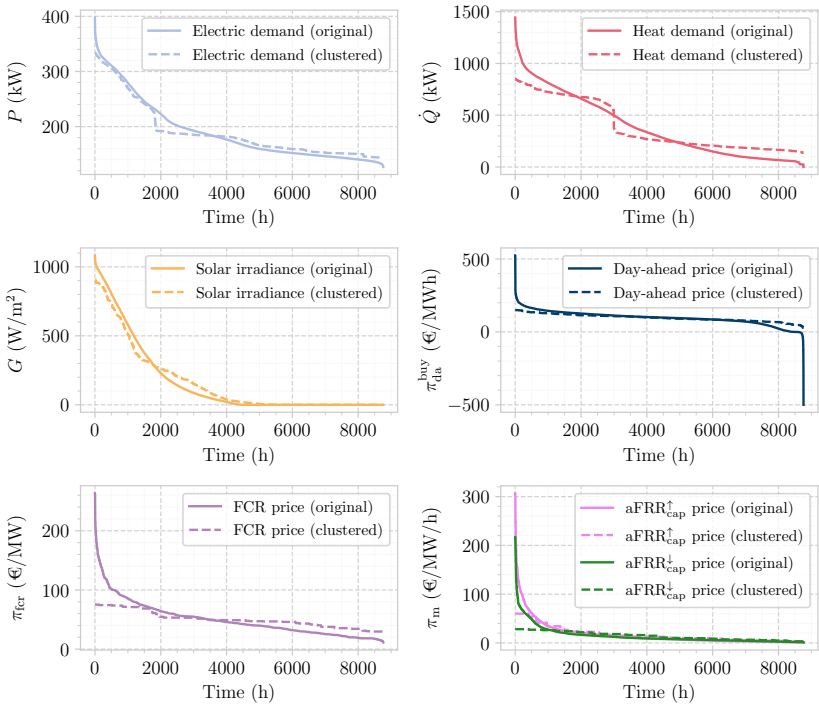

Fig. D.2: Duration curves for the district-scale case study in Chapter 5 for six representative clustering days, with the non-dashed line representing the original data set, while the dashed lines depict the duration curves of the clustered data set.

References

[1] C. Thelen, H. Nolte, M. Kaiser, P. Jürgens, P. Müller, C. Senkpiel, and C. Kost, "Wege zu einem klimaneutralen Energiesystem – Bundesländer im Transformationsprozess," technical report, Fraunhofer ISE, 2024. Cited on page 2.

[2] A. Borghetti, G. Graditi, T. Harighi, S. Lilla, F. Napolitano, C. A. Nucci, A. Prevedi, and F. Tossani, "How can energy communities be part of the urban energy transition?: A focus on electrical perspectives," *IEEE Power and Energy Magazine*, vol. 23, no. 3, pp. 78–88, 2025. Cited on page 2.

[3] G. Chicco, S. Riaz, A. Mazza, and P. Mancarella, "Flexibility from distributed multi-energy systems," *Proceedings of the IEEE*, vol. 108, pp. 1496–1517, Sept. 2020. Cited on pages 2, 3, 50, and 51.

[4] P. Mancarella, "MES (multi-energy systems): An overview of concepts and evaluation models," *Energy*, vol. 65, pp. 1–17, Feb. 2014. Cited on pages 2, 3, 29, 49, and 50.

[5] T. Weckesser, D. F. Dominković, E. M. Blomgren, A. Schledorn, and H. Madsen, "Renewable energy communities: Optimal sizing and distribution grid impact of photo-voltaics and battery storage," *Applied Energy*, vol. 301, p. 117408, 2021. Cited on page 2.

[6] A.-G. Chronis and N. Hatziargyriou, "The role of energy communities in enhancing sustainability in Europe: Successes and challenges," *IEEE Energy Sustainability Magazine*, vol. 1, no. 1, pp. 42–52, 2025. Cited on pages 2 and 3.

[7] European University Institute, A. Nouicer, A. Kehoe, J. Nysten, D. Fouquet, L. Meeus, and L. Hancher, *The EU clean energy package: (2020 ed.)*. European University Institute, 2020. Cited on pages 2 and 3.

[8] S. Backe, S. Zwickl-Bernhard, D. Schwabeneder, H. Auer, M. Korpås, and A. Tomasgard, "Impact of energy communities on the European electricity and heating system decarbonization pathway: Comparing local and global flexibility responses," *Applied Energy*, vol. 323, p. 119470, 2022. Cited on page 2.

[9] B. P. Koirala, E. Koliou, J. Friege, R. A. Hakvoort, and P. M. Herder, "Energetic communities for community energy: A review of key issues and trends shaping integrated community energy systems," *Renewable and Sustainable Energy Reviews*, vol. 56, pp. 722–744, 2016. Cited on page 2.

[10] M. Lynch, G. Longoria, and J. Curtis, "Market design options for electricity markets with high variable renewable generation," *Utilities Policy*, vol. 73, p. 101312, 2021. Cited on pages 2, 87, and 98.

[11] D. Ritter, D. Grafmüller, D. Bauknecht, M. Wingenbach, and K. Dünzen, "Electricity market design for 100 % renewable energy in Germany – Challenges and solutions," *Energy Reports*, vol. 14, pp. 634–647, 2025. Cited on page 2.

[12] D. Kirschen and G. Strbac, *Fundamentals of Power System Economics*. Wiley, 2nd ed., 2019. Cited on pages 3 and 6.

[13] L. Viola, S. Mohammadi, D. Dotta, M. R. Hesamzadeh, R. Baldick, and D. Flynn, "Ancillary services in power system transition toward a 100 % non-fossil future: Market design challenges in the United States and Europe," *Electric Power Systems Research*, vol. 236, p. 110885, 2024. Cited on pages 3 and 6.

[14] N. Good and P. Mancarella, "Flexibility in multi-energy communities with electrical and thermal storage: A stochastic, robust approach for multi-service demand response," *IEEE Transactions on Smart Grid*, vol. 10, no. 1, pp. 503–513, 2019. Cited on pages 3, 51, and 75.

[15] I.-I. Avramidis, F. Capitanescu, G. Deconinck, H. Nagpal, P. Heiselberg, and A. Madureira, "From the humble building to the smart sustainable grid: Empowering consumers, nurturing bottom-up electricity markets, and building collaborative power systems," *IEEE Power and Energy Magazine*, vol. 21, no. 4, pp. 53–63, 2023. Cited on page 51.

[16] G. Mokhtari, A. Ghosh, G. Nourbakhsh, and G. Ledwich, "Smart robust resources control in LV network to deal with voltage rise issue," *IEEE Transactions on Sustainable Energy*, vol. 4, no. 4, pp. 1043–1050, 2013. Cited on pages 75, 81, and 88.

[17] Z. Li, J. Wang, H. Sun, F. Qiu, and Q. Guo, "Robust estimation of reactive power for an active distribution system," *IEEE Transactions on Power Systems*, vol. 34, no. 5, pp. 3395–3407, 2019. Cited on pages 3 and 81.

[18] L. Canals Casals, J. Zhu, and L. F. Ochoa, "The potential of V2G considering EV charging behaviors, battery lifespan, and distribution networks," *Sustainable Energy, Grids and Networks*, vol. 42, p. 101706, 2025. Cited on page 4.

[19] C. Li, D. Carta, and A. Benigni, "EV charging station placement considering V2G and human factors in multi-energy systems," *IEEE Transactions on Smart Grid*, vol. 16, no. 1, pp. 529–540, 2025. Cited on page 4.

[20] D. Hering, M. E. Cansev, E. Tamassia, A. Xhonneux, and D. Müller, "Temperature control of a low-temperature district heating network with model predictive control and mixed-integer quadratically constrained programming," *Energy*, vol. 224, p. 120140, 2021. Cited on pages 15 and 21.

[21] E. Bettanini, A. Gastaldello, and L. Schibuola, "Simplified models to simulate part load performances of air conditioning equipments," *Proc. IBPSA 8th Int. Conf. Building Simulation '03*, p. 107 – 114, 2003. Cited on page 15.

[22] D. A. Waddicor, E. Fuentes, M. Azar, and J. Salom, "Partial load efficiency degradation of a water-to-water heat pump under fixed set-point control," *Applied Thermal Engineering*, vol. 106, pp. 275–285, 2016. Cited on pages 15 and 16.

[23] E. Sperber, U. Frey, and V. Bertsch, "Reduced-order models for assessing demand response with heat pumps – insights from the German energy system," *Energy and Buildings*, vol. 223, p. 110144, 2020. Cited on page 16.

[24] D. Romanchenko, J. Kensby, M. Odenberger, and F. Johnsson, "Thermal energy storage in district heating: Centralised storage vs. storage in thermal inertia of buildings," *Energy Conversion and Management*, vol. 162, pp. 26–38, 2018. Cited on page 17.

[25] H. Niyas, L. Prasad, and P. Muthukumar, "Performance investigation of high-temperature sensible heat thermal energy storage system during charging and discharging cycles," *Clean Technologies and Environmental Policy*, vol. 17, no. 2, pp. 501–513, 2015. Cited on page 18.

[26] Gurobi Optimization, LLC, "Gurobi Optimizer Reference Manual," 2023. Cited on pages 19 and 26.

[27] S. Frank and S. Rebennack, "An introduction to optimal power flow: Theory, formulation, and examples," *IIE Transactions*, vol. 48, no. 12, pp. 1172–1197, 2016. Cited on pages 19 and 20.

[28] J. C. Naughton, *A modelling framework for virtual power plants under uncertainty*. Phd thesis, University of Birmingham, 2022. Cited on page 20.

[29] J. A. Taylor, *Convex Optimization of Power Systems*. Cambridge: Cambridge University Press, 2015. Cited on page 20.

[30] S. H. Low, "Convex relaxation of optimal power flow—part i: Formulations and equivalence," *IEEE Transactions on Control of Network Systems*, vol. 1, no. 1, pp. 15–27, 2014. Cited on page 21.

[31] Bundesverband der Energie- und Wasserwirtschaft e.V. (BDEW), "BDEW-Strompreisanalyse März 2025," tech. rep., Bundesverband der Energie- und Wasserwirtschaft e.V. (BDEW), March 2025. accessed on 05/05/2025. Cited on pages 22 and 93.

[32] Bundesnetzagentur, "EEG-Förderung und -Fördersätze." Available at `https://www.bundesnetzagentur.de/DE/Fachthemen/ElektrizitaetundGas/ErneuerbareEnergien/EEG_Foerderung/start.html` (accessed on 29/05/2025), 2025. Cited on page 22.

[33] H.-G. Beyer and B. Sendhoff, "Robust optimization – a comprehensive survey," *Computer Methods in Applied Mechanics and Engineering*, vol. 196, no. 33, pp. 3190–3218, 2007. Cited on page 22.

[34] X. Lu, Z. Liu, L. Ma, L. Wang, K. Zhou, and S. Yang, "A robust optimization approach for coordinated operation of multiple energy hubs," *Energy*, vol. 197, p. 117171, 2020. Cited on page 22.

[35] A. Charnes and W. W. Cooper, "Chance-constrained programming," *Management Science*, vol. 6, no. 1, pp. 73–79, 1959. Publisher: INFORMS. Cited on page 22.

[36] M. Jasinski, A. Najafi, O. Homaee, M. Kermani, G. Tsaousoglou, Z. Leonowicz, and T. Novak, "Operation and planning of energy hubs under uncertainty—a review of mathematical optimization approaches," *IEEE Access*, vol. 11, pp. 7208–7228, 2023. Cited on page 23.

[37] P. Li, H. Arellano-Garcia, and G. Wozny, "Chance constrained programming approach to process optimization under uncertainty," *Computers & Chemical Engineering*, vol. 32, no. 1, pp. 25–45, 2008. Process Systems Engineering: Contributions on the State-of-the-Art. Cited on page 22.

[38] G. B. Dantzig, "Linear programming under uncertainty," *Management Science*, vol. 1, no. 3, pp. 197–206, 1955. Publisher: INFORMS. Cited on page 22.

[39] J. R. Birge and F. Louveaux, *Introduction to Stochastic Programming*. Springer Science & Business Media, 2011. Cited on page 22.

[40] M. Langiu, D. Y. Shu, F. J. Baader, D. Hering, U. Bau, A. Xhonneux, D. Müller, A. Bardow, A. Mitsos, and M. Dahmen, "Comando: A next-generation open-source framework for energy systems optimization," *Computers & Chemical Engineering*, vol. 152, p. 107366, 2021. Cited on pages 22, 23, and 91.

[41] X. Li and P. I. Barton, "Optimal design and operation of energy systems under uncertainty," *Journal of Process Control*, vol. 30, pp. 1–9, 2015. CAB/DYCOPS 2013. Cited on page 23.

[42] L. Kotzur, P. Markewitz, M. Robinius, and D. Stolten, "Time series aggregation for energy system design: Modeling seasonal storage," *Applied Energy*, vol. 213, pp. 123–135, 2018. Cited on page 23.

[43] T. Schütz, M. H. Schraven, M. Fuchs, P. Remmen, and D. Müller, "Comparison of clustering algorithms for the selection of typical demand days for energy system synthesis," *Renewable Energy*, vol. 129, pp. 570–582, 2018. Cited on page 23.

[44] F. Domínguez-Muñoz, J. M. Cejudo-López, A. Carrillo-Andrés, and M. Gallardo-Salazar, "Selection of typical demand days for chp optimization," *Energy and Buildings*, vol. 43, no. 11, pp. 3036–3043, 2011. Cited on page 23.

[45] M. D. Hering, *Optimization of district heating networks using mixed integer quadratically constrained programs*. Phd thesis, RWTH Aachen University, 2023. Cited on page 23.

[46] G. Mancò, U. Tesio, E. Guelpa, and V. Verda, "A review on multi energy systems modelling and optimization," *Applied Thermal Engineering*, vol. 236, p. 121871, 2024. Cited on page 27.

[47] A. Najafi, H. Falaghi, J. Contreras, and M. Ramezani, "Medium-term energy hub management subject to electricity price and wind uncertainty," *Applied Energy*, vol. 168, pp. 418–433, 2016. Cited on page 27.

[48] N. Liu, L. Tan, H. Sun, Z. Zhou, and B. Guo, "Bilevel heat–electricity energy sharing for integrated energy systems with energy hubs and prosumers," *IEEE Transactions on Industrial Informatics*, vol. 18, no. 6, pp. 3754–3765, 2022. Cited on page 27.

[49] R. Li and V. Mahalec, "Integrated design and operation of energy systems for residential buildings, commercial buildings, and light industries," *Applied Energy*, vol. 305, p. 117822, 2022. Cited on page 27.

[50] G. Piazza, F. Delfino, S. Bergero, M. Di Somma, G. Graditi, and S. Bracco, "Economic and environmental optimal design of a multi-vector energy hub feeding a local energy community," *Applied Energy*, vol. 347, p. 121259, 2023. Cited on page 28.

[51] A. Maroufmashat, S. Sattari, R. Roshandel, M. Fowler, and A. Elkamel, "Multi-objective optimization for design and operation of distributed energy systems through the multi-energy hub network approach," *Industrial & Engineering Chemistry Research*, vol. 55, pp. 8950–8966, Aug. 2016. Cited on page 28.

[52] T. Terlouw, P. Gabrielli, T. AlSkaif, C. Bauer, R. McKenna, and M. Mazzotti, "Optimal economic and environmental design of multi-energy systems," *Applied Energy*, vol. 347, p. 121374, 2023. Cited on page 28.

[53] H. Lv, Q. Wu, H. Ren, Q. Li, and W. Zhou, "A two-stage decision-making approach for optimal design and operation of integrated energy systems considering multiple uncertainties and diverse resilience needs," *Energy*, vol. 305, p. 132375, 2024. Cited on page 28.

[54] G. De Carne, S. M. Maroufi, H. Beiranvand, V. De Angelis, S. D'Arco, V. Gevorgian, S. Waczowicz, B. Mather, M. Liserre, and V. Hagenmeyer, "The role of energy storage systems for a secure energy supply: A comprehensive review of system needs and technology solutions," *Electric Power Systems Research*, vol. 236, p. 110963, 2024. Cited on pages 28 and 75.

[55] F. Calero, C. A. Cañizares, K. Bhattacharya, C. Anierobi, I. Calero, M. F. Z. de Souza, M. Farrokhabadi, N. S. Guzman, W. Mendieta, D. Peralta, B. V. Solanki, N. Padmanabhan, and W. Violante, "A review of modeling and applications of energy storage systems in power grids," *Proceedings of the IEEE*, vol. 111, no. 7, pp. 806–831, 2023. Cited on page 28.

[56] S. Dong, E. Kremers, M. Brucoli, R. Rothman, and S. Brown, "Techno-enviro-economic assessment of household and community energy storage in the UK," *Energy Conversion and Management*, vol. 205, p. 112330, 2020. Cited on page 28.

[57] L. Li, X. Cao, and S. Zhang, "Shared energy storage system for prosumers in a community: Investment decision, economic operation, and benefits allocation under a cost-effective way," *Journal of Energy Storage*, vol. 50, p. 104710, 2022. Cited on page 28.

[58] S. van der Stelt, T. AlSkaif, and W. van Sark, "Techno-economic analysis of household and community energy storage for residential prosumers with smart appliances," *Applied Energy*, vol. 209, pp. 266–276, 2018. Cited on page 28.

[59] M. Stecca, L. R. Elizondo, T. B. Soeiro, P. Bauer, and P. Palensky, "A comprehensive review of the integration of battery energy storage systems into distribution networks," *IEEE Open Journal of the Industrial Electronics Society*, vol. 1, pp. 46–65, 2020. Cited on page 28.

[60] R. Dai, R. Esmaeilbeigi, and H. Charkhgard, "The utilization of shared energy storage in energy systems: A comprehensive review," *IEEE Transactions on Smart Grid*, vol. 12, no. 4, pp. 3163–3174, 2021. Cited on pages 28 and 29.

[61] A. Walker and S. Kwon, "Analysis on impact of shared energy storage in residential community: Individual versus shared energy storage," *Applied Energy*, vol. 282, p. 116172, 2021. Cited on page 28.

[62] J.-W. Xiao, Y.-B. Yang, S. Cui, and X.-K. Liu, "A new energy storage sharing framework with regard to both storage capacity and power capacity," *Applied Energy*, vol. 307, p. 118171, 2022. Cited on page 28.

[63] E. Barbour, D. Parra, Z. Awwad, and M. C. González, "Community energy storage: A smart choice for the smart grid?," *Applied Energy*, vol. 212, pp. 489–497, 2018. Cited on page 28.

[64] T. Weckesser, D. F. Dominković, E. M. Blomgren, A. Schledorn, and H. Madsen, "Renewable energy communities: Optimal sizing and distribution grid impact of photo-voltaics and battery storage," *Applied Energy*, vol. 301, p. 117408, 2021. Cited on page 28.

[65] N. Pompern, S. Premrudeepreechacharn, A. Siritaratiwat, and S. Khunkitti, "Optimal placement and capacity of battery energy storage system in distribution networks

integrated with PV and EVs using metaheuristic algorithms," *IEEE Access*, vol. 11, pp. 68379–68394, 2023. Cited on page 29.

[66] X. Wu, A. J. Conejo, and S. Mathew, "Optimal siting of batteries in distribution systems to enhance reliability," *IEEE Transactions on Power Delivery*, vol. 36, no. 5, pp. 3118–3127, 2021. Cited on page 29.

[67] L. Mallier, G. Hétreux, R. Thery-Hetreux, and P. Baudet, "A modelling framework for energy system planning: Application to chp plants participating in the electricity market," *Energy*, 2021. Cited on page 29.

[68] P. Mancarella, G. Andersson, J. Peças-Lopes, and K. Bell, "Modelling of integrated multi-energy systems: Drivers, requirements, and opportunities," in *2016 Power Systems Computation Conference (PSCC)*, pp. 1–22, June 2016. Cited on page 29.

[69] J. Allegrini, K. Orehounig, G. Mavromatidis, F. Ruesch, V. Dorer, and R. Evins, "A review of modelling approaches and tools for the simulation of district-scale energy systems," *Renewable and Sustainable Energy Reviews*, vol. 52, pp. 1391–1404, 2015. Cited on page 29.

[70] T. Capuder and P. Mancarella, "Techno-economic and environmental modelling and optimization of flexible distributed multi-generation options," *Energy*, vol. 71, pp. 516–533, 2014. Cited on page 29.

[71] P. Gabrielli, M. Gazzani, E. Martelli, and M. Mazzotti, "A milp model for the design of multi-energy systems with long-term energy storage," in *27th European Symposium on Computer Aided Process Engineering* (A. Espuña, M. Graells, and L. Puigjaner, eds.), vol. 40 of *Computer Aided Chemical Engineering*, pp. 2437–2442, Elsevier, 2017. Cited on page 29.

[72] P. Gabrielli, M. Gazzani, E. Martelli, and M. Mazzotti, "Optimal design of multi-energy systems with seasonal storage," *Applied Energy*, vol. 219, pp. 408–424, 2018. Cited on page 29.

[73] B. H. Bakken, H. I. Skjelbred, and O. Wolfgang, "eTransport: Investment planning in energy supply systems with multiple energy carriers," *Energy*, vol. 32, no. 9, pp. 1676–1689, 2007. Cited on page 29.

[74] S. Clegg and P. Mancarella, "Integrated electricity-heat-gas modelling and assessment, with applications to the Great Britain system. part ii: Transmission network analysis and low carbon technology and resilience case studies," *Energy*, vol. 184, pp. 191–203, 2019. Shaping research in gas-, heat- and electric- energy infrastructures. Cited on page 29.

[75] M. Geidl, G. Koeppel, P. Favre-Perrod, B. Klockl, G. Andersson, and K. Frohlich, "Energy hubs for the future," *IEEE Power and Energy Magazine*, vol. 5, no. 1, pp. 24–30, 2007. Cited on page 29.

[76] S. Geng, M. Vrakopoulou, and I. A. Hiskens, "Optimal capacity design and operation of energy hub systems," *Proceedings of the IEEE*, vol. 108, no. 9, pp. 1475–1495, 2020. Cited on page 29.

[77] B. Morvaj, R. Evins, and J. Carmeliet, "Optimising urban energy systems: Simultaneous system sizing, operation and district heating network layout," *Energy*, vol. 116, pp. 619–636, Dec. 2016. Cited on page 29.

[78] X. Liu, P. Zhang, A. Pimm, D. Feng, and M. Zheng, "Optimal design and operation of PV-battery systems considering the interdependency of heat pumps," *Journal of Energy Storage*, vol. 23, pp. 526–536, June 2019. Cited on page 30.

[79] E. A. Martínez Ceseña and P. Mancarella, "Energy systems integration in smart districts: Robust optimisation of multi-energy flows in integrated electricity, heat and gas networks," *IEEE Transactions on Smart Grid*, vol. 10, pp. 1122–1131, Jan. 2019. Conference Name: IEEE Transactions on Smart Grid. Cited on page 30.

[80] X. Liu, J. Wu, N. Jenkins, and A. Bagdanavicius, "Combined analysis of electricity and heat networks," *Applied Energy*, vol. 162, pp. 1238–1250, Jan. 2016. Cited on page 30.

[81] X. Liu, Z. Yan, and J. Wu, "Optimal coordinated operation of a multi-energy community considering interactions between energy storage and conversion devices," *Applied Energy*, vol. 248, pp. 256–273, Aug. 2019. Cited on page 30.

[82] A. Walker and S. Kwon, "Analysis on impact of shared energy storage in residential community: Individual versus shared energy storage," *Applied Energy*, vol. 282, p. 116172, 2021. Cited on page 30.

[83] J.-W. Xiao, Y.-B. Yang, S. Cui, and X.-K. Liu, "A new energy storage sharing framework with regard to both storage capacity and power capacity," *Applied Energy*, vol. 307, p. 118171, 2022. Cited on page 30.

[84] V. Masson-Delmotte, P. Zhai, H.-O. Pörtner, D. Roberts, J. Skea, P. R. Shukla, A. Pirani, W. Moufouma-Okia, C. Péan, R. Pidcock, S. Connors, J. Matthews, Y. Chen, X. Zhou, M. I. Gomis, E. Lonnoy, T. Maycock, M. Tignor, and T. W. (eds.), *Global Warming of 1.5°C: IPCC Special Report on Impacts of Global Warming of 1.5°C above Pre-industrial Levels in Context of Strengthening Response to Climate Change, Sustainable Development, and Efforts to Eradicate Poverty*. Cambridge University Press, 1 ed., 2018. Cited on page 32.

[85] S. Pfenninger and I. Staffell, "Long-term patterns of European PV output using 30 years of validated hourly reanalysis and satellite data," *Energy*, vol. 114, pp. 1251–1265, 2016. Cited on page 35.

[86] S. B. Sepúlveda-Mora and S. Hegedus, "Making the case for time-of-use electric rates to boost the value of battery storage in commercial buildings with grid connected PV systems," *Energy*, vol. 218, p. 119447, 2021. Cited on page 35.

[87] N. Baumgärtner, R. Delorme, M. Hennen, and A. Bardow, "Design of low-carbon utility systems: Exploiting time-dependent grid emissions for climate-friendly demand-side management," *Applied Energy*, vol. 247, pp. 755–765, 2019. Cited on page 35.

[88] P. Graham, J. Hayward, and J. Foster, "GenCost 2023-24: Final report," tech. rep., CSIRO, 2024. Cited on pages 35, 62, and 92.

[89] S. H. M. Germscheid, B. Nilges, N. von der Assen, A. Mitsos, and M. Dahmen, "Optimal design of a local renewable electricity supply system for power-intensive production processes with demand response," *Computers & Chemical Engineering*, vol. 185, p. 108656, 2024. Cited on page 35.

[90] G. Wernet, C. Bauer, B. Steubing, J. Reinhard, E. Moreno-Ruiz, and B. Weidema, "The ecoinvent database version 3 (part i): Overview and methodology," *The International Journal of Life Cycle Assessment*, vol. 21, no. 9, pp. 1218–1230, 2016. Cited on page 35.

[91] A. A. Mohamed, R. J. Best, X. Liu, and D. J. Morrow, "A comprehensive robust techno-economic analysis and sizing tool for the small-scale PV and BESS," *IEEE Transactions on Energy Conversion*, vol. 37, no. 1, pp. 560–572, 2022. Cited on page 43.

[92] J. E. T. Bistline, C. W. Roney, D. L. McCollum, and G. J. Blanford, "Deep decarbonization impacts on electric load shapes and peak demand," *Environmental Research Letters*, vol. 16, p. 094054, sep 2021. Cited on page 49.

[93] A. Rinaldi, M. C. Soini, K. Streicher, M. K. Patel, and D. Parra, "Decarbonising heat with optimal PV and storage investments: A detailed sector coupling modelling framework with flexible heat pump operation," *Applied Energy*, vol. 282, p. 116110, 2021. Cited on page 50.

[94] A. Akrami, M. Doostizadeh, and F. Aminifar, "Power system flexibility: an overview of emergence to evolution," *Journal of Modern Power Systems and Clean Energy*, vol. 7, no. 5, pp. 987–1007, 2019. Cited on page 49.

[95] A. Ulbig and G. Andersson, "Analyzing operational flexibility of electric power systems," *International Journal of Electrical Power & Energy Systems*, vol. 72, pp. 155–164, 2015. Cited on page 50.

[96] J. Zhao, T. Zheng, and E. Litvinov, "A unified framework for defining and measuring flexibility in power system," *IEEE Transactions on Power Systems*, vol. 31, no. 1, pp. 339–347, 2016. Cited on page 50.

[97] S. Riaz and P. Mancarella, "Modelling and characterisation of flexibility from distributed energy resources," *IEEE Transactions on Power Systems*, vol. 37, no. 1, pp. 38–50, 2022. Cited on pages 50, 51, 54, 55, and 59.

[98] Y. Wang, T. Levin, J. Kwon, and E. Baker, "The value of hydropower flexibility for electricity system decarbonization," *Energy Reports*, vol. 13, pp. 2711–2721, 2025. Cited on page 50.

[99] D. Enescu, G. Chicco, R. Porumb, and G. Seritan, "Thermal energy storage for grid applications: Current status and emerging trends," *Energies*, vol. 13, no. 2, p. 340, 2020. Cited on page 50.

[100] H. Nagpal, I.-I. Avramidis, F. Capitanescu, and A. G. Madureira, "Local energy communities in service of sustainability and grid flexibility provision: Hierarchical management of shared energy storage," *IEEE Transactions on Sustainable Energy*, vol. 13, no. 3, pp. 1523–1535, 2022. Cited on page 50.

[101] I.-I. Avramidis, H. Nagpal, M. Mehrtash, and F. Capitanescu, "gENESiS: Design, operation and integration of smart sustainable buildings in smart power grids," in *2021 29th Mediterranean Conference on Control and Automation (MED)*, pp. 45–52, 2021. ISSN: 2473-3504. Cited on page 51.

[102] M. Z. Liu, L. N. Ochoa, S. Riaz, P. Mancarella, T. Ting, J. San, and J. Theunissen, "Grid and market services from the edge: Using operating envelopes to unlock network-aware bottom-up flexibility," *IEEE Power and Energy Magazine*, vol. 19, no. 4, pp. 52–62, 2021. Cited on page 51.

[103] A. Vandermeulen, B. van der Heijde, and L. Helsen, "Controlling district heating and cooling networks to unlock flexibility: A review," *Energy*, vol. 151, pp. 103–115, 2018. Cited on page 51.

[104] A. De Corato, I. Saedi, S. Riaz, and P. Mancarella, "Aggregated flexibility from multiple power-to-gas units in integrated electricity-gas-hydrogen distribution systems," *Electric Power Systems Research*, vol. 212, p. 108409, 2022. Cited on pages 51 and 55.

[105] R. Heffron, M.-F. Körner, J. Wagner, M. Weibelzahl, and G. Fridgen, "Industrial demand-side flexibility: A key element of a just energy transition and industrial development," *Applied Energy*, vol. 269, p. 115026, 2020. Cited on page 51.

[106] Q. Zhang and I. E. Grossmann, "Enterprise-wide optimization for industrial demand side management: Fundamentals, advances, and perspectives," *Chemical Engineering Research and Design*, vol. 116, pp. 114–131, 2016. Process Systems Engineering - A Celebration in Professor Roger Sargent's 90th Year. Cited on page 51.

[107] F. T. C. Röben, D. Liu, M. A. Reuter, M. Dahmen, and A. Bardow, "The demand response potential in copper production," *Journal of Cleaner Production*, vol. 362, p. 132221, 2022. Cited on page 51.

[108] M. Paulus and F. Borggrefe, "The potential of demand-side management in energy-intensive industries for electricity markets in Germany," *Applied Energy*, vol. 88, no. 2, pp. 432–441, 2011. Cited on page 51.

[109] J. C. Richstein and S. S. Hosseinioun, "Industrial demand response: How network tariffs and regulation (do not) impact flexibility provision in electricity markets and reserves," *Applied Energy*, vol. 278, p. 115431, 2020. Cited on page 51.

[110] M. Bohlayer, M. Fleschutz, M. Braun, and G. Zöttl, "Energy-intense production-inventory planning with participation in sequential energy markets," *Applied Energy*, vol. 258, p. 113954, 2020. Cited on pages 51, 77, and 95.

[111] S. Ledur, R. Molinier, F. Sossan, J.-C. Alais, M.-D. El Alaoui Faris, and G. Kariniotakis, "Identification and quantification of the flexibility potential of a complex industrial process for ancillary services provision," *Electric Power Systems Research*, vol. 212, p. 108396, 2022. Cited on pages 52 and 55.

[112] H. Hui, M. Bao, Y. Ding, and Y. Song, "Exploring the integrated flexible region of distributed multi-energy systems with process industry," *Applied Energy*, vol. 311, p. 118590, 2022. Cited on page 52.

[113] H. Hui, M. Bao, Y. Ding, J. Yan, and Y. Song, "Probabilistic integrated flexible regions of multi-energy industrial parks: Conceptualization and characterization," *Applied Energy*, vol. 349, p. 121521, 2023. Cited on page 52.

[114] H. Hui, M. Bao, Y. Ding, and C. J. Meinrenken, "Incorporating multi-energy industrial parks into power system operations: A high-dimensional flexible region method," *IEEE Transactions on Smart Grid*, vol. 16, no. 1, pp. 463–477, 2025. Cited on page 52.

[115] X. Zang, H. Li, and S. Wang, "Levelized cost quantification of energy flexibility in high-density cities and evaluation of demand-side technologies for providing grid services," *Renewable and Sustainable Energy Reviews*, vol. 211, p. 115290, 2025. Cited on page 52.

[116] H. Wang, S. Riaz, and P. Mancarella, "Integrated techno-economic modeling, flexibility analysis, and business case assessment of an urban virtual power plant with multi-market co-optimization," *Applied Energy*, vol. 259, p. 114142, 2020. Cited on page 52.

[117] N. Čović, F. Braeuer, R. McKenna, and H. Pandžić, "Optimal PV and battery investment of market-participating industry facilities," *IEEE Transactions on Power Systems*, vol. 36, no. 4, pp. 3441–3452, 2021. Cited on page 52.

[118] M. Fleschutz, M. Bohlayer, M. Braun, and M. D. Murphy, "From prosumer to flexumer: Case study on the value of flexibility in decarbonizing the multi-energy system of a manufacturing company," *Applied Energy*, vol. 347, p. 121430, 2023. Cited on pages 52 and 77.

[119] P. Schäfer, T. M. Daun, and A. Mitsos, "Do investments in flexibility enhance sustainability? A simulative study considering the German electricity sector," *AIChE Journal*, vol. 66, no. 11, p. e17010, 2020. Cited on page 53.

[120] M. Z. Liu, L. F. Ochoa, P. K. C. Wong, and J. Theunissen, "Using OPF-based operating envelopes to facilitate residential DER services," *IEEE Transactions on Smart Grid*, vol. 13, no. 6, pp. 4494–4504, 2022. Cited on page 54.

[121] Bundesnetzagentur, "Beschaffungskonzept für die Spezifikationen und technischen Anforderungen der transparenten, diskriminierungsfreien und marktgestützten Beschaffung der nicht frequenzgebundenen Systemdienstleistung 'Dienstleistungen zur Spannungsregelung' ('Blindleistung') gem. § 12h Abs. 1 S. 1 Nr. 1, Abs. 5 EnWG," 2024. Available at https://www.bundesnetzagentur.de/DE/Beschlusskammern/1_GZ/BK6-GZ/2023/BK6-23-072/BK6-23-072_beschaffungskonzept.pdf?__blob=publicationFile&v=4, accessed on 27/09/2024. Cited on page 59.

[122] Netztransparenz.de, "Blindleistung - Einheitliche Auslegung von E-STATCOM," 2024. Available at ttps://www.netztransparenz.de/de-de/Systemdienstleistungen/Spannungshaltung/Blindleistung, accessed on 27/09/2024. Cited on page 59.

[123] M. Wirtz, "npro: A web-based planning tool for designing district energy systems and thermal networks," *Energy*, vol. 268, p. 126575, 2023. Cited on page 61.

[124] Solcast, "Global solar irradiance data and PV system power output data," 2024. Available at https://solcast.com/, accessed on 02/08/2023. Cited on page 61.

[125] N. Baumgärtner, R. Delorme, M. Hennen, and A. Bardow, "Design of low-carbon utility systems: Exploiting time-dependent grid emissions for climate-friendly demand-side management," *Applied Energy*, vol. 247, pp. 755–765, 2019. Cited on pages 62 and 92.

[126] D. Hering, A. Xhonneux, and D. Müller, "Design optimization of a heating network with multiple heat pumps using mixed integer quadratically constrained programming," *Energy*, vol. 226, p. 120384, 2021. Cited on pages 62 and 92.

[127] Ofenseite, "Pufferspeicher 500," 2024. Available at https://www.ofenseite.com/6100108-pufferspeicher-500, accessed on 31/10/2024. Cited on pages 62 and 92.

[128] M. Evens and A. Arteconi, "Design energy flexibility within a comfort and climate box – an experimental evaluation of the internal heat pump control effects," *Applied Thermal Engineering*, vol. 254, p. 123842, 2024. Cited on page 62.

[129] E. Ubachukwu, J. Pick, L. Riebesel, P. Lieberenz, P. Althaus, A. Xhonneux, and D. Müller, "User engagement for thermal energy-efficient behavior in office buildings using dashboards and gamification," *Applied Thermal Engineering*, vol. 266, p. 125598, 2025. Cited on page 72.

[130] A. Srivastava, J. Zhao, H. Zhu, F. Ding, S. Lei, I. Zografopoulos, R. Haider, S. Vahedi, W. Wang, G. Valverde, A. Gomez-Exposito, A. Dubey, C. Konstantinou, N. Yu, S. Brahma, Y. R. Rodrigues, M. Ben-Idris, B. Liu, A. Annaswamy, F. Bu, Y. Wang, D. Espín-Sarzosa, F. Valencia, J. Gabrielski, S. M. Mohseni-Bonab, J. Jazaeri, Z. Wang, and A. Srivastava, "Distribution system behind-the-meter DERs: Estimation, uncertainty quantification, and control," *IEEE Transactions on Power Systems*, vol. 40, no. 1, pp. 1060–1077, 2025. Cited on page 76.

[131] G. G. Farivar, W. Manalastas, H. D. Tafti, S. Ceballos, A. Sanchez-Ruiz, E. C. Lovell, G. Konstantinou, C. D. Townsend, M. Srinivasan, and J. Pou, "Grid-connected energy storage systems: State-of-the-art and emerging technologies," *Proceedings of the IEEE*, vol. 111, no. 4, pp. 397–420, 2023. Cited on page 76.

[132] M. Kazemi, H. Zareipour, N. Amjady, W. D. Rosehart, and M. Ehsan, "Operation scheduling of battery storage systems in joint energy and ancillary services markets," *IEEE Transactions on Sustainable Energy*, vol. 8, no. 4, pp. 1726–1735, 2017. Conference Name: IEEE Transactions on Sustainable Energy. Cited on page 76.

[133] M. Karasavvidis, A. Stratis, D. Papadaskalopoulos, and G. Strbac, "Optimal offering of energy storage in UK day-ahead energy and frequency response markets," *Journal of Modern Power Systems and Clean Energy*, vol. 12, no. 2, pp. 415–426, 2024. Cited on page 76.

[134] Y. Shi, B. Xu, D. Wang, and B. Zhang, "Using battery storage for peak shaving and frequency regulation: Joint optimization for superlinear gains," *IEEE Transactions on Power Systems*, vol. 33, no. 3, pp. 2882–2894, 2018. Cited on page 76.

[135] S. Chen, J. Zhou, H. Han, X. Zhang, Y. Zhou, and Z. Wei, "Investment strategies for energy storage systems in a joint energy and frequency ancillary service market," *Journal of Energy Storage*, vol. 116, p. 115798, 2025. Cited on page 76.

[136] L. Maeyaert, L. Vandevelde, and T. Döring, "Battery storage for ancillary services in smart distribution grids," *Journal of Energy Storage*, vol. 30, p. 101524, 2020. Cited on page 76.

[137] J. Bian, Y. Song, C. Ding, J. Cheng, S. Li, and G. Li, "Optimal bidding strategy for PV and BESSs in joint energy and frequency regulation markets considering carbon reduction benefits," *Journal of Modern Power Systems and Clean Energy*, vol. 12, no. 2, pp. 427–439, 2024. Cited on page 76.

[138] S. Kortmann, J. Jeup, C. Ernst, F. Schmidtke, and A. Ulbig, "A two-stage optimization for multi-use operation of BESS with peak shaving and FCR applications," in *2024 IEEE Power & Energy Society General Meeting (PESGM)*, pp. 1–5, 2024. Cited on page 76.

[139] C. B. Domenech, A. M. De Corato, and P. Mancarella, "Co-optimization of behind-the-meter and front-of-meter value streams in community batteries," *Journal of Modern Power Systems and Clean Energy*, vol. 12, no. 2, pp. 334–345, 2024. Cited on page 76.

[140] A. Muqbel, A. T. Al-Awami, and M. Parvania, "Optimal planning of distributed battery energy storage systems in unbalanced distribution networks," *IEEE Systems Journal*, vol. 16, no. 1, pp. 1194–1205, 2022. Cited on page 76.

[141] N. B. Arias, J. C. López, S. Hashemi, J. F. Franco, and M. J. Rider, "Multi-objective sizing of battery energy storage systems for stackable grid applications," *IEEE Transactions on Smart Grid*, vol. 12, no. 3, pp. 2708–2721, 2021. Cited on page 76.

[142] Y. Zhang, A. Anvari-Moghaddam, S. Peyghami, Y. Li, T. Dragičević, and F. Blaabjerg, "Optimal sizing of behind-the-meter battery storage for providing profit-oriented stackable services," *IEEE Transactions on Smart Grid*, vol. 15, no. 2, pp. 1481–1494, 2024. Cited on pages 76 and 77.

[143] H. Khaloie, A. Abdollahi, M. Shafie-khah, A. Anvari-Moghaddam, S. Nojavan, P. Siano, and J. P. S. Catalão, "Coordinated wind-thermal-energy storage offering strategy in energy and spinning reserve markets using a multi-stage model," *Applied Energy*, vol. 259, p. 114168, 2020. Cited on page 77.

[144] E. Finhold, C. Gärtner, R. Grindel, T. Heller, N. Leithäuser, E. Röger, and F. Schirra, "Optimizing the marketing of flexibility for a virtual battery in day-ahead and balancing markets: A rolling horizon case study," *Applied Energy*, vol. 352, p. 121667, 2023. Cited on page 77.

[145] J. Naughton, H. Wang, M. Cantoni, and P. Mancarella, "Co-optimizing virtual power plant services under uncertainty: A robust scheduling and receding horizon dispatch approach," *IEEE Transactions on Power Systems*, vol. 36, no. 5, pp. 3960–3972, 2021. Cited on page 77.

[146] H. Wang, S. Riaz, and P. Mancarella, "Integrated techno-economic modeling, flexibility analysis, and business case assessment of an urban virtual power plant with multi-market co-optimization," *Applied Energy*, vol. 259, p. 114142, 2020. Cited on page 77.

[147] G. Cardoso, M. Stadler, S. Mashayekh, and E. Hartvigsson, "The impact of ancillary services in optimal DER investment decisions," *Energy*, vol. 130, pp. 99–112, 2017. Cited on page 77.

[148] C. Li, P. Li, H. Yu, H. Li, J. Zhao, S. Li, and C. Wang, "Optimal planning of community integrated energy station considering frequency regulation service," *Journal of Modern Power Systems and Clean Energy*, vol. 9, no. 2, pp. 264–273, 2021. Cited on page 77.

[149] N. Nolzen, L. Leenders, and A. Bardow, "Flexibility-expansion planning of multi-energy systems by energy storage for participating in balancing-power markets," *Frontiers in Energy Research*, vol. 11, 2023. Publisher: Frontiers. Cited on page 77.

[150] S. F. Contreras, C. A. Cortes, and J. M. A. Myrzik, "Optimal microgrid planning for enhancing ancillary service provision," *Journal of Modern Power Systems and Clean Energy*, vol. 7, no. 4, pp. 862–875, 2019. Cited on page 77.

[151] Next Kraftwerke, "What is frequency containment reserve (FCR)?," 2025. Available at `https://www.next-kraftwerke.de/wissen/ausgleichsenergie`, accessed on 09/02/2025. Cited on pages 79 and 80.

[152] Epex Spot, "Annual trading results of 2024 – power trading on epex spot reaches all-time high," 2025. Available at https://www.epexspot.com/sites/default/files/download_center_files/, accessed on 14/04/2025. Cited on page 80.

[153] Epex Spot, "Trading products," 2025. Available at https://www.epexspot.com/en/tradingproducts, accessed on 14/04/2025. Cited on page 80.

[154] ENTSOE, "Electricity balancing guidelines," 2025. Available at https://www.entsoe.eu/network_codes/eb, accessed on 09/02/2025. Cited on page 80.

[155] 50 Hertz Transmission GmbH, Amprion GmbH, TenneT TSO GmbH, and TransnetBW GmbH, "Prequalification Process for Balancing Service Providers (FCR, aFRR, mFRR) in Germany ("PQ conditions")," tech. rep., Berlin, 2024. Cited on pages 80, 84, and 85.

[156] Regelleistung.net, "Platform for control reserve market information," 2025. Available at https://www.regelleistung.net/, accessed on 29/03/2025. Cited on pages 81 and 93.

[157] D. Wibmer, "Strommarkttreffen 'Speicher' - Realistischer Blick auf die Erlöspotentiale von Batteriespeichern in der Sekundärregelreserve (SRL)." Available at https://www.strommarkttreffen.org/vergangene-treffen/, accessed on 25/03/2025, 2025. Cited on pages 81 and 96.

[158] Deutsche Energie-Agentur GmbH (dena), TU Dortmund and ef.Ruhr GmbH, "dena-Studie Systemdienstleistungen 2030 - Sicherheit und Zuverlässigkeit einer Stromversorgung mit hohem Anteil erneuerbarer Energien.," tech. rep., Berlin, 2014. Cited on page 81.

[159] Bundesnetzagentur, "Beschaffungskonzept für die Spezifikationen und technischen Anforderungen der transparenten, diskriminierungsfreien und marktgestützten Beschaffung der nicht frequenzgebundenen Systemdienstleistung 'Dienstleistungen zur Spannungsregelung' ('Blindleistung') gem. § 12h Abs. 1 S. 1 Nr. 1, Abs. 5 EnWG," 2024. Cited on page 81.

[160] Federal Ministry for Economic Affairs and Climate Action Germany, "Roadmap Systemstabilität," 2023. Cited on page 81.

[161] Energate - Ron-David Heinen, "50 Hertz launches reactive power market," 2025. Available at https://www.energate-messenger.com/news/252209/50-hertz-launches-reactive-power-market, accessed on 06/06/2025. Cited on pages 81 and 106.

[162] 50 Hertz Transmission GmbH, "Marktgestützte Beschaffung von Blindleistung - Q&A," 2025. Available at https://www.50hertz.com/de/Vertragspartner/Systemdienstleistungen/Spannungshaltung/Blindleistungsanbieterwerden, accessed on 04/04/2025. Cited on pages 81 and 106.

[163] 50 Hertz Transmission GmbH, Amprion GmbH, TenneT TSO GmbH and TransnetBW GmbH, "Netzentwicklungsplan Strom 2035, Systemstabilität, zweiter Entwurf," tech. rep., Berlin, 2021. Cited on page 81.

[164] J. Jomaux, "The emergence of duck curves in Europe," 2024. Available at https://gemenergyanalytics.substack.com/p/the-emergence-of-duck-curves-in-europe, accessed on 28/03/2024. Cited on page 87.

[165] Australian Market Energy Operator (AEMO), "Quarterly Energy Dynamics Q4 2024," tech. rep., AEMO, 2025. Cited on page 87.

[166] J. Jomaux, "The duck is growing," 2025. Available at https://gemenergyanalytics.substack.com/p/the-duck-is-growing, accessed on 17/03/2025. Cited on page 87.

[167] Clean Horizon Consulting - Michael Salmon, "Ancillary services trending downward change the business model for storage," 2025. LinkedIn post, Available at https://gemenergyanalytics.substack.com/p/the-duck-is-growing, accessed on 28/03/2025. Cited on page 87.

[168] 50 Hertz Transmission GmbH, "Marktgestützte Beschaffung von Blindleistung - Ausschreibungsunterlagen 2025." Available at https://www.50hertz.com/xspProxy/api/staticfiles/50hertz-client/dokumente/vertragspartner/systemdienstleistungen/blindleistungsanbieter_werden_02_2025, accessed on 15/04/2025. Cited on pages 88 and 104.

[169] Bundesnetzagentur, "Diskussionspapier - Blindleistungsbereitstellung für den Netzbetrieb," tech. rep., Berlin, 2018. Cited on page 88.

[170] L. Bobo, A. Venzke, and S. Chatzivasileiadis, "Second-order cone relaxations of the optimal power flow for active distribution grids: Comparison of methods," *International Journal of Electrical Power & Energy Systems*, vol. 127, p. 106625, 2021. Cited on page 89.

[171] R. R. Jha and A. Dubey, "Network-level optimization for unbalanced power distribution system: Approximation and relaxation," *IEEE Transactions on Power Systems*, vol. 36, no. 5, pp. 4126–4139, 2021. Cited on pages 89 and 90.

[172] C. B. Domenech, J. Naughton, S. Riaz, and P. Mancarella, "Towards distributed energy markets: Accurate and intuitive DLMP decomposition," *IEEE Transactions on Energy Markets, Policy and Regulation*, vol. 2, no. 2, pp. 240–253, 2024. Cited on pages 89 and 90.

[173] Fraunhofer Institute for Solar Energy Systems ISE, "Energy charts," 2021. Available at https://www.energy-charts.info., accessed on 02/03/2025. Cited on page 93.

[174] Netztransparenz.de, "Netztransparenz: Information Platform of the German Transmission System Operators," 2025. Available at https://www.netztransparenz.de/, accessed on 02/04/2025. Cited on page 93.

[175] DVLP.energy, "Changes to the building cost subsidies (BKZ): What will change in 2025," 2025. Available at ttps://www.dvlp.energy/post-eng/changes-to-the-building-cost-subsidies-bkz-what-will-change-in-2025, accessed on 04/06/2025. Cited on page 94.

[176] A. J. Conejo, M. Carrión, and J. M. Morales, *Decision Making Under Uncertainty in Electricity Markets*, vol. 153 of *International Series in Operations Research & Management Science*. Springer US, 2010. Cited on page 94.

[177] R. Sioshansi, P. Denholm, J. Arteaga, S. Awara, S. Bhattacharjee, A. Botterud, W. Cole, A. Cortés, A. d. Queiroz, J. DeCarolis, Z. Ding, N. DiOrio, Y. Dvorkin, U. Helman, J. X. Johnson, I. Konstantelos, T. Mai, H. Pandžić, D. Sodano, G. Stephen, A. Svoboda, H. Zareipour, and Z. Zhang, "Energy-storage modeling: State-of-the-art and future research directions," *IEEE Transactions on Power Systems*, vol. 37, no. 2, pp. 860–875, 2022. Cited on page 94.

[178] L. Koltermann, K. Jacqué, J. Figgener, S. Zurmühlen, and D. Uwe Sauer, "Balancing group deviation & balancing energy costs due to the provision of frequency containment reserve with a battery storage system in Germany," *International Journal of Electrical Power & Energy Systems*, vol. 142, p. 108327, 2022. Cited on page 95.

[179] N. Naseri, Y. Ghiassi-Farrokhfal, W. Ketter, and J. Collins, "Understanding and managing the participation of batteries in reserve electricity markets," *Decision Support Systems*, vol. 165, p. 113895, 2023. Cited on page 95.

[180] M. Backer, D. Keles, and E. Kraft, "The economic impacts of integrating European balancing markets: The case of the newly installed aFRR energy market-coupling platform PICASSO," *Energy Economics*, vol. 128, p. 107124, 2023. Cited on page 95.

[181] E. Kraft, M. Russo, D. Keles, and V. Bertsch, "Stochastic optimization of trading strategies in sequential electricity markets," *European Journal of Operational Research*, vol. 308, no. 1, pp. 400–421, 2023. Cited on page 95.

[182] J. Jomaux, "Daily spreads on the day-ahead markets," 2025. Available at https://gemenergyanalytics.substack.com/p/daily-spreads-on-the-day-ahead-markets, accessed on 24/04/2025. Cited on page 97.

[183] L. Hirth, "The market value of variable renewables: The effect of solar wind power variability on their relative price," *Energy Economics*, vol. 38, pp. 218–236, 2013. Cited on page 98.

[184] D. E. Bell, "Regret in decision making under uncertainty," *Operations Research*, vol. 30, no. 5, pp. 961–981, 1982. Cited on page 101.

Band / Volume 678
Deployment of Fuel Cell Vehicles in Road Transport and the Expansion of the Hydrogen Refueling Station Network
T. Grube, M. Sander (2025), iv, 61 pp
ISBN: 978-3-95806-859-9

Band / Volume 679
Entwicklung von nickelbasierten katalysatorbeschichteten Diaphragmen für die alkalische Wasserelektrolyse
C. B. Karacan (2025), 146 pp
ISBN: 978-3-95806-860-5

Band / Volume 680
Bewertung lokaler Eigenspannungsverteilungen bei der lokalen Bauteilreparatur durch Kaltgasspritzen
J.-C. Schmitt (2025), 154, xxvii pp
ISBN: 978-3-95806-861-2

Band / Volume 681
First principles study of the effect of substitution\doping on the performance of layered oxide cathode materials for secondary batteries
N. Yaqoob (2025), iii, 126 pp
ISBN: 978-3-95806-864-3

Band / Volume 682
Field assisted sintering technology/spark plasma sintering in the direct recycling of hot-deformed Nd-Fe-B scrap and PM T15 steel swarf
M. T. M. Keszler (2025), viii, 173 pp
ISBN: 978-3-95806-866-7

Band / Volume 683
Assessment of erosion in recessed areas of fusion devices using multi-scale computer simulations
S. W. Rode (2025), viii, 196 pp
ISBN: 978-3-95806-867-4

Band / Volume 684
Europäische Energiewende – Deutschland im Herzen Europas
T. Klütz, P. Dunkel, T. Busch, J. Linssen, D. Stolten (2025), IV, 56 pp
ISBN: 978-3-95806-870-4

Band / Volume 685
Performance and stability of solar cells and modules: From laboratory characterization to field data analysis
T. S. Vaas (2025), xvii, 146 pp
ISBN: 978-3-95806-871-1

Band / Volume 686
From Soil Legacy to Wheat Yield Decline: Studying the Plant-Soil Feedback Mechanisms in Wheat Rotations
N. Kaloterakis (2025), XXIX, 188 pp
ISBN: 978-3-95806-874-2

Band / Volume 687
Entwicklung von Beschichtungsverfahren für die Herstellung von Wärmedämmschichten auf additiv gefertigten Komponenten
M. Rüßmann (2026), ix, 188 pp
ISBN: 978-3-95806-877-3

Band / Volume 688
Model Perovskite Oxide Electrocatalysts for the Oxygen Evolution Reaction and their Material Sustainability Evaluation
L. Heymann (2026), vi, 174 pp
ISBN: 978-3-95806-878-0

Band / Volume 689
Development of an oxygen ion conducting solid oxide electrolysis cell based on gadolinium-doped cerium oxide as fuel electrode and electrolyte material
D. Ramler (2026), ix, 162 pp
ISBN: 978-3-95806-879-7

Band / Volume 690
Design of Local Multi-Energy Systems: Impact of Coupled Energy Vector Integration and Grid Service Participation
P. S. Glücker (2026), xxviii, 145 pp
ISBN: 978-3-95806-880-3

Energie & Umwelt / Energy & Environment
Band / Volume 690
ISBN 978-3-95806-880-3

Mitglied der Helmholtz-Gemeinschaft

JÜLICH
Forschungszentrum